TECHNICAL UNIVERSITY OF LIBEREC

FACULTY OF TEXTILE ENGINEERING

DIPLOMA THESIS

2011 **Nkululeko Muzi Patrick Dlamini**

TECHNICAL UNIVERSITY OF LIBEREC

Textile engineering

Department of Textile Chemistry

FINISHING OF BASALT FIBRES

Supervisor : Assoc. Prof. Jakub Wiener, PhD.

Consultants : Ing. Jana Šašková

Ing. Marie Štěpánková

Number of pages : 98

Number of figures : 57

Number of tables : 23

Number of references : 35

Statement

I, Nkululeko Muzi Patrick Dlamini, have been informed that my thesis is fully applicable to the Act No. 121/2000 Coll. about copyright, especially §60 - school work.

I acknowledge that Technical University of Liberec (TUL) does not breach my copyright when using my thesis for internal needs.

Shall I use my thesis or shall I award a licence for its utilisation, I acknowledge that I am obliged to inform TUL about this fact, TUL has right to claim expenses incurred for this thesis up to amount of actual full expenses.

I have elaborate the thesis alone utilising the listed references and on basis of consultations with supervisor.

Date: 13 May 2011

Signature:

Nkululeko Muzi Patrick Dlamini

ACKNOWLEDGEMENT

Firstly I would like to express my sincere gratitude to my supervisor, Assoc. Prof. Jakub Wiener, for his support and inspiration throughout the course of my project. Also I would like to express my genuine thanks to, Jana Šašková Ing; Marie Štěpánková Ing and Mirka Maršálková PhD, for their assistance during my lab work. I really appreciate all their inputs, time and efforts towards the success of this project.

I acknowledge all the staff members working under the Textile Chemistry department, the department of Textile Materials and all the lectures of Technical University of Liberec who have been assisting and imparting tons of knowledge to South African students without any reservations. Not forgetting Hana Musilova and Dr Rajesh Mishra (International Officer) for their patience and making our lives easier during our stay in the Czech Republic.

I am dedicating this project to my family and friends, who have been very supportive right from the beginning of my studies up until now. Much appreciation goes to my mother, Busisiwe Dlamini, my father, Mandla Dlamini, my brother, Sibusiso and my Sister Thokozani, for being my pillars of strength and sources of inspiration at all times. Lastly I would like to thank my God, for being faithful to me, at all times.

ABSTRACT

Basalt fibre (BF) is a material made from extremely fine fibres of basalt, which is composed of the minerals plagioclase, pyroxene, and olivine. It is almost similar to its mineral fibre counterparts, like carbon fibre and glass fibre, having better physical mechanical properties than glass fibre, but being significantly cheaper than carbon fibre. In this study a series of investigations are conducted, to explore and develop other techniques which could be useful for basalt fibre finishing. The first investigation is piloted by qualitatively analysing the atomic element(s) composition of basalt fibre, with a use of Laser-Induced Breakdown Spectroscopy (LIBS). The inter-facial interaction relationship between basalt fibre, acids and alkalis is also explored as a means to determine the degree of BF resistance against corrosion. An attempt to modify BF surface properties is conducted by means of IR laser (CO_2 laser) irradiation. A degree of BF surface damage due to different CO_2 laser beam intensity levels is classified accordingly. An attempt to deposit carbon on BF surface, by IR laser method is explored. Lastly, a carbon matrix (C-matrix) is prepared from different concentrates of sucrose solution. This C-matrix is then used as a binding resin for BF reinforced composite material. Porous carbon composites rods (carbon electrode) are produced and tested for electrical conductivity, mechanical properties and thermo stability. To assess and evaluate properties of the specimens prepared, the following instruments are used: Scanning Electron microscopy (SEM), Tera 2300 mechanical tester, X-ray florescence (XRF), and Dynamic mechanical analyser (DMA).

Key words: Basalt fibre, IR laser (CO_2 laser), Carbon matrix, Electrical conductivity

Table of Contents

LIST OF TABLES

1. INTRODUCTION

The growing use of composite materials for non-structural and structural applications demands the development of products which are able to fulfil both technical and strict environmental requirements. At the present time, the typical reinforcements of composite materials are glass, carbon and aramid fibres (or a combination). Due to environmental concerns, natural fibres have been gaining a considerable attention during the last years. Despite the advantages of natural fibres over traditional ones (low cost, low density, acceptable specific strength properties, reduced tool wear and biodegradability), they suffer from several drawbacks, such as their hydrophilic nature (which affects the compatibility with hydrophobic polymeric matrix), the scattering in mechanical properties and the low processing temperature required. As a consequence, new reinforcement materials are currently under investigation.

Mineral fibres from basalt are not new, but their suitability as reinforcement in polymer composites is a relatively new issue. These emerging mineral fibres are natural, safe and easy to process also at the recycling stage. They also show high modulus, excellent heat resistance, heat and sound insulating properties, good resistance to chemical attack and low water absorption [1].

For these reasons, basalt fibres are wildly applied to many fields, such as corrosion resistance material in the chemical industry, wear and friction stuff in the auto-mobile industry, target area of anti-low viscosity impact, and reinforcement in contraction. Apart from this, basalt fibres could be made into various products, such as mat, fabric, and strip. Therefore, the basalt fibre is now regarded as a new generation fibre with high performance and has received enormous attention in many countries lately [2].

Countries like Ukraine, Russia, USA and China have mastered continuous basalt filament production technology. Just like other materials, basalt fibres also have surface defects, which make the measured mechanical properties remarkably lower than their maximum theoretical values. As a reinforcing material, the basalt fibre's superficial performance immediately influences its composite materials' final performance.

Although lots of studies about this continuous textile fibre production technology have already been reported, the reports about fibre surface modification are few. The application possibilities of the BF are determined by their chemical and mechanical properties. The mechanical strength of basalt fibres is thought to be closely related to the presence of surface heterogeneities such as surface flaws, structure defects and impurities. Surface heterogeneities are expected to act as stress-concentrators facilitating the fracture development, and enhance water adsorption. The fibre surface modification technology has been listed as one of the four most useful technologies in the composite materials area. The fibre surface modification is implemented mainly using the plasma modification technology, the oxidized modification technology or the coating modification technology. Among these modification technologies, the coating modification technology does not change the fibre's main body structure. Simultaneously, the coatings' forms are varied and the coating structure could be designed freely. Furthermore, the coatings could heal the surface flaws in the range of a few of hundred nano-meters and prolong many traditional materials' lifetime. Therefore, the coating modification technology, especially the organic/inorganic hybrid coating technology, has drawn more and more attention. The hybrid coating technology is a newly developed technology and it can combine organic, bio and inorganic components in a single material. It has been proved that the sol–gel chemistry allows the combination of inorganic and organic or even bioactive component at a nano-sized level in a single hybrid composite [2].

However this study investigated the interrelations between basalt fibre/chemical resistance inter-facial properties. Furthermore the investigation is carried out by analysing the atomic elements composition of basalt fibre by Laser-Induced Breakdown Spectroscopy (LIBS). Most of this work is based on finishing methods using BF as reinforcement for carbon composite material. All the properties are investigated using different mechanical test methods, and electrical conductivity test methods.

LITERATURE REVIEW

2. THEORETICAL PART

2.1 Basalt

Basalt originates from volcanic magma and flood volcanoes, a very hot fluid or semifluid material under the earth's crust, solidified in the open air. Basalt is a common term used for a variety of volcanic rocks, which are grey, dark in colour, formed from the molten lava after solidification. When magma reaches the surface it cools down and can be mined as a raw material. This volcanic rock contains in addition to its main components silicon and oxygen plus other valuable elements such as calcium, magnesium, iron, sodium, potassium, aluminium and titanium [3].

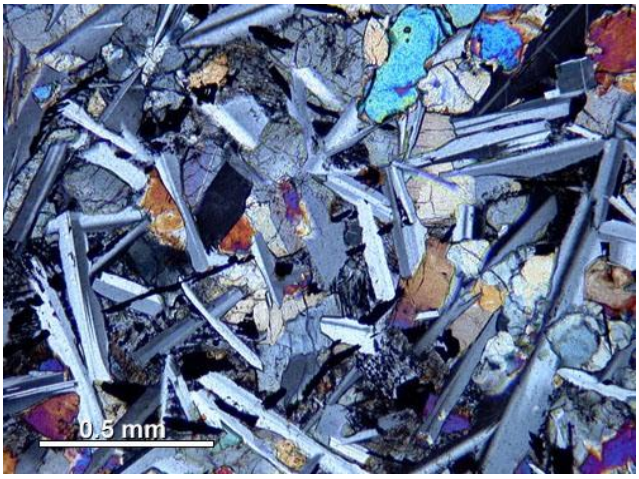

(*Fig. 1) A thin section, of a typical pertrographic basalt micrograph, viewed in polarized light. The gray mineral is plagioclase, bluish green to blue grains near the top are olivine, and the remainder is mostly high-Ca pyroxene [4]*.

Basaltic rocks are melted approximately in the range 1400 – 1600 ^{o}C. Glass like nearly amorphous solid is result of quickly quenched melt. Slow cooling leads to more or less complete crystallization, to an assembly of minerals. Most basalt consist predominantly of the normative minerals - Olivine, Clinopyroxene, Plagioclase, and Quartz or Nepheline (figure 2) [5].Two essential minerals plagioclase and pyroxene make up perhaps 80% of many types of basalt and the rest could be Oliven [6], (see Figure 1).

2.1.1 Basalt Mineral contents

Plagioclase – Na & Ca silicates ($Na4Si_xO_y$, $CaSi_xO_y$)

Clinopyroxene – Silicates + metal oxides (Mg, Fe, Ca)

Olivine – $(Mg, Fe)_2SiO_4$

[7]

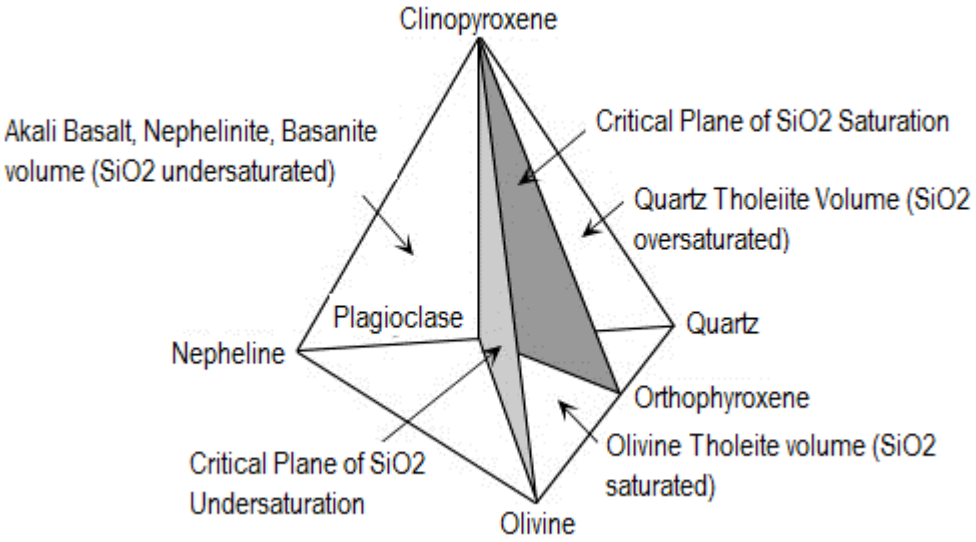

(Figure. 2) Basalt tetrahedron system of Ol-Ne-Cpx-Qtz

These minerals are in the 4 component normative system Ol-Ne-Cpx-Qtz, shown here as a tetrahedron. In the tetrahedron, plagioclase plots between Ne and Qtz, and Opx plots between Ol and Qtz. The basalt tetrahedron can be divided into three compositional volumes, separated by planes.

- The plane Cpx-Plag-Opx is the critical plane of silica saturation. Basalts that plot in this volume are called ***Quartz Tholeiites***.
- The plane Ol - Plag - Cpx is the critical plane of silica undersaturation (***Olivine Tholeiites***).
- Normative compositions that contain no Qtz or Opx, but contain Ne are silica undersaturated (the volume Ne-Plag-Cpx-Ol). Alkali Basalts, Basanites, Nephelinites, and other silica undersaturated compositions lie in the silica undersaturated volume [5].

When looking at the chemical composition of basalt rocks, the silicon oxide dominates, Al_2O_3 is next in abundance and CaO, MgO and FeO are closely similar. Other oxides are almost always below 5% level [6].

Table 1: Chemical composition of Basalt fibre forming rocks

	Basalt Vestany	**Basalt standard**
SiO2	51,56	13,5 – 47
Al_2O_3	18,24	11 – 18
CaO	1,3	10 – 15
MgO	0,00	8 - 11
B_2O_3	6,36	0,00
Na_2O	4,5	2 – 3,5
K_2O	1,23	1- 2
TiO_2	1,02	2 – 3,5
Fe_2O_3	2,14	4 -7
FeO	0,28	5 – 8
MnO	0,28	0,2 -0,3
H_2O	0,46	0,00
P_2O_5	0,26	0,00

Basalt can be classified into three groups, according to its content of SiO_2 as follows

1. Alkaline basalt with the contents of SiO2 below 42%;
2. Slightly acidic basalt with the contents of SiO2 from 43 to 46%,
3. Acid basalt with the content of SiO2 over 46%. [6]

2.1.2 Brief History about basalt fibre

Paul Dhé from Paris, France, was the first with the idea to extrude fibres from basalt. He was granted a U.S. patent in 1923. Around 1960, both the U.S. and the former Soviet Union (USSR) began to investigate basalt fibre applications, particularly in military hardware, such as missiles.

In the north-western U.S., where large basalt formations are concentrated, Prof. R.V. Subramanian of Washington State University (Pullman, Wash.) conducted research that

correlated the chemical composition of basalt with the conditions for extrudability and physio-chemical characteristics of the resulting fibre. The research in Eastern Europe, which had been carried out in the 1950s by independent groups in Moscow, Prague and other locales, was nationalized by the USSR's Defence Ministry and concentrated in Kyiv, Ukraine, where technology was subsequently developed in closed institutes and factories. After the breakup of the Soviet Union in 1991, the results of Soviet research were declassified and made available for civilian applications.

Today, basalt fibre research, production and most marketing efforts are based in countries once aligned with the Soviet bloc. Companies currently involved in production and marketing include Kamenny Vek (Dubna, Russia), Technobasalt (Kyiv, Ukraine), Hengdian Group Shanghai Russia & Gold Basalt Fibre Co. (Shanghai, China), and OJSC Research Institute Glassplastics and Fiber (Bucha, Ukraine). Basaltex, a division of Masureel Holding (Wevelgem, Belgium), Sudaglass Fiber Technology Inc. (Houston, Texas) and Incotelogy Limited, convert basalt fiber into woven and nonwoven reinforcement forms for the European and North American markets, respectively [8].

2.1.3 Manufacturing of basalt fibre

The technology process of basalt fibre manufacturing is based on the following major steps:

- Basalt rock pre-treatment.
- Melt furnace processing for continuous fibres.
- Processing for continuous threads.
- Downstream processing for fabric (cloth) and other applications to specific end-uses [9]

The manufacturing of the fibres materials, based on mineral, vitreous, kaolin and other fibres is widely known and intensively developed in the world [9]. Basalt fibres are continuously extruded from high temperature melt of selected basalt stones as a raw material [5]. This rocks are first pulverised (crushed) to particles of 8 - 10 cm for traditional furnace and 0.6 - 0.8 cm for the microwave oven, and then fed into a furnace [6;9]. When raw material comes into the plant, it is preheated in the oblong loading

without contact to existing melt. As these crushed basalt rock particles enters the furnace, the material is liquefied at a temperature of 1500°C/2732°F [2]. After reaching the wanted quality the melt is flowing from the bath to the production part and then goes through the spherical gauze filter with wanted temperature and viscosity .The melt is now in the fibre forming zone with spinneret plate on its bottom (figure 3). All melting basin is closed hermetically to atmosphere. The melting bath and the spherical production vessel have a special computer relation between depth and sphere diameter of both of them [3]. In addition, the basalt fibre does not contain any other additives in a single production process, which makes them have an additional advantage in cost [10].

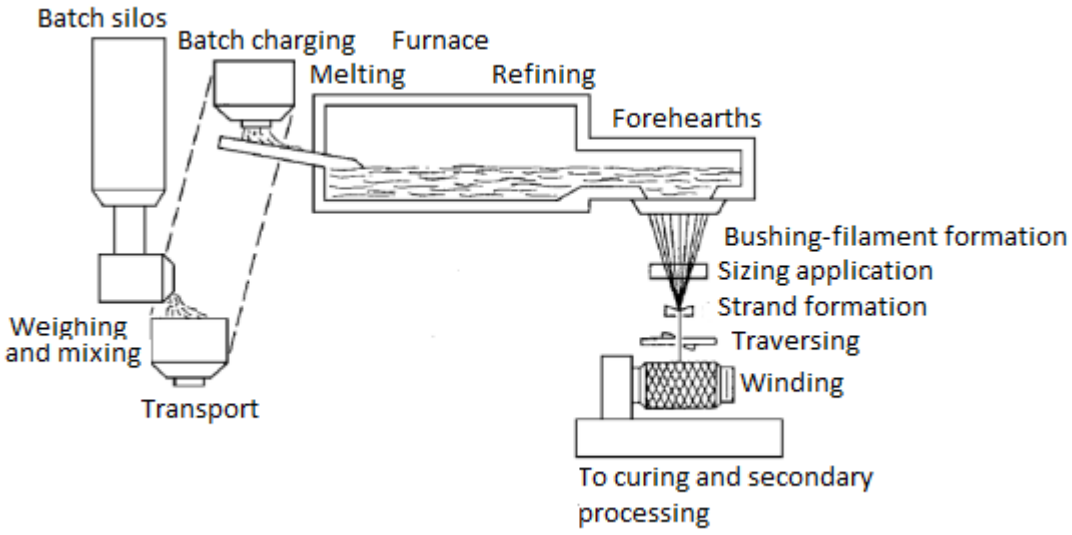

Figure 3: An illustration of a direct melt process for basalt continuous filaments production [11]

The continuous fibres produced from pure basalt igneous rock has some problems during manufacturing process. Typical samples of basalt rock with different deposits contain about 2-3% of ferric oxide and 11-13% of ferrous oxide, i. e. approximately the same ratio. The big iron oxide content of basalt stone, painting a melt dark colour, increase homogenization period, crystallization temperature and make viscosity curve much more abrupt in comparison with aggregated glass compositions [3].

In order to produce fibres the acid basalt are used. Basalt rocks suitable for the preparation of

Fibres must meet the following requirements:

(i) SiO_2 content around 46% and constant chemical composition;
(ii) The ability to melt without solid residues;
(iii) The optimal viscosity of the melted basalt;
(iv) The ability of the cooling without significant crystallization.

The basic criterion for the selection of technology suitable for the manufacture of basalt fibre

is the *acidity coefficient* M_k defined by

$$M_k = (SiO_2 + Al_2O_3) / (CaO + MgO) \quad [6]$$

M_k value must be within the range from 1.1 to 3.0. The ideal technological conditions for production of fibres are at M_k = 1.65. Basaltic rocks suitability for the manufacture of fibre is connected not only with chemical and mineralogical composition, but also with the texture of rocks [6].

2.2 Basic properties of Basalt fibre

As known basalt fibres has high tensile strength then E-glass and their strain to failure is larger than carbon fibre [12]. The tensile strength of virgin basalt fibres varies in the range of 2– 4 GPa, depending on drawing conditions [3].

2.2.1 Some basalt technical advantages are:

- High chemical resistance, (especially to concentrated acids based materials).
- High thermal resistance (thermo stability) and low flammability.
- Low strength degradation at temperatures as low as – 200…250 deg. C and as high as +700…900 deg. C., and of high humidity.
- High thermal and acoustic insulation properties.
- Excellent adhesion to polymer resins and rubbers.

- Relatively high mechanical strength, abrasion resistance and elasticity.
- High dielectric properties.
- Low water absorption.
- Ecologically clean and non-toxic. [9]

Table 2: Typical basalt fibre properties

Characteristics	Standard	Unit	Specification
Material	-	-	Volcanic rock
Roving density	-	tex	50 - 4800
Mono-filament diameter	DIN 53811	µm	10 – 30
colour	-	-	Gold brown
Odor	-	-	No smell
density	EN 1097-6	g/cm^3	2,8
Typical mechanical properties with epoxy-resin-system			
ILSS	-	MPa	80
Compressive strength	-	MPa	1300
Tensile strength	-	MPa	1700
Flexural strength	-	MPa	2000
Type of sizing	-	-	Silane-based sizing for plastics
Sizing content	DIN ISO 1887	%	0,1 - 1
Resin compatibility			Special sizing assures usability of Epoxy, MAH-pp reinforcement
Moisture content	ISO 3344:1997	%	< 0,2
Flow point	DIN 51730	^oC	1280 - 1310
Half sphere point	DIN 51730	^oC	Approx. 1160
Softening point	DIN 51730	^oC	Approx. 1115
Application temperature	-	^oC	-260 to approx. 650 (at 300oC/ 2h: 6% loss of strength
Electronical conditivity	-	Ω	$4,5 \times 10^9$
Bobbin type	-	Mm	Cylindical bobbin for external and internal unwinding
Optimal treatment	-	^oC	Approx. 22 (at 60% relative moisture)

[12]

2.2.2 Comparison of basalt and E-glass fibre properties

Table 3: Typical basalt vs. glass fibre properties

No.	Characteristic	Basalt fiber	Glass fibre
1.	Fibre diameter, micron	9	9
2.	Specific gravity, g/ccm	2.65	2.54
3.	Operative temperature, C	-200 … +900	-60 … +500
4.	Sintering temperature, C	+1050	+600
5.	Hygroscopic, %	0.5…1.0	5.0…20.0
6.	Moisture regain, %	1.0	2.7
7.	Coefficient of filtering	0.7…0.9	-
8.	Chemical resistance:		
	To 0,5N NaOH	73…99%	50%
	To 2.0N NaOH	48…92%	-
	To 2.0N HCl	35…75% and 90…92% after crystallization	1.2%
9.	Sound proofing for 400…1800 Hz	80…95%	-

These technical futures and apparent superior cost-effective position make basalt fibre suitable material to fill in the gap between fibre glass and more resistant but much more expensive fibres, like ceramic, carbon, etc [9].

3. LIBS ANALYSIS

The first experiments using Laser-Induced Breakdown Spectroscopy (LIBS) were done by Brech and Cross, more than 45 years ago. LIBS experiences a lively renaissance as analytical method for elemental analysis in several areas of industrial and environmental monitoring and screening [13]. LIBS can be used on geological samples for quantification of major elemental abundances, e.g. Al, Ca, Fe, K, Mg, Mn, Na, Si, and Ti. These elements (with oxygen) typically account for >99% of the mass of the sample [14].

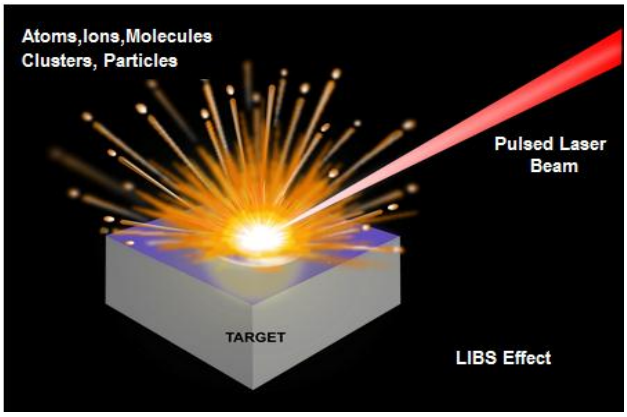

Fig,4: Laser Ablation: The removal of a small quantity of mass from a sample's surface using a focused, pulsed laser beam [15]

The most significant, representative and recent applications of LIBS described in the literature are analysis of alloys (molten samples, samples under water, detection of defects, surface analysis, analysis of light elements, fully automated systems with auto-samplers an so on), archaeological materials and art objects (low invasive analysis, possibility to perform in-situ measurements, high spatial discrimination, rapidity and capability for direct analysis without sample pre-treatment, connection of analytical and cleaning process), pharmaceutical products (fast multi-elemental analysis), aerosols (mobile systems for direct analysis of automatically acquired aerosol filter samples), military, homeland security and forensic samples [14] LIBS requires little or no sample preparation and can provide simultaneous multi-element analysis. Typically, these applications occur under standard Earth atmospheric conditions. However, interest in

LIBS under other atmospheric conditions has been a growing area of study both for fundamental knowledge and challenging applications [16].

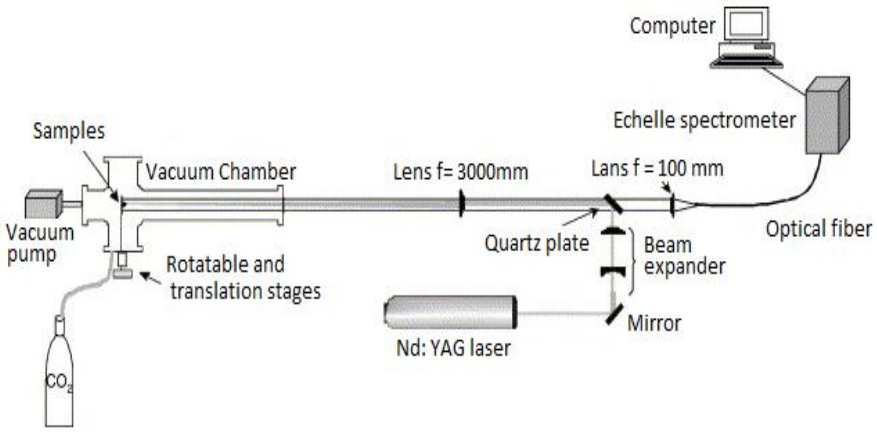

Figure 5: Typical apparatus for a pressure and gas composition LIBS studies. [16]

In LIBS, a high power laser pulse is focused on a small spot of the sample which ablates the surface layer, and successively heats and ionises the vaporised matter, producing the plasma. The spectral emission, which occurs as a result of the subsequent relaxation of constituent excited species, is measured by an appropriate spectrometer. LIBS method is also useful for the analyses of many elements in textile structure and especially in metal oxides of Al, Ca, Fe, K, Mg, Mn, Na, Si and Ti found in basalt fibres which are important from practical point of view. [17]. All these combination of metal oxide molecules gives basalt fibres its unique chemical and machenical properties. The chemical elements analysis of basalt fibres in this regard is realised by LIBS spectrometer.

4. CORROSION RESISTANCE OF BASALT FIBRES

High performance filaments are frequently used as the reinforcement of the composites, such as carbon fibres, glass fibres and ceramic fibres. Fibres in the composites are known to confer strength and rigidity to the weak matrix. Most of the external load is undertaken by the reinforcement filaments when the materials are in service. Chemical corrosion on the composites is unavoidable in some applications. For example, some containers, vessels, tubes, off-shore platforms, and equipment's in marine applications, may be corroded after long-term service in an alkali environment like seawater. It is believed that one of the obstacles preventing the extensive use of composites is the lack of long-term durability and performance data when servicing in critical environments. Consequently, it is necessary to understand how the materials behave during long-term applications. Most of the previous studies on the degradation of the reinforcement fibres in chemical environments are focused on the fabricated materials in which the fibres are covered by the matrix. The resistance of the filament to corrosion is mainly dependant on the resin's corrosion resistance, and the corrosion crack propagation is also related to the resin toughness. The lack of complete understanding of the basic mechanisms of damage and degradation of the fibre is obvious. [6]. Acid penetration to composites occurs from external surfaces of samples. In applications such as composite pipes, acid is in contact with composites just from one side. When PH of a corrosive acidic medium changes, the acid power also changes and automatically affects the stress corrosion behaviour of samples. Therefore, PH of a corrosive medium is one of the important parameters in stress corrosion tests. In long-term stress corrosion tests, constant PH value is preferred. Also, for the case of flowing corrosive fluids in composite pipes, constant PH value is essential. While for corrosive fluid storage tanks, it is not necessary to fix the PH value of the corrosive medium [18].

The composition of the basalt fibre is more complex than that of the glass fibre. Especially, there is Fe element existing in the former with mainly Fe^{2+}. .During immersion in seawater, H_2O, O_2, CO_2 molecules and Cl^-, Na^+ ions can penetrate into the matrix (including the resin and the interface) through channels and/or voids and react with the resin and/or fibre. At the same time, there are some components leached out from the fibre, including Ca, Mg, Al, and K and so on. These leached elements may form

a hydrated layer at the interface. As a result, the microstructure of the composite is changed and the cracks are consequently formed, leading to the sporadic breaking of fibres in the mechanical test. This implies that the bonding effect of the matrix on the fibres has been greatly reduced. Also the leaching of network modifying elements plays a minor role in the mechanical property deterioration. The degradation mechanism originates from chemical reactions involving Cl^- and Fe^{2+}. This can be seen by the colour when the basalt fibre is immersed in sea water after treatment, since iron (II) chloride is known to be yellow. The chemical reactions involved are described as follows:

$$Fe^{2+} + Cl^- = [FeCl\ complex]^- \quad (2)$$

$$[FeCl\ complex]^- + OH = Fe(OH)_2 + Cl^- \quad (3)$$

$$Fe(OH)_2 + O_2 + H_2O + Fe(OH)_3 = Fe_2O_3 + nH_2O \quad (4)$$

There into, reaction (2) occurs under the condition of $Cl^-/OH^- > 0,6$
Until the reaction product can be detected, the whole reaction process above may take a long time [19].
It is unclear whether the iron element in the structure plays a role of the framework former. The following views have been established: in the basalt fibre structure, the Fe^{3+} ion content is much less than the Fe^{2+} ion one in the basalt fibres. The existence of Fe^{3+} in basalt fibres is helpful to its high temperature-resistance property. The Fe^{2+} ions are in the octahedral coordination and the Fe^{3+} ions are also in the octahedral coordination. Some conditions the Fe3+ ions (half of the Fe^{3+} in the Fe_3O_4 structure) are in the tetrahedron coordination meaning that some cases the Fe3+ ions may form alumina-silica-oxygen frameworks [6, 20].

In this study the degradation rate of basalt filaments in hydrochloride acid HCl and sodium NaOH hydroxides is investigated. Where by the increasing of pH in acid solution after degradation is expected to be accordance with assumption that HCl reacts with cations and destroying the glass like network. The chloride salts replace the intermediate oxides as MnO_2, Fe_2O_3 and Al_2O_3. These salts are typically well soluble in water and these phenomena supported the basalt degradation due to action of acid. It is known that alkali attacks the silica network directly.

The hydroxyl ion of the alkali breaks the Si-O-Si linkage. The presence of intermediate oxides like MnO_2, Fe_2O_3 and Al_2O_3 always improve the alkaline durability. Degradation in alkaline solutions is relatively small [6].

5. LASER MODIFICATION OF FIBRES

Chemical treatment methods are most often used in the present for textile material surface modification; however, these methods are frequently "environmentally unfriendly". So, new technologies are now considered, especially in physical treatment methods. This is the case of laser technologies, like CO_2 laser radiation. Morphological modifications can be produced on the surface of any material, resulting in changes in the physical and chemical properties of the materials [21].

CO_2 lasers have average powers up to tens of kilowatts. This gas laser uses electric discharge for exciting of atoms. Energy is transferred from the discharge to the atoms by the form of collisions. The CO_2 laser ranges between 9.3 – 11.5μm wavelengths. This range of wavelength is in the invisible, infra-red (IR) part of the electromagnetic spectrum. This laser produces powers up to 100kW and pulsed energies of about 10kJ [22].

The CO_2 laser can be continuous wave or pulsed modes. It depends mainly on the required end product. Pulsed mode is more appropriate when heating is not desirable for specific application in textile treatment of textile, as compared to continuous wave mode. One of the advantages of carbon dioxide infrared lasers is their large beam size, high efficiency, easy operation, use nontoxic gases and low costs of the equipment. The application of this type of lasers is of little in textile or polymer treatment likely due to the effect of infrared radiation which imparts thermal damage to the surface of the treated polymers. CO_2 pulsed lasers can be considered to be non-contact and environmentally friendly treatment for surface modification of textiles [23].

The mixture of carbon dioxide, nitrogen and helium are filled through the discharge tube which has a cross section of 1.5 cm^2 and a length of 26 cm. Carbon dioxide, nitrogen and helium gases are filled through the proportion 1:4:5 respectively. Light and electricity are the excitation mechanisms of choice for most lasers. In case of carbon dioxide lasers, electric discharge is used. A high voltage electric discharge is ignited into this mixture. The CO_2 molecule is being broken down during this process to form oxygen and carbon

monoxide, thus small amount of vapour is added to the gas mixture for the regeneration of CO_2.

The lasing mechanism of CO_2 is highly characterized by the vibration levels, whereby nitrogen is playing an important role. 10% - 30% of nitrogen is excited by the high voltage discharge. Nitrogen is homonuclear molecule and therefore it cannot lose energy by photon emission. CO_2 molecule undergoes vibrational oscillations known as vibrational modes, namely, stretching mode, the bending mode and the asymmetric stretching mode.

The molecules can only absorb infrared radiation if the dipole moments of that molecule changed by vibrations. The homonuclear diatomic molecule of N_2 has no dipole moments, no matter how far the atoms are separated, thus it cannot be affected by infrared spectra. It can neither be affected by microwave spectra. All heteronuclear atoms (e.g. HCl and CO) and polyatomics (three or more atoms) absorb infrared radiation because they have dipole moments due to their vibrations. Thus CO_2 is the used molecule in gas laser due to its bending mode of vibration which makes the molecule nonlinear, and thus creating dipole moments.

Nitrogen and carbon dioxide absorb energy from the discharge tube. The excited nitrogen molecule transfer energy to the carbon dioxide molecule through collisions. This results in carbon dioxide molecule being excited into highest energy level. Energy is then transferred to the lower energy level and population inversion is achieved [22, 23,24].

Fig. 6, shows a typical apparatus. The laser beam (usually from a high power CO_2 laser) is directed via a system of optical elements for beam homogenization under inert gas onto the sample, which is mounted on a computer-controlled working table [23].

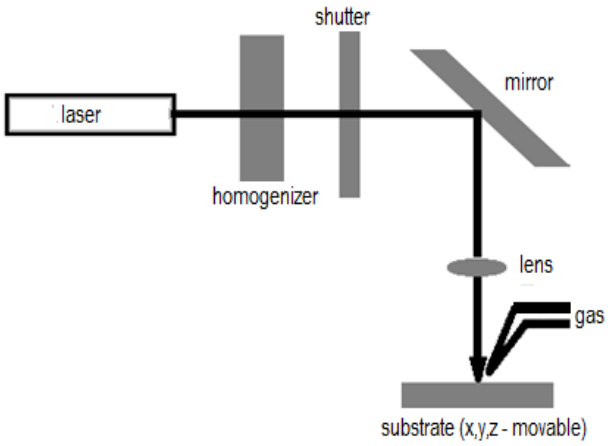

Figure 6: Set-up for industrial laser-heat treatment of materials

In order to start the phase transformation, the laser-induced increase in temperature has to overcome the transformation temperature, and also to be restricted to below the melting temperature.

If one stops the laser irradiation, cooling takes place with a cooling rate of usually more than 104 K/s. this results in a structure with a high internal stress and stable dislocations, i.e., a structure that is 'hard' and brittle compared with the initial structure. The depth of hardening depends on the rate of thermal carbon diffusion and thus the heating time. The hardness increases about 0,7% to 0,9% has been reached.[23].

Adequate power levels for a specific application are very important in surface modification processes because an excessive amount of energy can be supplied, with the consequent damage of the textile material. For instance, infrared lasers (CO_2) are the most powerful lasers and, with no suitable power level, severe thermal damage can result. However, this shortcoming can be overcome by the use of pulsed-mode CO_2 lasers, easier to control than lasers operating in continuous wave mode [21].

In this work, different experimental conditions were applied in CO_2 laser irradiation of basalt fibres, with the main purpose of choose the most appropriate values of the considered parameters.

6. POROUS CARBON MATERIALS

Porous carbon materials have attracted a lot of attention in these recent years, much of interest as they are potential candidates for large number of applications especially in catalytic supports, battery electrodes, capacitors, gas storage and biomedical engineering [25]. Such materials display a well-developed surface, large adsorption space created by homogeneous, relatively small mesopores with diameter 2-4 nm, and a certain amount of micropores; they hold interest, in particular, in regard to the preparation of efficient hydrogen absorbers and accumulators, the selective separation of hydrogen and methane from multicomponent gas mixtures, and the removal of impurities from such mixtures [26]. As porous carbons are mostly amorphous in nature, a little presence of sp2 carbon structures enhances the possibility of using these carbon materials for wider applications involving electrical conductivity. The porous carbon materials contain sp3 carbon fractions and a considerable sp2 carbon fractions depending upon the preparation conditions and the raw material used. The sp2 carbon sites in the carbon materials predominantly control the electronic and transport properties. The properties of carbon materials with poor crystallinity have not been explored in detail yet, despite these carbons available to application in much higher quantities than graphite. Even though the chemical applications of these materials have been investigated in recent years, the exploitation of materials for physical and nonchemical application for little perhaps nil. This material has very interesting micro structures consist of the following i) large density of the pores and defects, ii) dangling bonds particularly in the regions between the graphitic crystallites, iii) a large fractions of the carbons as surface atoms and iv) disordered crystallites. Because of these complexities it requires variety of experimental techniques to characterize both the surface and bulk properties [25].

There have been many recent advances in a field of chemistry known as “single-molecule” chemistry, whereas three-dimensional space is compartmentalized into small, usually nanometer-sized subunits or nanoreactors within molecular sieves. Molecular sieves are ordered, porous structures, with nanometer-scale pores, and include the naturally occurring zeolites. Because of their crystalline nature, pores of the same type are precisely the same size. Depending on the size of the pores, they can selectively adsorb or filter different molecules, thus functioning as molecular sieves [27,28].

6.1 Carbonization of sucrose

The most common way to produce amorphous porous carbons is the carbonisation of precursors of natural or synthetic origin, followed by activation. By this method, however, it is not possible to obtain carbon materials with a strictly controlled pore structure. New approaches have been proposed which are based on a replication technique starting from a silica material (mesoporous silica (MCM-48, SBA-15) used as porous solid template. The synthesis procedure consists of introducing a carbon precursor into the pores of the silica material and subsequent dissolution by chemical etching (HF) of the silica framework. A carbon material with a controlled porosity and which retained the initial silica morphology can then be obtained [28,29]. In a first step, the mesoporous silica "patrix" is filled with a carbon precursor either by impregnation with a carbon precursor such as sucrose, followed by carbonisation or by chemical vapour deposition. Once that the carbon structure is formed in the pores of the silica structure, the silica can be removed by dissolution in hydrofluoric acid or in diluted alkali hydroxides solution resulting in a mesoporous carbon replica ("matrix") of the silica patrix, where the pores correspond to the walls of the original silica structure and the carbon walls to the mesopores of the silica [30].

However, there still have not been sufficient systematic studies of the processes and products of the matrix carbonization of C-precursors in various carbon mesoporous molecular. One of the most important questions concerns the effect of the spatial organization and porous structure of the starting inorganic matrices, and nature of the carbon-containing precursors, occupancy of the matrix by the organic compound on the structure-related adsorption characteristics of the intermediate composites and final carbon products [26, 31].

Hence in this study the micro structure for which the electrical properties of basalt fibre reinforced materials based on porous carbon has been considered in our investigations. Basalt fibre based porous carbon composite material was prepared, which contains carbon fibre and sucrose carbonised matrix as components of the material. Sucrose assumed to act as carbon conductive binding matrix and a partial insulator. When sucrose (table sugar) is mixed with a concentrated sulfuric acid, soon an exothermic reaction takes places during which a carbonisation takes place and produces steam and sulphur dioxide. In the presence of concentrated sulphuric acid, sucrose is dehydrated to

produce carbon and water. The heat of the reaction vaporizes the water causing the carbon matrix to form.

$C_{12}H_{22}O_{11}$ (sugar) + H_2SO_4 (sulphuric acid) → 12 C (carbon) + 11 H_2O (water) + mixture water and acid. (5)

This aqueous sucrose carbon matrix has adequate binding ability which can be used to bind fibres in composite material with limited mechanical stability. The electrical conductivity properties of the composite are assumed to be due to carbon components of the material. Hence this study also focused on the assessment of electrical conductivity mechanism, due to the presence of carbon components in composite material.

6.2 Electrical conductivity of carbon materials

Carbon reinforced composite material are known for being brittle, with low tensile strength and low strain capacity that result in low resistance to cracking or totally breaking. To improve such properties, mixed fibre reinforced composite material has been developed. This new fibres are intended to improve tensile strength, flexural strength, toughness and impact strength, to change failure mode by means of improving post-cracking ductility, and to control cracking. Tensile strength of the composite, is related more to the stress at which matrix develops a macrocrack, will not differ much for most conventional fibre reinforced composite materials. The addition of carbon fibres can also have a strong effect on the electrical properties (DC conductivity and AC impedance) of the composite, but only when the added fibres are highly conductive compared to the matrix. Currently different kinds of fibres are used with different kinds of matrix. Conventional fibres such as steel and glass; new fibres such as carbon, Kevlar, basalt; and low modulus fibres, either man-made (polypropylene, nylon) or natural (e.g. cellulose). These types of fibres vary considerably in mechanical properties, effectiveness, cost and geometry[32].

Composite containing conductive fibres, such as steel and carbon, have many structural as well as non-structural applications. For example, electromagnetic interface shielding, electrostatic discharge, self-regulated heater, conductive floor panels and cathodic protection of reinforcing steel in concrete structures. Besides these, carbon fibre reinforced composites have been considered as intrinsically stress/strain sensor for

damage assessment. This is due to the effect of strain on the electrical resistivity. The resistivity in both stress direction and transverse direction increases upon tension, because of slight fibre pull-out that accompanies crack opening, and decreases upon compression, due to slight fibre push-in that accompanies crack closing [31,32]

The present study addresses the electrical resistivity of carbon and basalt fibre reinforced composite material with carbonised sucrose matrix. Firstly, the properties of carbon and basal fibres are explained. After that, resistivity measurements techniques will are discussed. Usually, the effect of conductive fibres is explained with reference to the percolation threshold of the fibres, so this topic will also be mentioned briefly. Finally, damage detection, which is one application of carbon fibre reinforced composites, is reviewed.

6.3 CARBON FIBERS

Carbon fibres are inert in aggressive environments, abrasion-resistant and stable at high temperatures, medically safe, as strong as steel fibres and more chemically stable than glass fibres in alkaline environments. Moreover, carbon fibres are low in density, especially when compared to steel fibres, and their strength to density ratio is one of the highest among all fibre types. The main drawback of carbon fibres has been their high cost - and low cost is essential for most applications concerning composites material. Carbon fibres possess an additional advantage of having a high electrical conductivity. The presence of carbon fibres greatly increases the electrical conductivity of the composite. The two main processes for making carbon fibres are based on different starting materials; either PAN (polyacrylonitrite) carbon fibres or petroleum and coal tar pitch (pitch-based carbon 6 fibres). Both processes utilize heat treatments, and various grades of carbon fibres can be obtained with each, depending on the combination of heat treatment, stretching and oxidation.

In order to strengthen the matrix, the specific fibre spacing must be decreased to reduce the allowable flaw size. This may be achieved by using fine short discrete fibres, such as carbon fibres of approximately a few microns in diameter. These fibres can provide bridging of the microcracks before they reach the critical flaw size. Carbon reinforced

composites can be produced by hand lay-up of continuous fibres or mats, filament winding, spraying, and conventional mixing. The maximum carbon fibre content that can be incorporated in a matrix is based on the assumption that the diameter of the filament (≈ 10μm) is of the same order of magnitude as the amount of matrix used. For matrix to be able to penetrate between the individual filaments, the maximum fibre content is about 12% by volume for unidirectional orientation, and less than 4-5 % for random orientation. Different attempts to improve bond and to compensate for potentially poor dispersion have also been made, e.g. using filament winding [32].

The engineering properties of carbon fibre reinforced composites have been studied by many researchers. It has been noticed that a 3% (by volume) addition of high-modulus carbon fibre to the composite results in a two-fold increase in the modulus of elasticity and a five-fold increase in tensile strength over similar values for the unreinforced matrix . However, the compressive strength slightly decreases with increasing carbon fibre content or with increasing carbon fibre length, and this has been attributed to the increase in air void content as the fibre content increases.

6.4 RESISTIVITY AND CONDUCTIVITY

Electrical resistivity measurements on solids are often made by applying a known D.C. current, *I*, to two electrodes connected to the specimen made with the material under investigation. Then, the electrical resistance, R, is determined by measuring the resultant drop in the voltage across the specimen [31]. According to the definition of electrical conductivity of a specimen, electrical resistivity and conductivity can be calculated using the following equation, starting from the following well known Ohm's law [34, 35].

$$R = \frac{V}{I} \tag{6}$$

The resistivity of the material, ρ , which is a material constant, is defined as:

$$\rho = R\,\frac{b}{L} \tag{7}$$

Where *L* is the length of the specimen, and *b* is the specimen cross sectional area.

$$\sigma = \frac{1}{\rho} \quad (8)$$

Although D.C. current has been used for determining the electrical resistivity of composite, it is recognized that the true resistivity of composite materials may not be determined by a single measurement of V and *I* as in equation 6. This fact is due to polarization that occurs at the electrodes [31,32]

6.4.1 Polarization Effects

Generally, there are two basic types of electrical conduction in moist specimens: electronic and electrolytic. The former is through the motion of free electrons in the conductive phases, e.g. carbon or steel fibres, and the latter is through the motion of ions in the pore solution [34, 36]. Due to electrolytic conduction, chemical reactions take place at the electrodes and hydrogen and oxygen gases are liberated that deposit around the electrodes in the form of thin film, which eventually results in polarization effect [34]. The conductivity measurement, therefore, requires the elimination of the effect of electrolytic conduction. Three methods have been used: one way is to use completely dried specimens. Another method it is assumed that the polarization potential opposes the flow and manifests itself in the form of reduced current for a given applied voltage V

$$I = \frac{V - V_p}{R} \quad (9)$$

Where, V_P is the polarization potential. It follows that in this case at least two different values of the applied voltage should be used to determine the two unknowns VP and R. However, the best method is through using alternating currents. In this method the effect of polarization is considered by introducing a capacitor in series or parallel with the resistance, and equation 9 takes the form 10:

$$Z = \frac{V}{I} \quad (10)$$

Where Z is the system impedance in Ohms. Also, Z and R are related as:

$$Z = \frac{R}{\sqrt{(1-\omega^2 C^2 R^2)}} \quad (11)$$

and ω=2πf, where f is the applied frequency in cycle per second (Hz), and C is the capacitance

in farads. It can be seen that by increasing the frequency, we can reduce the effect of the capacitor. Usually impedance can be deduced by plotting R versus frequency, and the frequency in which the impedance gets constant can be calculated. From this frequency Z approaches R [32].

7. APPLICATIONS OF BASALT FIBRES

Basalt roving:

Applications: High pressure vessels, tanks & cylinders, pipes. Concentrate reinforcing bars, load bearing profiles and gratings, windmill blades, boats, automotive parts.

Basalt chopped strand:

Applications: - BMC parts for the automotive industry, friction materials, surface finishing for fire protection, fibre reinforced concrete

Basalt non-woven and roving fabrics:

Applications: - blade for wind power generators, boat hulls

Basalt yarns, woven fabrics and braided sleeves:

Application: - curtains for fire protection, heat and sound insulation, braided sleeves for tubes and electric insulation, ballistic protection

EXPERIMENTAL PART 1

8. OBJECTIVES

8.1 Qualitative analysis of Basalt fibre material by LIBS method

The first objective of this study was to qualitatively determine minor elements (e.g. Al, Ca, Fe, K, Mg, Mn, Si, or Ti) in basalt fibres sample. The sample was obtained from *Incotelogy Ltd (Germany).*

8.1.1 Materials and method

The LIBS spectrometer (LEA S500, Solar TII Ltd., Belarus) was used for this investigation. The instrument integrates a dual pulse Q-switched Nd:YAG laser, operating at 1064 nm. The laser emits two collinear pulses of about 10 ns duration with energy per pulse variable between 80– 150 mJ at maximum repetition rate of 20 Hz. The inter-pulse delay can be set from 0 to 20 ms. The spectrograph with focal length 500 mm and grating 1800 lines mm^{-1}. The wavelength range of the spectrograph was set to 385–413.995 nm (lower visible spectrum range). Recording of spectra was carried out by means of a back thinned and front illuminated CCD camera (2048 _ 14 pixels) with a minimal integration time of 1 ms to record the emissions of a single laser shot. The spectral emission results were then compared with the ones obtained from the NIST Atomic Spectra Database [35].

8.1.2 REULTS AND DISCUSSIONS

A quantitative analysis using LIBS, which produced a high power laser pulse was focused on a small spot of a basalt specimen, which ablated the surface layer, and successively heated and ionises the vaporised matter, producing the plasma. The spectral emission, occurred as a result of the subsequent relaxation of constituent excited species, it was measured by spectrometer (LEA S500, Solar TII Ltd., Belarus). The spectral emission results were generated as see on figure 7.

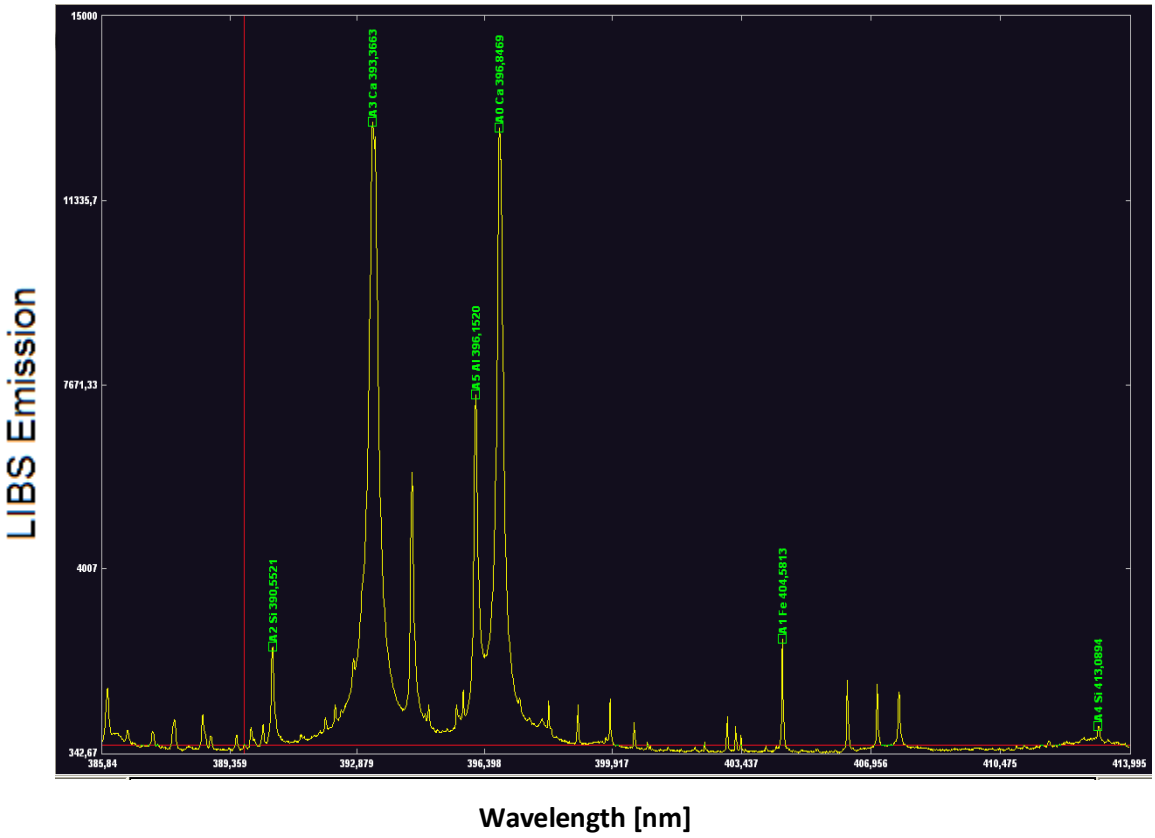

Figure 7: VIS (380-414nm), spectral emission of basalt fibre. Graphical spectral generated by LIBS spectrometer (LEA S500, Solar TII Ltd., Belarus).

Table 4: Wavelengths corresponding to several trace elements from LIBS emitted spectra, along with possible emissions and configurations taken from the NIST Atomic Spectra Database using their listed precision.

Element (s)	**Peak (nm)**	**NIST Database Possible Matches (nm)**	**Configurations**
Si	390.551	Si IV : 390.511	$2p^6 3p - 2p^6 7d$
	413.089	Si VII: 413.805	$2s2p^4(^4P)3s - 2s^2 2p^3(^2P°)4d$
Ca	393.663	Mg X 393.314	$1s^2 4p - 1s^2 5d$
	396.847	Ca IX: 395.024	3s3p -3s3d
Fe	404.581	Fe XV: 404.842	3s3d - 3p3d
Al	396.152	Al IX : 396.05 , 396.09	$2s2p^2 - 2p^3$

The qualitative analysis was based on results generated by LIBS (fig. 7) at lower visible spectral range (*VIS 380-414nm)*. These results reviled that tested specimen had Si, Ca, Fe and Al, by choosing the peak which best correlated with each trace element (Table 4). These wavelengths correlate with standard data obtained from NIST database which gave the wavelength and configurations associated with that particular element. E.g. Si wavelengths 390.511 and 413.805 nm corresponded with Si V : 390.511 and Si VII 413.805nm, which were associated with $2p^6 3p - 2p^6 7d$ and $2s2p^4(^4P)3s - 2s^2 2p^3(^2P°)4d$ configurations respectively. In others, there is no known emission line for that element in the nearby wavelength range (e.g. 393.314 nm). It is then apparent that the trace element is being hidden or captured by another element of similar size and charge or one having a higher ionic potential (cf. Goldschmidt's Rules of Substitution). This can be seen on figure 8 (magnified version of fig. 7), for example, in the case of Ca being visible over Mg, which is directly above it on the periodic table.

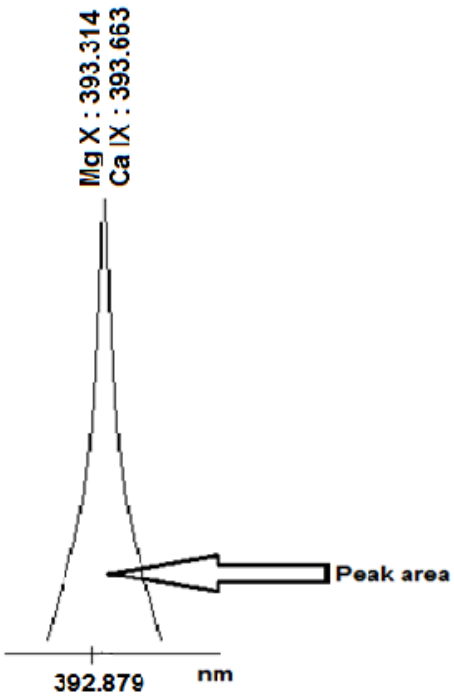

Fig.8: A spectral emission peak area of Mg X and Ca IX

Such substitutions are not unexpected in basalt fibre samples since they originated from mineral rocks. Form analysis of these experimental results it is noted that many lines do

not precisely correspond to those in the NIST database. The acquisition conditions of those reference spectra are likely very different from LIBS. These results thus highlight the need for careful studies of emission lines in both simple systems (pure elements, elemental oxides, binary compounds, etc.) especially when analysing fibres which originated from minerals rock sources. In order for a better qualitative analyses relating peak areas to element-specific emissions to be made in basalt fibre samples, there is a need to find multiple peaks unmistakeably associated with each element. This work shows that for many trace elements, useful lines corresponding to emission from minor elements do exist and may be used for qualitative identifications and even quantitative analysis. This study lays the foundation for and it a crucial step toward more detailed studies with more sophisticated analytical techniques which utilize more spectral information than a single peak area.

EXPERIMENTAL PART 2

9. OBJECTIVES

9.1 Basalt fibres chemical resistance

According to the previous studies done by other researchers, it was proven that the stability of Basalt in alkalis is generally very good. The chemical resistance of Basalt fibres in acids is comparatively small. Prolonged acids action leads to the full disintegration of fibres [3,6]. However these studies were done under high pH concentration and temperature, which is generally not the case in our surrounding environment, hence this part of the study depicts the possible and realistic environmental pH conditions into which basalt fibre material could be exposed. Therefore suggests are made from generalisation of possible solutions and precautions.

9.1.1 Materials and method

Chemical resistance of basalt fibre was investigated by treating its multifilament fibres with 2g/l solution of HCl and NaOH. Basalt fibres with a density of 2.75g.cm^3 and an average diameter of 13 µm were used. Small specimens (30) were cut and weighed to equal mass (g) (about 2g each). These samples were then divided into sets of three. All samples were washed with acetone for 24 hour and then washed again softly with running hot water before drying at 105^{o}C to remove all sizing agent. Each set of three desized basalt samples were then treated with HCl and NaOH (totalling to 15 samples per each chemical type treatment). The treating time ranged from 2, 4, 24, 48 and 72 hours and the experimental solution maintained at room temperature. After selected times the specimens were removed and rinsed gently three times with hot water, removing the residual chemicals. The specimens were dried again in an oven at 105^{o}C for 30min in order to totally remove moisture precisely. The weight losses of fibers after the treatment were examined using an electronic analytical balance with a precision of 0.001 g. The rest weight after degradation was recorded for evaluation.

9.1.2 Scanning electron microscopic test

The surface morphological changes of chemical treated basalt multifilament specimens were characterized by coating the samples with a gold–palladium alloy and studied with the Scan Electron Microscopy SEM (Vega©Tescan), operating at 30.0 kV. The samples were analysed at different magnifications (5000x).

9.2 RESULTS AND DISCUSSIONS

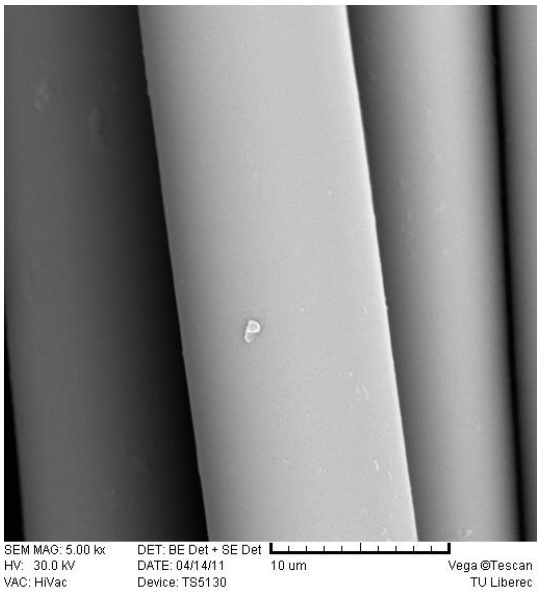

Fig 9:-SEM image, after 4hour in 2g/l HCl

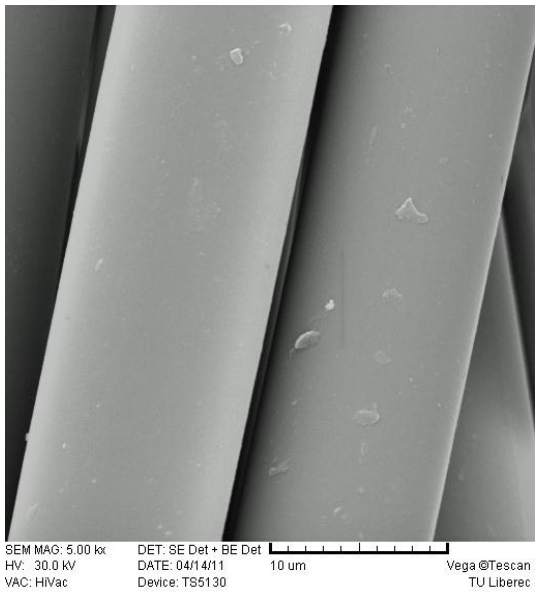

Fig. 10:-SEM image, after 72hour in 2g/lHCl

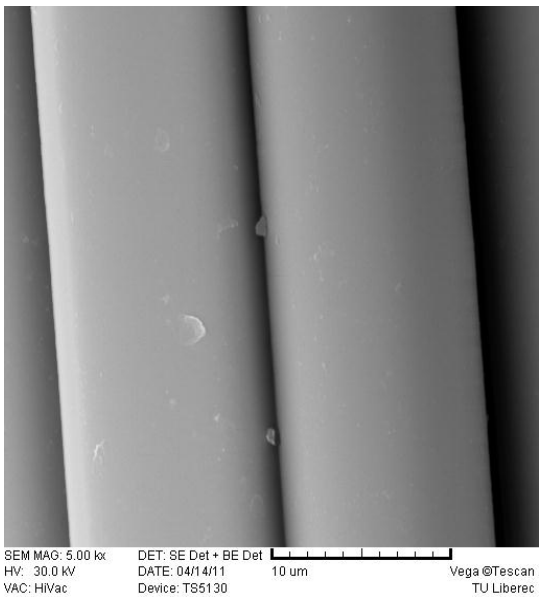

Fig. 11:-SEM image, after 4hour in 2g/l NaOH

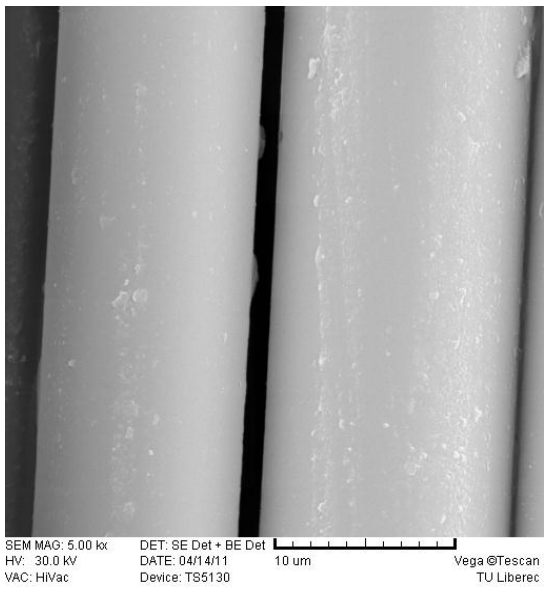

Fig. 12:-SEM image, after 4hour in 2g/l NaOH

The SEM results (fig. 9 to 10) show the degree and the effect of peeling off as a result of leaching out of elements from the surface of basalt fibre into the solution. These results were quantified as see in the table 5 and 6. Seemingly, there is little change in the surface morphology after 2g/l of HCl acid treatment for 4 to 72 hour, but it may be seen that there are local small flacks and cracks on the fibre with a size of about 1 to 2 micrometres. An almost similar effect could be seen on SEM images (figure 11 and 12), whereby there is little change in the surface morphology after 2g/l of NaOH alkali treatment for 4 to 72 hour, however it may be seen that there are also local smaller flacks on the fibre surfaces with a size of about 0,5 to 1 micrometres. This flakes peeling off effect directly result in the decrease of the relative volume and weight of fibre, which lead to a decrease in machenical strength of basalt fibres.

9.2.1 Chemical resistance

Assuming the initial weight of fibres is Mp [g] (Cleaned with Acetone); the mass of chemical treated state fibres is M_k [g].

$$R_z = \frac{M_k}{M_p}.100[\%] \tag{11}$$

For chemical resistance of basalt fibre it is necessary to compare the using the relative rate of degradation in various times as defined by relation.

$$K_p = \frac{M_p - M_k}{t_p \cdot M_p} = \frac{100 - R_z}{t_p}[\%.hour^{-1}] \tag{12}$$

Where, t_p is degradation time [hours]. Higher relative degradation rate corresponds to more severe action of degradation agents. The values R_Z and K_p for acid are in the table 5 and for alkalis in the table 6.

Table 5: Rest weights and relative degradation rates in 2g/l of HCl

Time [hours]	1/ t [hr-1]	R_z [%]	ΔRz %	1/ΔRz [per %]	K_p[% hours^{-1}]
0	0,000	100,00	0,00	0,000	0,000
2	0,500	99,89	0,11	9,091	0,055
4	0,250	99,85	0,15	6,667	0,037
24	0,0417	99,64	0,36	2,778	0,015
48	0,0208	99,50	0,50	2,000	0,010
72	0,0138	99,44	0,56	1,786	0,008

Table 6: Rest weights and relative degradation rates in 2g/l of NaOH

Time [hours]	1/ t [hr-1]	R_z [%]	ΔRz %	1/ΔRz [per %]	K_p[% hours^{-1}]
0	0,000	100,00	0.000	0.00	0,000
2	0,500	99,95	0.050	20.0	0,025
4	0,250	99,88	0.120	8.33	0,068
24	0,042	99,72	0.280	3.57	0,012
48	0,021	99,70	0.300	3.33	0,0062
72	0,0139	99,68	0.320	3.13	0,0044

9.2.2 Chemical resistance and degradation kinetics

During the degradation process the chemical solution attacks the surface and subsurface layers. An investigation of fibres weight after long-term chemical treatment has shown that the amount of solid fibre decrease to a significant degree level. This is a step by step removal of surface layers by peeling off mechanism. Therefore the reason of degradation can be associated with the reaction of chemical solution with some cations (in the case of acids) or anions (in the case of alkalis) from the surface of Basalt fibre. The kinetic model is therefore based on the assumption model by Cegarra-Puent equation 15.

The instantaneous rate of degradation is dependent on the difference between actual weight and weight in equilibrium as defined by Cegarra-Puent equation,

$$\frac{dM_t}{dt} = K \,.\frac{M_\infty^2 - M_t^2}{M_t} \tag{12}$$

Solving of the this equation by integration within the intervals limits t =t, $M_t = M_t$, the following equation results.

$$\ln\left(-\frac{M_t^2}{M_\infty^2}\right) = -kt \tag{13}$$

Which can also be rewritten in the form of:

$$\frac{M_t}{M_\infty} = \sqrt{(1 - e^{-kt})} \tag{14}$$

After introducing the change in rest weight the final relation is obtained.

$$\Delta R_z = \Delta R_\infty \,.\sqrt{[1 - e^{-kt}]} \tag{15}$$

where ΔR_∞ [%] is a rate of equilibrium rest weight, $(R_0\text{-}R_\infty) = \Delta R_\infty$ and K [%.hour^{-1}] is degradation rate constant.

$\Delta M_t = \Delta R_z$ - change in total weight of basalt at time t [%]

R_o = total weight of basalt at time t=0, (100% weight)

K = rate constant.

Parameter to be determined by graphical model were :

ΔR_∞, k

9.2.3 Hydrochloric acid aqueous solution treatment results

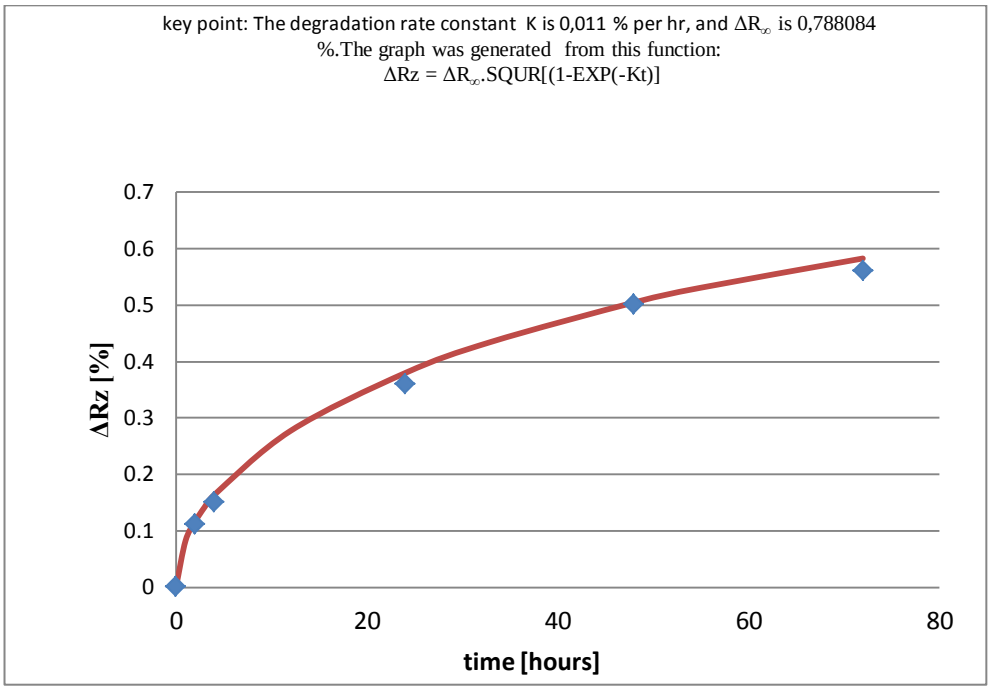

Fig. 13, Degradation Kinetics of basalt fibres in 2g/l HCl described by eqn. (15)

Fig. 12 shows the Δ mass loss ratio (ΔRz) as a function of treating time for basalt fibres treated with 2g/l of HCl. As seen, the Δ mass loss ratio (ΔRz) increases sharply before 4 h. After that, it rises slowly until 24 h and continuously and slowly until the maximum treating time (72 h) is reached. All other parameters characterizing weight loss for degradation in HCl are shown in the table 5. The parameters of degradation model ΔR = 0,788 [%] and K = 0,011 [%.hour^{-1}] were obtained by using an equation # 15 to generate the exponential model curve are shown in the Fig. 13.

It is very interesting to note that degradation is due to peeling and creation of small flacks on the fibre surface. After long-term exposure (72h) the flakes which even more vivid appeared.

The degradation is accompanied by the great loss of mechanical properties especially tensile strength. The increasing of pH acid solution after degradation is in accordance with assumption of reaction of HCl with cations and destroying the glass like network. The chloride salts replace the intermediate oxides as MnO_2, Fe_2O_3 and Al_2O_3. These salts

are typically well soluble in water and these phenomena supported the Basalt degradation due to action of acid [3, 6]

9.2.4 Sodium hydroxide aqueous solution treatment results

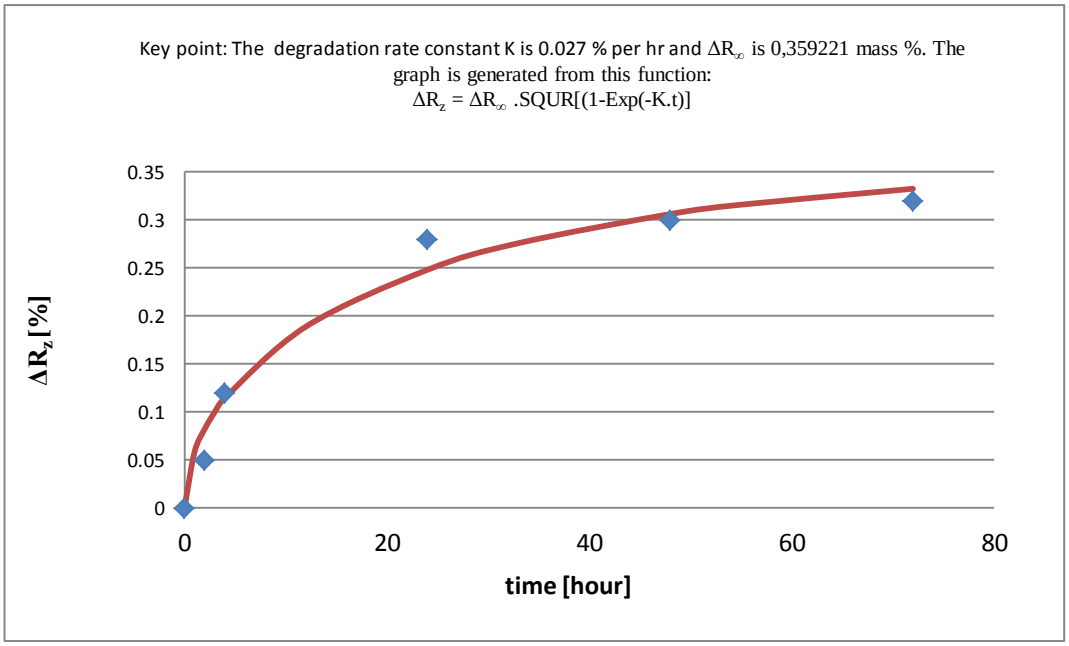

Fig. 14, Degradation Kinetics of basalt fibre in 2g/l NaOH described by eqn. (15)

Fig. 14 shows the Δ mass loss ratio (ΔRz) as a function of treating time for basalt fibers treated with 2g/l of NaOH. As seen, the Δ mass loss ratio (ΔRz) increases sharply before 4 h just like in the acidic solution. After that, it rises slowly until 24 h and continuously and slowly until the maximum treating time (72 h) is reached. All other parameters characterizing weight loss for degradation in HCl are shown in the table 6. The parameters of degradation model ΔR = 0,359 [%] and K = 0,027 [%.hour-1] were obtained by using an equation # 15 to generate the exponential model curve are shown in the Fig. 14. The corrosion in alkaline media is mainly controlled by the dissolving of the SiO_2-network, and not by diffusion like in acid media. The hydroxyl ions of the solution disrupt the siloxane bonds in the glass like network and, as a consequence, silicates migrate into solution:

$$[–Si–O–Si–] + OH^- \rightarrow [–Si–OH] + [–SiO]^-$$

Hence the strength of the fibres after treatment in alkali solution is decreased slowly. Their alkali corrosion resistance is relatively better as compared to acid corrosion resistance. This probably because the –Si–O–Si structure is inert to the acid except for hydrofluoric acid and phosphorous acid [6]. However the presence of intermediate oxides like MnO_2, Fe_2O_3 and Al_2O_3 should always improve the alkaline durability [3]

On the surface of basalt fibres, the formation of small brittle flakes like layers occurred after it was treated for 4 h in NaOH solution as see on SEM image 11 and 12 . These flakes were formed with a certain thickness around the filament and were partially peeled off in some areas. Therefore, it can be deduced that this phenomenon is typical for the treatment in NaOH solution. Water and NaOH reagents may penetrate into the flakes net structure of the fibre and cause some reactions to destroy the original structure. Meanwhile, some constituents inside the basalt fibre could migrate outside and dissolve in the solution. In addition, hydrolytic action may exist on the alkali silicate of the fibres.

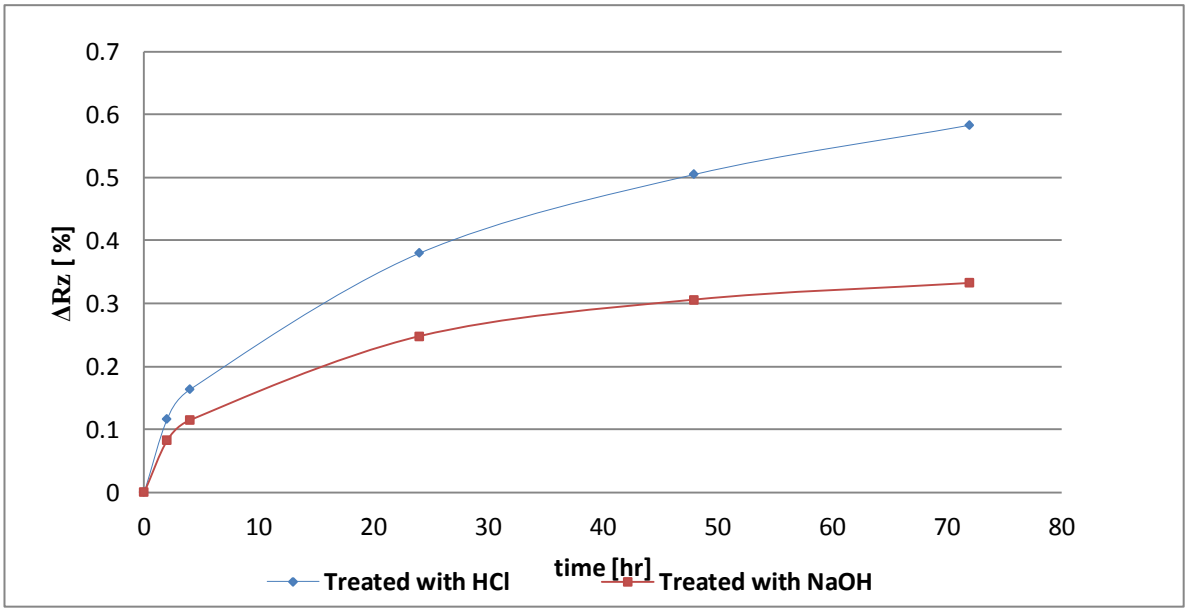

Fig. 15: The degradation rate of basalt fibre in 2g/l NaOH and 2g/l HCl, as described by eqn. (15)

In addition, the Δ mass loss ratio was found to be much lower for the basalt fibres treated with NaOH than that of basalt treated with HCl (~45% lower). As a result, the basalt fibres are much more resistant to acid corrosion as compared to the alkali corrosion.

EXPERIMENTAL PART 3

10. OBJECTIVES

10.1 Effects of IR laser treatment on basalt fibres

Infra-red (IR) laser is known to produces power of up to 100kW and pulsed energies of about 10kJ [22]. In most cases the application of IR radiation results in thermal damage to the surface of the treated materials. Depending on the objective of the user this phenomena can be considered good or bad, for instance if the user wants to change only the surface properties of the fibre and the fibre gets damaged by treatment with high IR energy laser, that effect could be considered as being negative. However, if the purpose is to cut the material to a particular shape or design, IR laser can be considered as a very useful and neat method. For such reasons we have performed some experiments to investigate the effects on basalt fibre.

10.1.1 Materials and methods

Irradiation was carried out on a 450g/m^2 basalt plain weave fabric using a commercial pulsed CO_2 laser (MARCATEX 150 FLEXI, EasyLaser), used for cutting and marking textiles. This laser provided a laser beam of frequency of 5 KHz and delivering a power of 100 W. The Pixel time [μs] – time used to mark each pixel of the image (in microseconds) was observed and recorded. Different experimental conditions concerning laser radiation were tested, in order to select the most adequate situation or situations to surface modification of basalt, with pulsed CO_2 laser, with visible thermal damage on the fabric. In all situations, irradiation was performed only in one side of the fabric and within a specific marked area.

10.1.2 Scanning electron microscopic analysis

The surface morphological changes on basalt fabric (450g/m^2 plain weave), were characterized by coating the specimens with a gold–palladium alloy and studied with the Scanning Electron Microscopy SEM (Vega©Tescan), operating at 30.0 kV. The samples were analysed at different magnifications (50x and 500x).

10.1.3 Mechanical properties testing

The tensile strength and elongation at break of laser treated basalt fibres were measured using the tensile tester (TIRA test 2300). The samples were cut into specific dimensions: 30x5cm^2. The test for mechanical properties was done on weft direction only. The distance between the two collets of the specimen was kept at 20cm and the crosshead speed was 100 mm/min. All the samples were maintained under an environment of relative humidity 65% and 25 ◦C for 24 hour before the test. The mechanical test was done on the non-irradiated specimens and likewise the irradiated samples, for comparisons to check the effect of laser treatment. The results of strength, modulus and elongation at break were recorded and the results were evaluated.

10.2 RESULTS AND DISCUSSIONS

10.2.1 CO_2 laser irradiation

The experimental data summarizing all experimental conditions investigated in CO_2 laser irradiation and observed results are given in Table 7and 8. The indicated parameters are directly related to commercial equipment and modification of those factors caused significant changes on experimental conditions and final results. D is a parameter related with applied power and represents the ratio between laser activation and inactivation time; the highest value of this parameter, 50%, corresponds to a maximum power. The frequency F was kept constant at 5 KHz, power radiation (P) was kept constant was well at 100W. The pixel time was the only parameter changing in this aspect. Therefore, observing pixel time values it was possible to search out for the best experimental conditions with this specific equipment, with significant thermal changes of the basalt fibre surface.

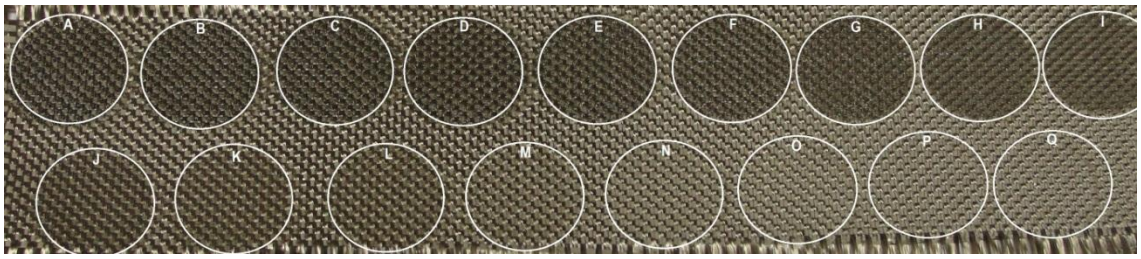

Figure 16: Marking points on basalt fabric irradiated with CO_2 laser

Table 7: Experimental conditions of CO_2 laser

Circle	Pixel time [µs]	D (duty cycle,%)	F (frequency, KHz)	Obs.
A	800	50	5	YES
B	755	50	5	YES
C	710	50	5	YES
D	665	50	5	YES
E	620	50	5	YES
F	575	50	5	YES
G	530	50	5	YES
H	485	50	5	YES
I	440	50	5	YES
J	395	50	5	YES
K	350	50	5	YES
L	305	50	5	YES
M	260	50	5	NO
N	215	50	5	NO
O	170	50	5	NO
P	125	50	5	NO
Q	80	50	5	NO

Note: YES- Visible thermal damage on the fibre, NO- without visible thermal changes on the fibre

Figure 16, shows 17 marked spots or points which were formed as a result of irradiation by laser from energy per pixel time of 80 to 800 µs. These results are also represented on table 7, where by visible thermal damage are labelled as „YES "and non-visible or without visible damage marked as „NO". For instance Circle „A" treated with at 800µs pixel time was marked as a „YES" and circle Q was marked as a „NO". From this information it was possible to deduce the energy intensity range settings to be used for the real testing experiment.

10.2.2 SEM results

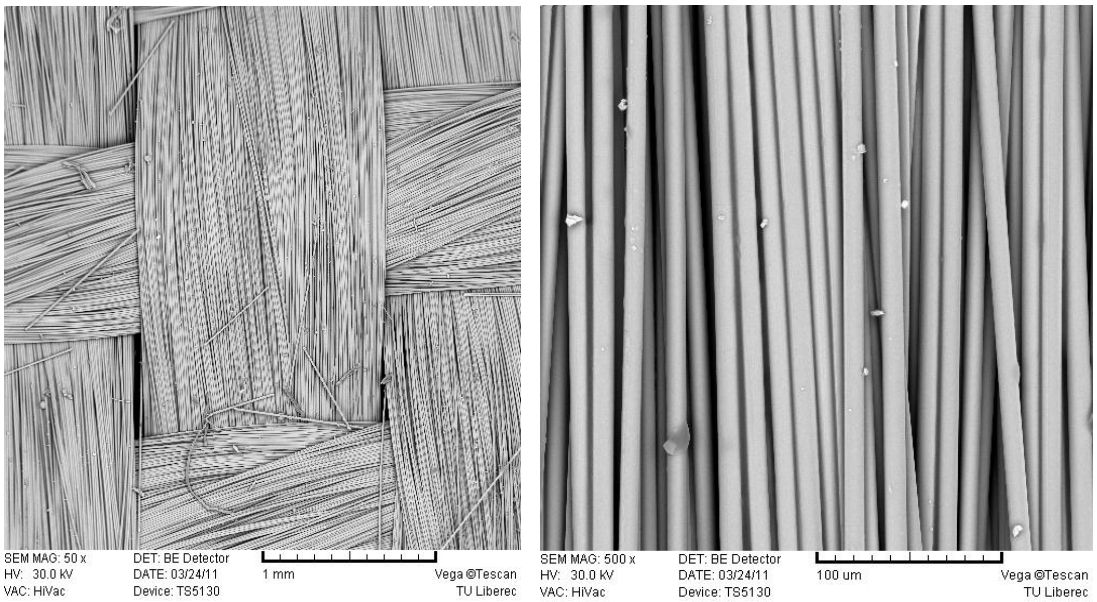

a **b**

figure 17: SEM image of a non-irradiated basalt specimen. (a) Magnification 50x and (b) 500x Mag.

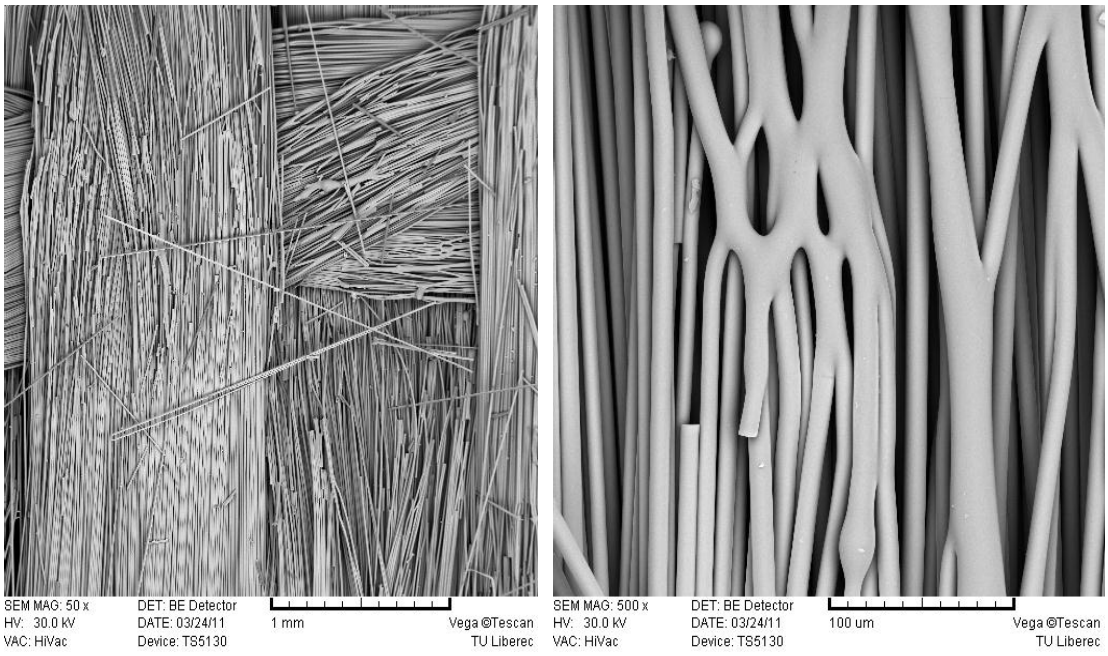

c **d**

Figure 18: SEM image of CO_2 laser irradiated basalt specimen at 260µs (Pixel time). (c) Magnification 50x and (d) 500x Mag.

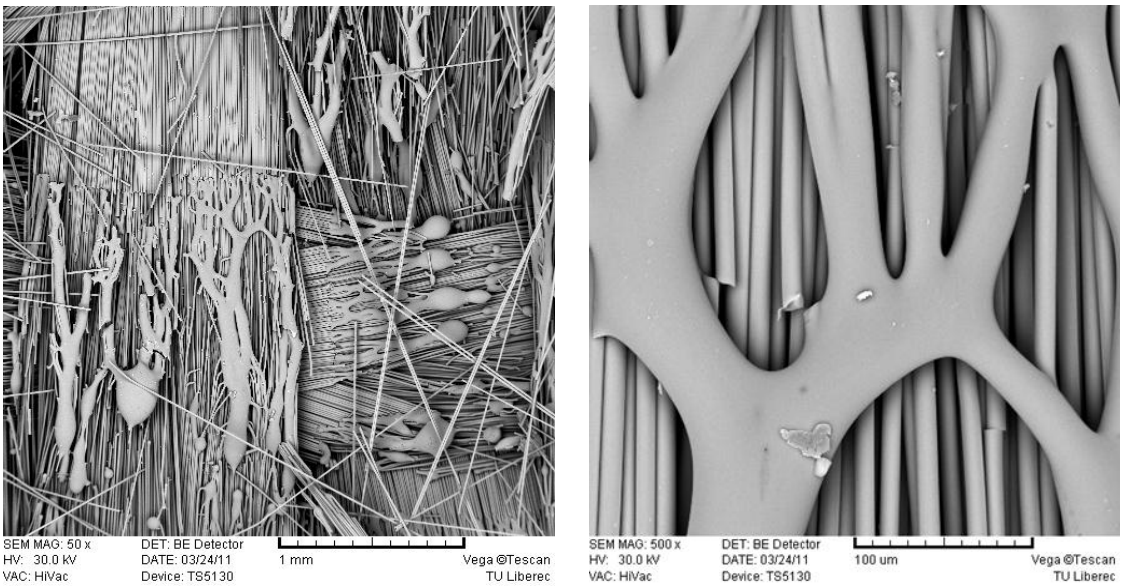

e f

Figure 19: SEM image of CO_2 laser irradiated basalt specimen at 620µs (Pixel time). (e) Magnification 50x and (f) 500x Mag.

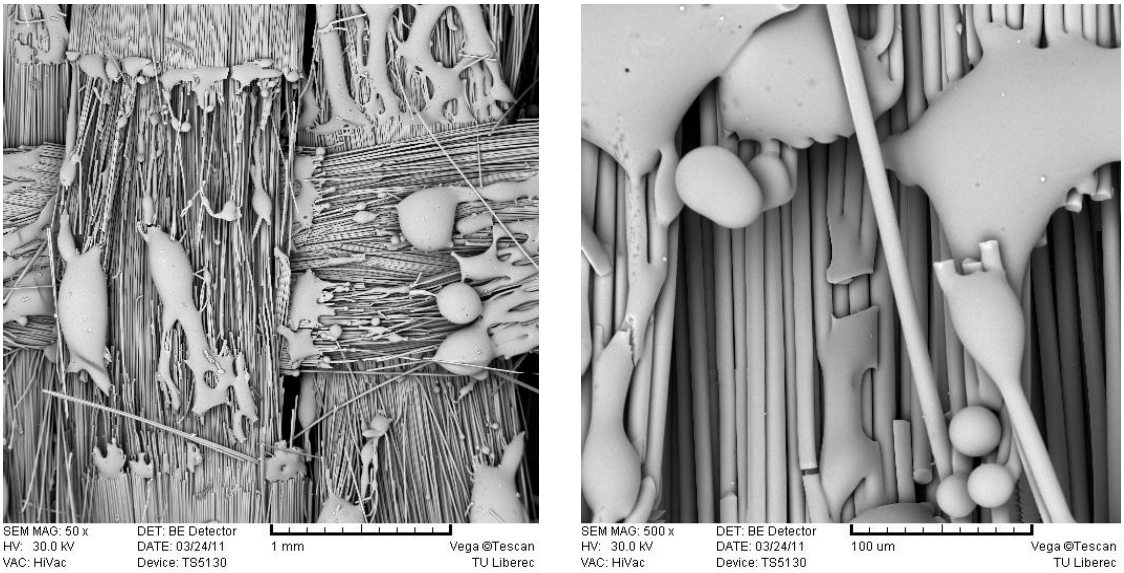

g h

Figure 20: SEM image of CO_2 laser irradiated basalt specimen 800µs (Pixel time) . (g) Magnification 50x and (h) 500x Mag.

Comparing untreated and treated material SEM images, a surface morphology modification can be observed after CO_2 laser irradiation, corresponding to irregularities on the surface. Swellings and certain roughness of basalt fibres, caused by the thermal effect of IR radiation are visible. In same marked spots visible damage was seen by naked eye however SEM revealed same damages to a certain degree. For instance circle „M“ at 260µs, there was no visible changes by naked eye, however SEM reviled that

there is a little swelling of fibre which took place there (Figure 18). SEM images also reviled that as more IR energy density was applied, more damaged occurred as a result (fig. 19 and 20). This effect not only creates damage but also some bonding spot were formed when the fibre melted (fig.19 SEM image f). This means that if the objective is to stabilise or bind the fibres by this method, there is a critical energy intensity level to be applied, beyond that energy density, the fibres could be damaged. The graph on fig 21 shows this energy intensity effect as relative to the damage area.

Table 8: The effect of energy density on a laser irradiated area of basalt fabric

Sample marking	Pixel time [µs]	Fibre damaged area [nm^2]	Fibre damaged area [%]
Untreated	0	0	0
M	260	73735	28.45102
I	440	119229	46.00511
E	620	131607	50.78122
A	800	183123	70.65893

Percentage (%) of fibre damage was calculated from a total area (259164.67 nm^2) , using Image J analysis prgram.

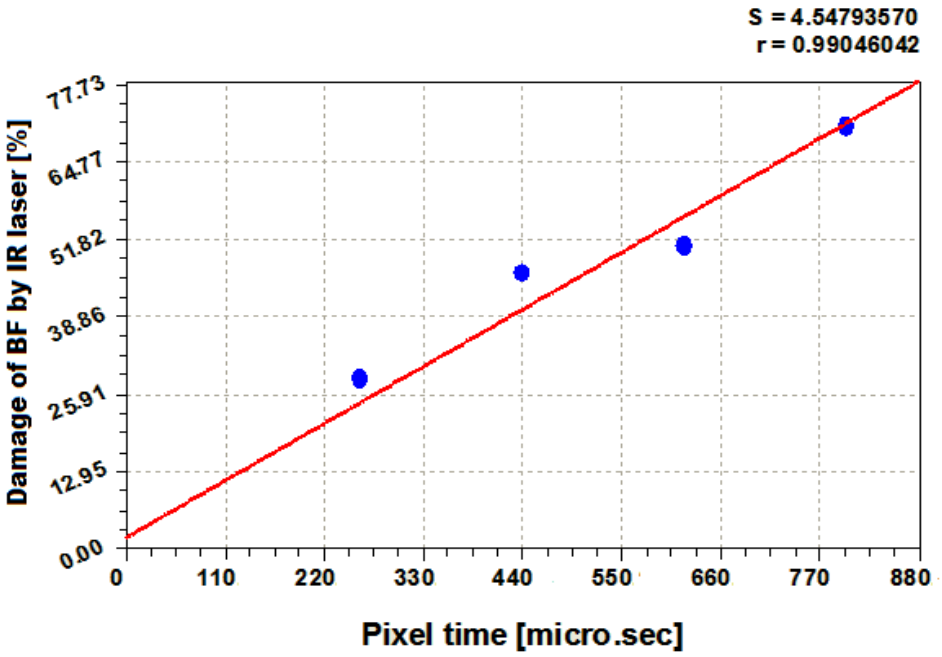

Figure 21: IR laser effects on basalt fibre

10.2.3 Laser Irradiation

To test for the machenical properties of the IR irradiated basalt samples the following experiment was conducted and the results recorded on table 8. The irradiated samples were varied according to different laser intensities. The irradiated area was 30x21 cm^2 and the settings were adjusted as per conditions prescribed by the above experiment.

Table 9. CO_2 laser irradiation BF treatment results

Pixel time [µs]	D (duty cycle,%)	F (frequency, KHz)	Marking time [s]	Marking time per area [s/cm^2]	Energy density [KJ/cm^2]	Obs.
800	50	5	121,484	192.8317	19.28317	YES
700	50	5	106,844	169.5937	16.95937	YES
600	50	5	92,187	146.3286	14.63286	YES
500	50	5	77,532	123.0667	12.30667	YES
400	50	5	62,891	99.82698	9.982698	YES
300	50	5	48,234	76.5619	7.65619	NO
200	50	5	33,578	53.29841	5.329841	NO
100	50	5	18,922	30.03492	3.003492	NO

Note: YES - Visible thermal damage on the fibre, NO-without visible thermal changes on the fibre

10.2.4 Mechanical test

Table 10: Mechanical properties of laser irradiated woven basalt fabric, using Tera test 2300, force applied in a weft direction on a 30x5cm^2 fabrics.

Pixel time µs	**Energy density [KJ/cm^2]**	**ε_u max mm**	**Fmax N**	**W J**	**E MPa**	**t sec**	**ε_u max %**
Untreated	0.00	7.87688	2111.4	7.31	4018.38	5.12	3.94
100	3.00349	7.44443	2110.41	12.49	3798.98	8.11	3.723
200	5.32984	8.20401	1950.76	8.863	3167.6	5.66	4.103
300	7.65619	7.92746	1656.93	8.4	2845.73	6.06	3.967
400	9.98269	8.03387	1366.81	7.62	2199.25	6.82	4.017
500	12.3066	6.6859	769.3	5.09	1954.35	7.59	3.34
600	14.6328	5.99197	435.06	3.63	269.55	8.933	2.997
700	16.9593	6.3148	365.61	3.757	354.17	10.77	3.16
800	19.2831	5.10549	159.95	0.95	157.99	6.393	2.553

Where ε_u max – is the elongation at break [in mm and %], Fmax – is the breaking strength [N],E – Young's Modulus [MPa],W – the work done (energy) [J], and t- time to break [sec]

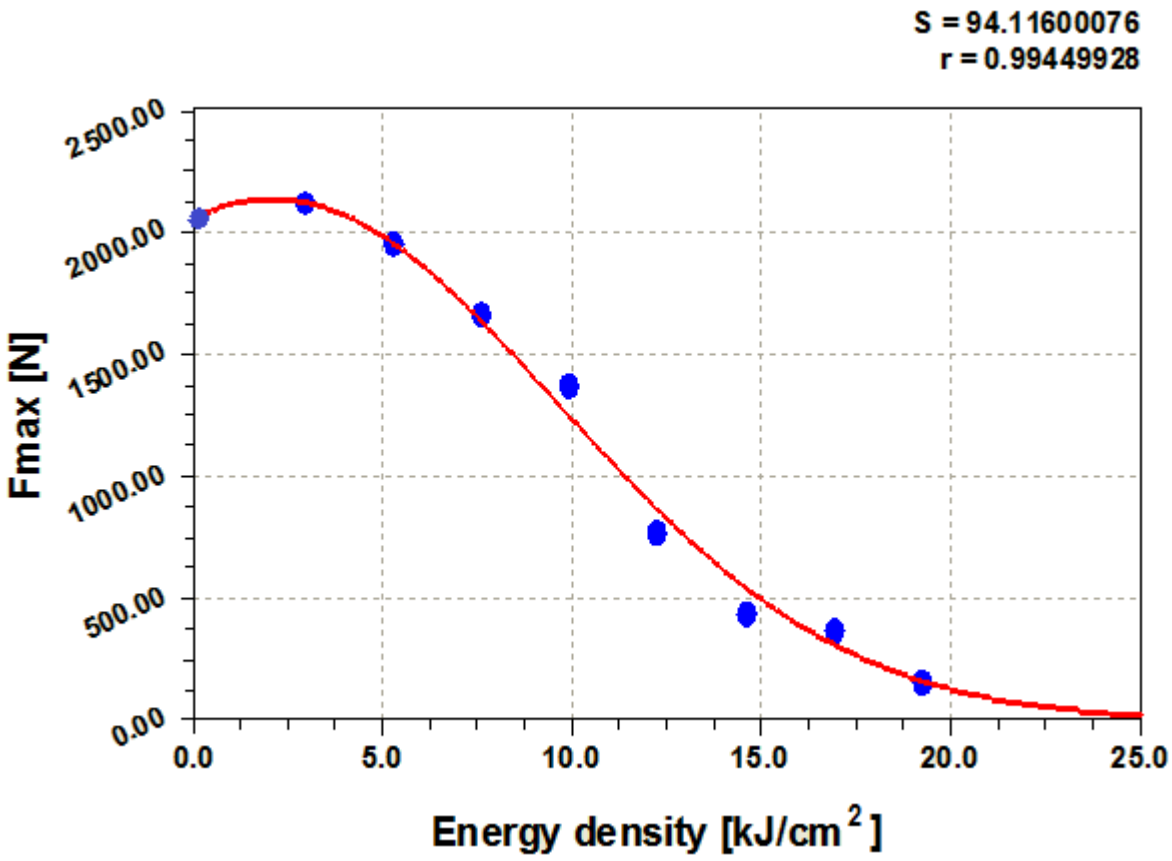

Figure 22: Strength of fabric (F_{max}) vs. Energy density (KJ/cm^2) of a laser treated basalt woven fabric ($450g/m^2$).

The graph above revealed that IR laser irradiation on basalt fibre has a huge influence on mechanical properties. The strength of the material tends to decrease due to thermal damage by the Infrared laser irradiation. The high order of decrease of strength was seen at basalt when the energy density of laser was increased. There is a slightest increase in strength up to 2.5 KJ/cm^2 energy input. This can be credited to the binding points formed during melting at this energy intensity. However beyond that the strength drops due to fibre damage.

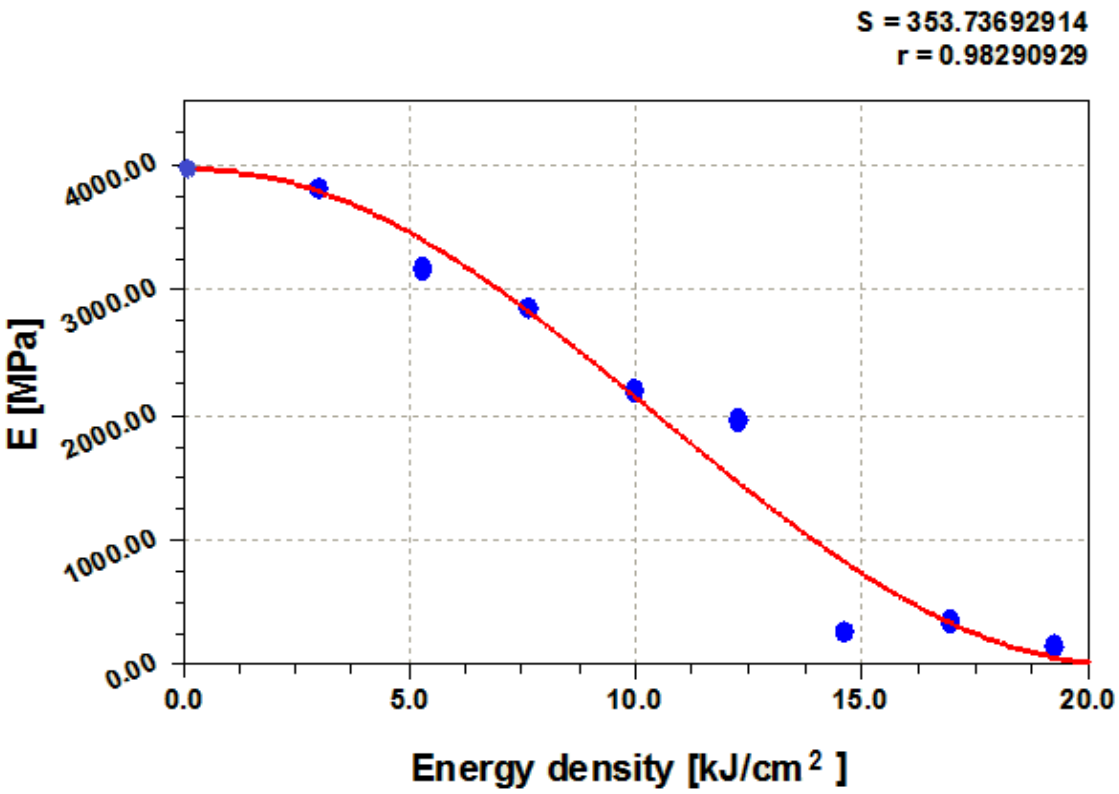

Figure 23: Elongation curve of E (Modulus) vs. Energy density (KJ/cm^2) of a laser treated basalt woven fabric (450g/m^2).

Likewise the tensile modulus is also affected by this effect of laser beam irradiation. Untreated basalt had a tensile modulus of about 4000Mpa. This decrease in modulus is related to the decrease in tensile strength. This effect was due to the fact that the wrinkles, bubbles which are formed on febrile axil orientation of the fibre created weak points on the fibre, leading to reduction in strength. The modulus dropped up to almost zero when 20KJ/cm^2 energy density was applied.

From these experiments it can be deduce that not much machenical and surface textural benefits can be obtained using IR laser treatment. However this technology could be useful when used as a cutting tool for basalt fibres.

EXPERIMENTAL PART 4

11. OBJECTIVES

11.1 CARBON DEPOSITION ON BASALT FIBRE

In efforts to find useful finishing techniques for basalt fibres, the application of carbon on basalt fibre could prove to be a very useful, attractive and even provide an alternative way of producing basalt fibres materials with carbon fibre like properties. This section of the experiment explores two ideas which could be a solution to this ambitious idea. Hence, part "A" of the study explores the effect of using CO_2 laser as a source of energy to dehydrate sucrose matrix, as an attempt to melt-bond the residual carbon to the surface of basalt fibres. Part "B" explores another possible way to chemically produce carbon matrix and then use it as a binging resin for *light duty*, electrical conductive basalt fibre composites material.

11.1 CO_2 LASER METHOD (PART A)

11.1.1 Materials and methods

A sucrose solution with a concentration of 300g/l was prepared by dissolving 30g of table sugar crystals with 100ml. Basalt woven fabric (450g/m^2) was then coated with this 300g/l sucrose solution and dried at 105^oC for 10 minutes. The sample was irradiated with CO_2 LASER (infrared), for a repeated number of cycles with laser density of 19.2831 KJ/cm^2 (at 800µs). This laser provided a laser beam of frequency of 5 KHz and delivering a power of 100 W.

11.1.3 Results

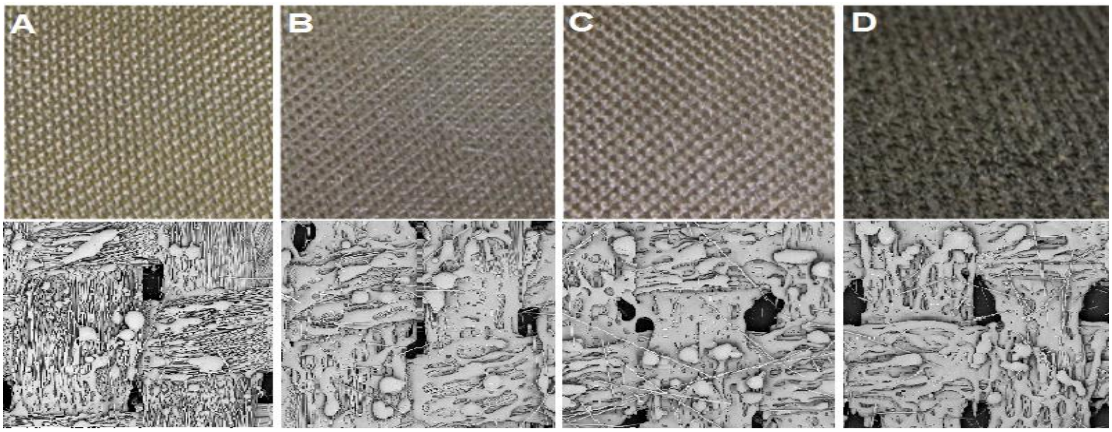

Figure 24, Actual and SEM images of CO_2 laser irradiated basalt fabric: Number of irradiation, cycles, (A) 800µS x1, (B) 800µS x 2, (C) 800µS x 3, (D) 800µS x 4. All SEM image magnification were taken at 1x Mag.

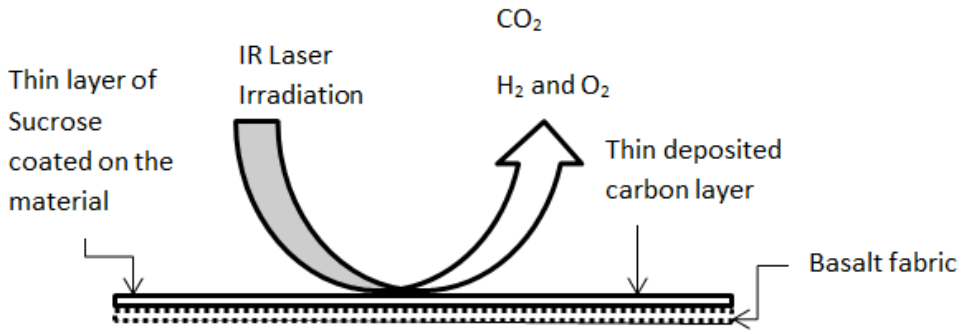

Figure 25: CO_2 laser irradiation on basalt fabric which was coated with a thin layer of sucrose solution (300g/l).

When IR laser was irradiated on the basalt fabric coated with a thin layer of sucrose matrix solution, dehydration of $C_{12}H_{22}O_{11}.nH_2O$ (sucrose) occurred, while a thin layer of carbon was formed, CO_2, H_2 and O_2 gases were generated and escaped. A gradual increase of the amount carbon deposited on a surface of basalt fabric was observed as the number of irradiation cycles increased.

The attempt to deposited carbon via laser dehydration of sucrose thin layer was not a fruitful one. Although a thin layer of carbon was formed on the surface of basalt fibre, however, high energy intensity destroyed the substrate material. This resulted into wrinkles, bubbles and big holes which created weak points on the fibre, and led to reduction in strength. On a positive note, it was observed that a layer of sucrose protected the material, in such a manner that it was able to withstand high level irradiation intensity (single cycle of 20kJ/cm^2) as compared to uncoated material.

11.2 CHEMICAL CARBON DEPOSITION (PART B)

11.2.1 Porous carbon based materials reinforced with basalt fibre

The following series of the experiments were divided into two phases. In Phase *I*, a non-woven glass fibre mat and basalt fibre woven fabrics specimens were coated with a carbonised sucrose matrix and then evaluated their properties. Phase *II* experiments investigated the electrical conductivity and dynamic machenical properties of carbon composite rods, which were prepared by mixing short carbon fibres (CF), basalt fibres (BF) and carbonised sucrose matrix.

11.2.2 Materials and methods (Phase I)

A sucrose solution with a concentration of 600g/l was prepared by dissolving 60g of table sugar crystals with 100ml. The solution was heated to about 60^{o} and vigorously shaking until all the particles completely dissolved. A 20ml volume of sucrose solution was taken from the main concentrate into three different beakers. On the 1^{st} beaker 0,5ml 96% H_2SO_4 was added while stirring and it was labelled as V0.5, for the 2^{nd} beaker, 1ml was added (V1) and likewise the 3^{rd} beaker 1.5ml was added as well (V1.5). Since the reaction between sugar and H_2SO_4 is exothermic, it releases a lot of heat, water vapour and sulphur dioxide, this experiment was done under the fume cupboard. The carbonised sucrose matrix was then cooled down for several minutes. This carbon matrix was then applied by a padding method on non-woven glass fibre mat and also on basalt fabric. All samples were dried at 105^{o}C for 30 minutes and then washed with running water, and dried again for another 30 in the oven at 105^{o}C. Lastly the samples were dried at 250^{o}C for 5 minutes to completely remove all of the excess acid impurities and moisture. This was done to minimise the effect of polarization during electrical conductivity measurements. Conductivity tests and measurements were done and recorded as seen on table 6 and 7.

11.2.3 Electrical conductivity

The test for electrical conductivity was done by a two-probe method using a Megaohmmeter C.A 6541, C.A 6543, CHAUVIN ARNOUX. The positive and the negative probe electrodes were places 10mm apart to measure the resistivity. The results were measured in sets of three per specimen.

11.3 RESULTS AND DISCUSSION (Phase I)

SEM images showing the binding effects of carbonised matrix, on glass fibre mat

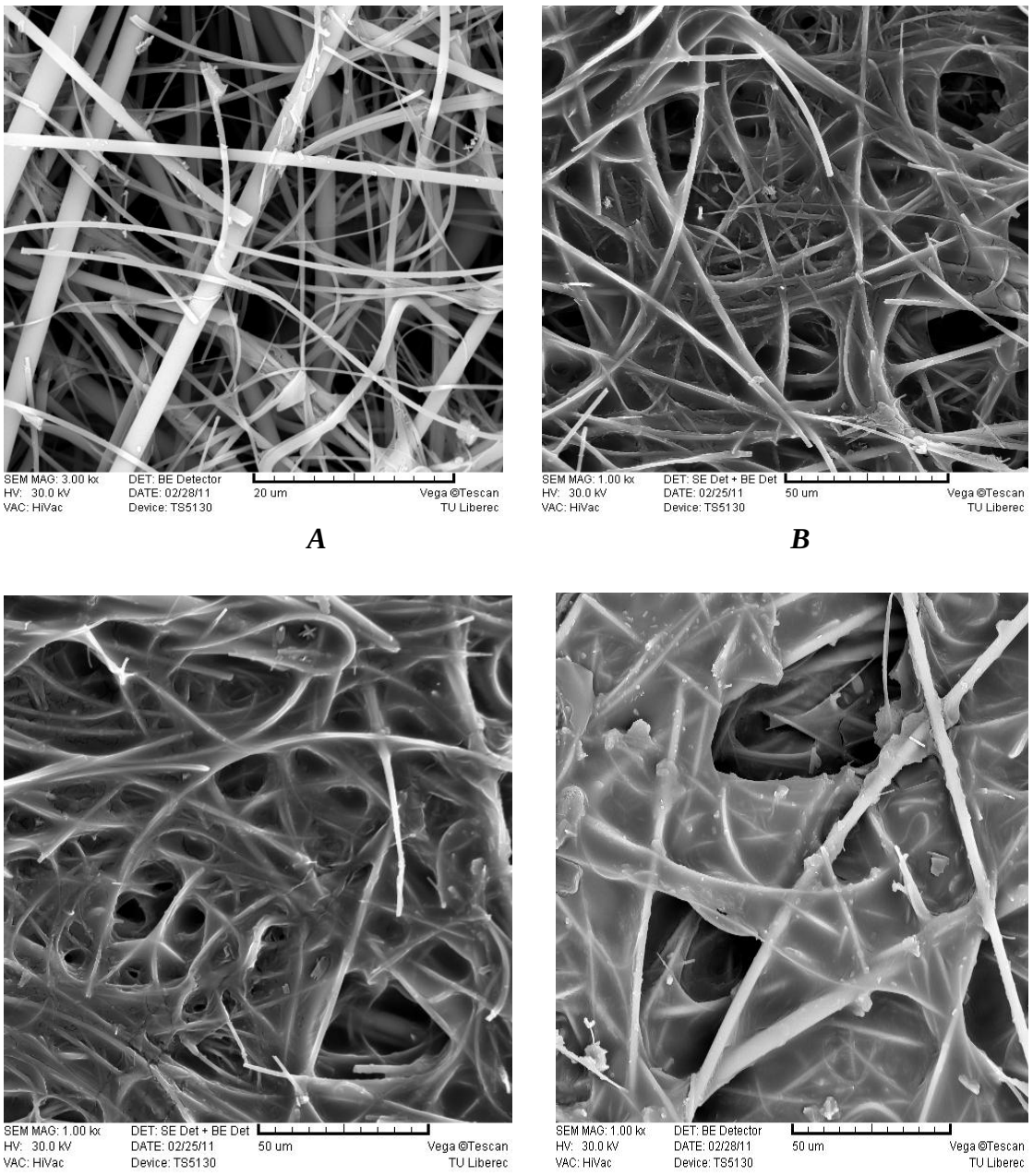

Figure 26.– SEM image of glass fibre mat (A) untreated treated, (B) treated with V05,(C) treated with V1 and (D) treated with V1.5 solutions

SEM images showing the binding effects of carbonised matrix, on basalt fibre fabric

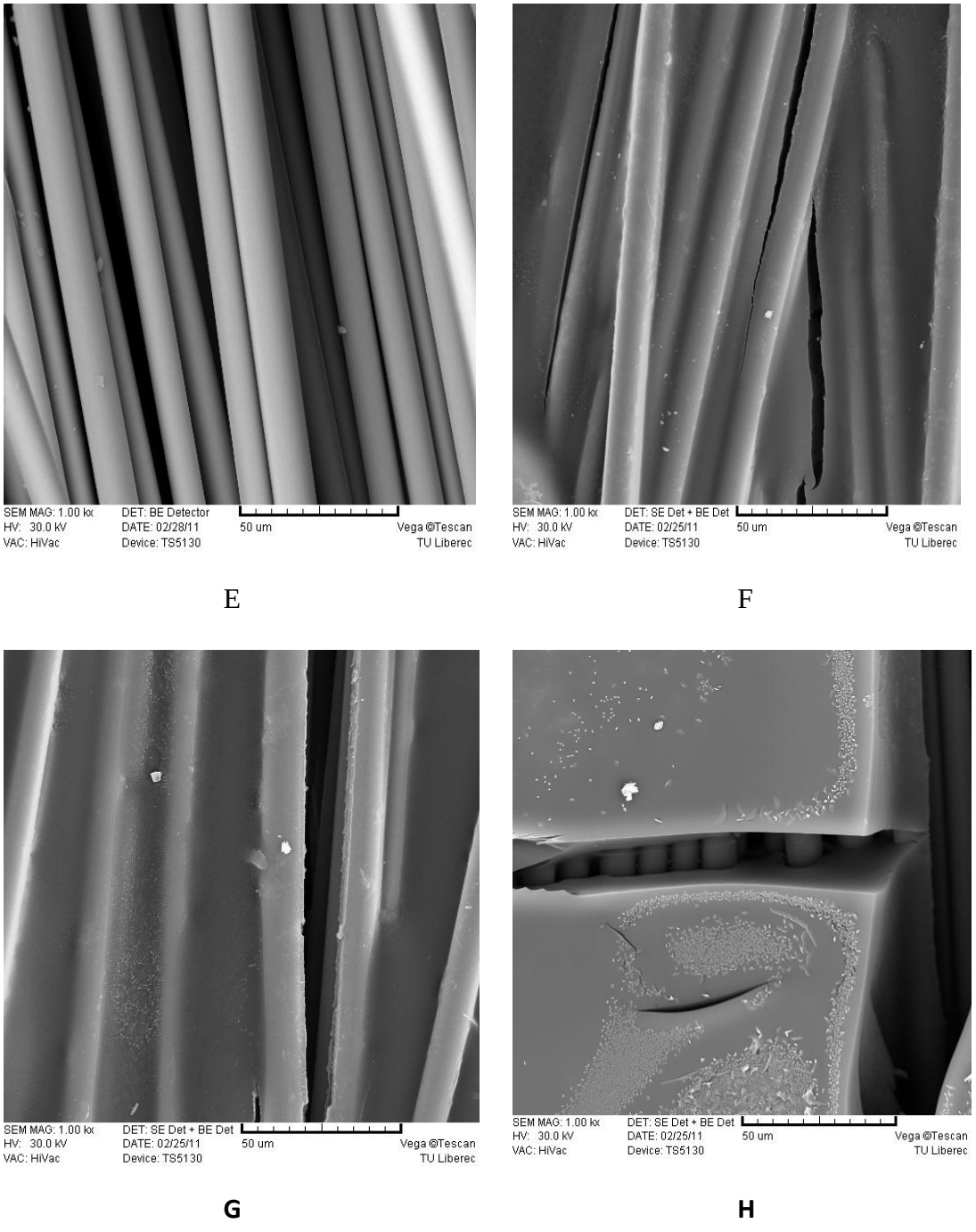

Figure 27.– SEM image of basalt fibre fabric (A) untreated treated, (B) treated with V05,(C) treated with V1 and (D) treated with V1.5 solutions

Table 11: Room temperature conductivities and resistivity of carbon coated basalt samples

No:	Volume of 96% H_2SO_4 added in 20ml sugar solution [ml]	Room temperature resistivity [Ω cm]	Room temp. Conductivity [S/cm]
1	Untreated	0	0
2	0,5	$2.34x10^{5}$	$4.27x10^{-6}$
3	1	$3.11x10^{4}$	$3.21x10^{-5}$
4	1,5	$2.04x10^{4}$	$2.45x10^{-5}$

Table 12: Room temperature conductivities and resistivity of carbon coated glass samples

No:	Volume of 96% H_2SO_4 added in 20ml sugar solution [ml]	Room temparature resistivity [Ω cm]	Room temp. Conductivity [S/cm]
1	0	0	0
2	0,5	$3.77x10^{6}$	$2.65x10^{-7}$
3	1	$2.58x10^{6}$	$3.87x10^{-7}$
4	1,5	$4.15x10^{5}$	$2.40x10^{-6}$

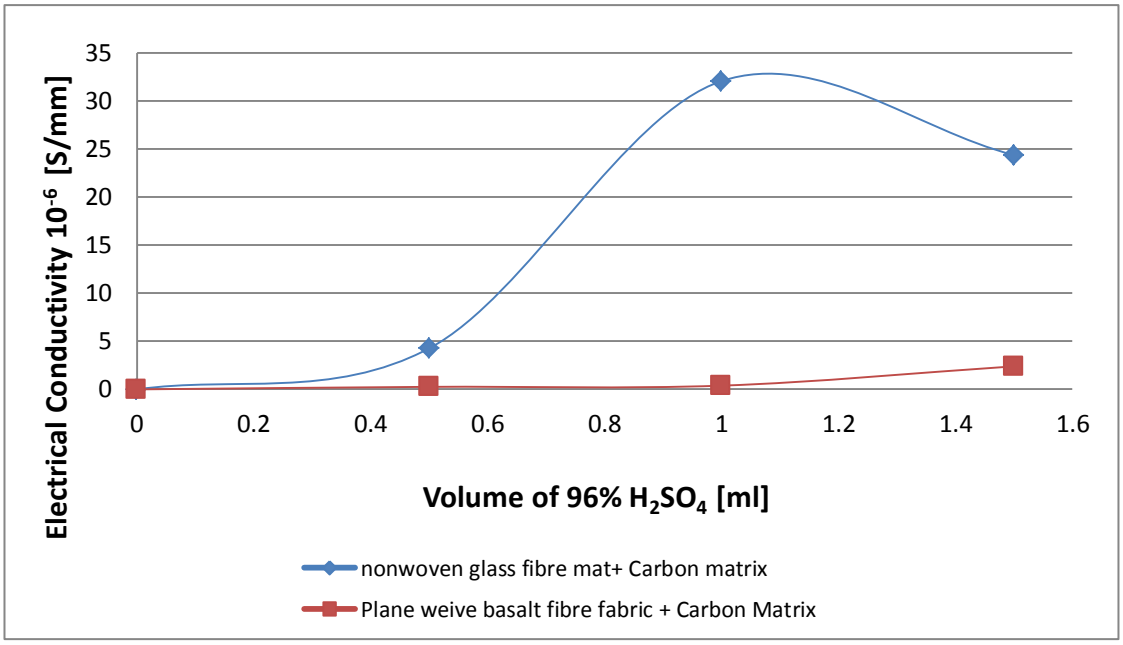

Figure 28: Graph showing the influence of increasing the volume of H_2SO_4, to carbonise the sucrose matrix, and the influence of geometrical structure of a substrate on electrical conductivity.

The above results revealed that, when more acid is added into sucrose solution, more carbon is generated. This is due to a dehydration process that take place during the reaction between acid and sucrose. From SEM images it can be deduced that, samples treated with solution V0,5 has lower bonding points as compared to sample treated with solution V1 and V1,5. Hence, SEM images on figure 26(A) (glass fibre mat) and figure 27 (E) (basalt fibre) had less thinner binding matrix as compared to a much thicker matrix on figure 26 (D) and 27(H). It is obvious that the thickness of the matrix is related to the amount of carbon deposited on the surface of the fabric. This phenomenon was also proven to be true when these materials were tested for the conductivity. The materials with a higher amount of carbon were more conductive as compared to the ones with a lower amount of carbon. This phenomenon was also related to the geometric structure of the substrate material. The samples with a substrate made from nonwoven (glass mat) structure were more conductive then the ones with woven fabric "basalt fabric" (figure 28). However the conductivity of the material was not connected with the type of fibre used but only connected to the geometrical connection of fibres. Since nonwoven material has irregular geometric structure, this allows it to have more binding points when bonded with matrix. The more bonding sites, the higher the surface area which allows the electron to move more freely. Therefore the resistance of the material becomes less, resulting in a much higher conductive material.

11.4 Titanium dioxide (TiO_2) effect on carbon matrix

The objective of this experimental part was to explore and investigate the effects of adding TiO_2 nanoparticles into a 600g/l concentrate of carbon matrix prepared on a previous section. A 20ml volume carbonised matrix solution was taken from a concentrate and places into beaker. 1g of TiO_2 powder was added and dispersion was prepared by homogenisation using the Ultrasonic Supersonic. This process was carried out by setting the ultrasonic capacity at 50% (50 kHz) for 1 minute. This new matrix was then padded on a nonwoven glass fibre mat, dried and tested with SEM & XRF (X-ray fluorescent).

11.4.1 Results

SEM images showing the effect of adding TiO_2 to a C-matrix.

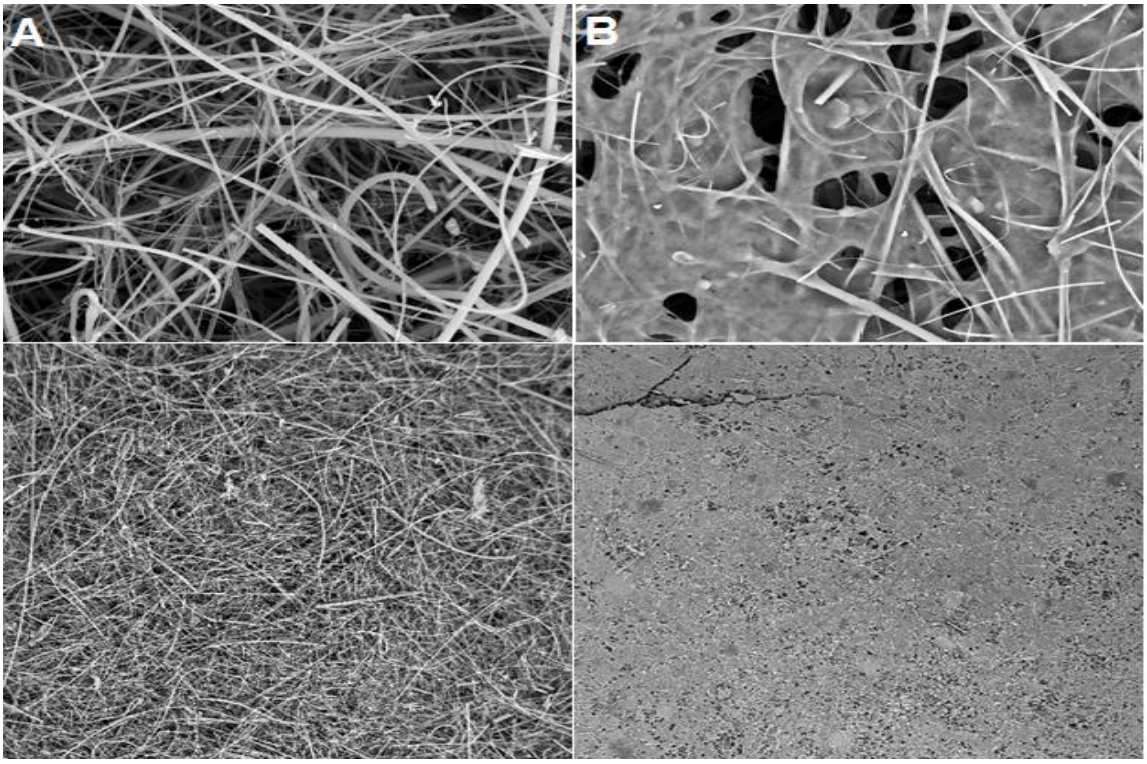

(Fig 29): SEM images of glass fibre mat untreated (A) and treated (B) with carbonised sucrose matrix, containing TiO_2 particles.

From SEM images it can be deduced that, samples treated with C-TiO_2 solution are more compact and stable as compared to untreated sample (figure 29).

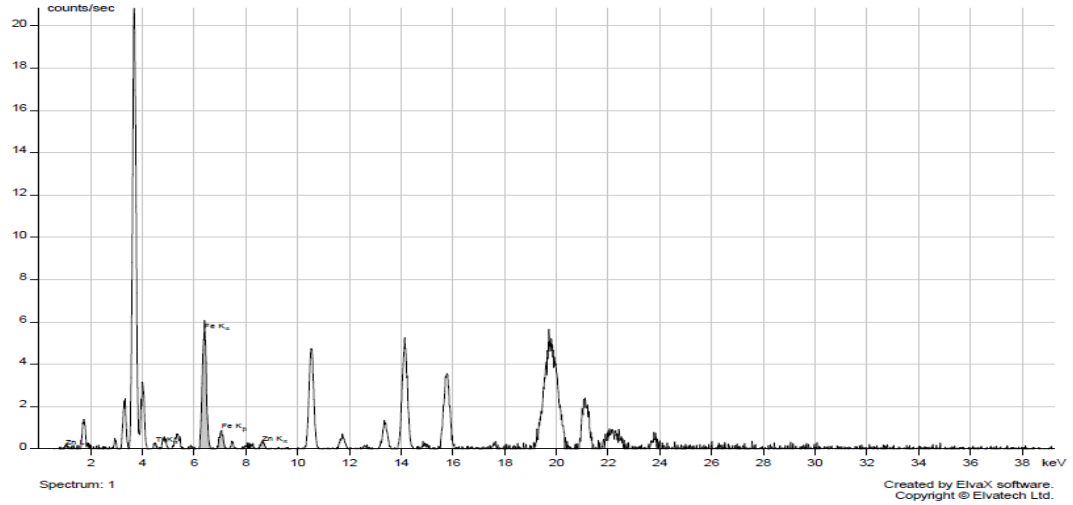

Figure 30: Untreated spectral image of glass fibre mat, generated by an XRF

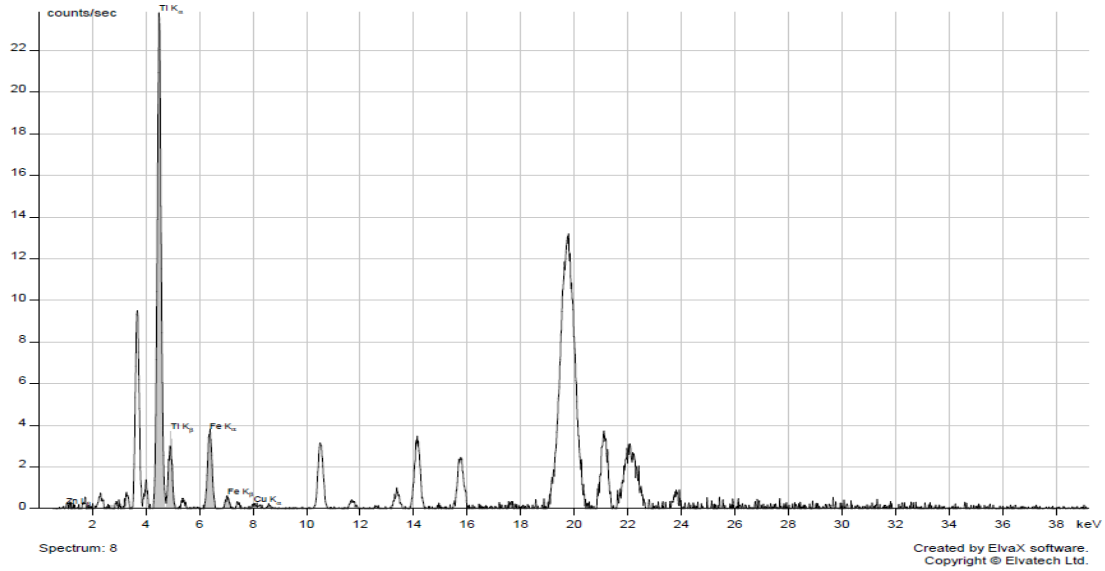

Figure 31: C-TiO_2 *treated spectral image of glass fibre mat, generated by an XRF*

X-rays generates energy per photon of 4,4keV, fluorescent X-rays are emitted by the material . A spectral peak at 4.4keV with approx. 23 counts/sec indicates that there was high Ti ions imparted on a glass fibre mat, after treatment with C-TiO_2 matrix (figure 31), whereas the untreated sample had none (figure 30). TiO_2 is well known for its photo-catalytic properties and it's used as a delustring agent in many textile applications. Therefore this method can be used to prepare a material with high photo-catalytic properties.

11.5 Phase II

11.5.1 Porous, conductive carbon composite rods preparations

The objective of this experimental part was to prepare composite rods which are porous, electrical conductive and low relative density. Such types of composite rods could well be suitable as an alternative to carbon electrodes, which are normally used in carbon-zinc batteries. The following series of experiments explains the procedure on how to carry out the preparation of these rods. Empirical mathematical models were generated for process optimisation.

11.5.2 Materials and methods

Matrix preparation method was almost similar to that used prepared in phase *I* . However, in this case sucrose solution with concentrations of 300, 600,900 and 1200g/l were prepared by dissolving 30,60, 90, 120 g of table sugar, with 100ml of water. These 4 different concentrated solutions were heated to about 60^{o} and while stirring until all the particles completely dissolved. Twenty samples (5 from each concentrate) of 25ml's sucrose solution were taken from each concentrate placed into different beakers. A volume of 1ml of 96% H_2SO_4 was added to all twenty beakers and 0.5ml of a surfactant known as Spolion S 50g/l was also added to each beaker (The addition of this surfactant was to promote the wetting ability of carbon and basalt fibre which will be used during impregnation with a matrix). Since the reaction between sugar and H_2SO_4 is exothermic, it releases a lot of heat, water vapour and sulphur dioxide, this experiment was done under the fume cupboard. The carbonised sucrose matrix was then cooled down for several minutes.

Basalt and carbon fibre were cut (chopped) to approx. 5mm length. A basalt fibre to carbon fibre [BF: CF] mass faction mixing ratio system was applied and expressed in % form. i.e. BF:CF (0:100 ; 33:66 ; 50:50 ; 66: 33; and 100:0) and the total fibre mass per each sample was 2g (e.g. for a mix ratio 33:66, the mass of BF was 0.66g and that of CF was 1.34g). (NB: carbon fibres are blended with basalt fibre because they possess high electrical conductivity properties).

A volume of 2.5ml of prepared carbonised sucrose matrix from each 4 different concentrates was then added to each of twenty, BF: CF mixed fibre samples and mixed together. Each mix was then loaded into 20 small test tubes, and applied some pressure to ensure proper compactness. All 20 samples were then dried at $150^{o}C$ for 60 minutes and furthermore dried at $450^{o}C$ for 15 minutes to completely remove all of the excess acid impurities and moisture, thus to minimise the effect of polarization during electrical resistance measurements.

To remove the composite rods from the test tube, it was necessary to carefully break each test tube by applying a little pressure therefore completely removing the specimen.

The conductivity tests and weight of each sample were measured and recorded as seen on table 8 and 9.

11.5.3 Electrical conductivity measurements

A DC electrical current was applied to test the rods specimens' electrical conductivity. This test was done by a two-probe method (total area of contact: $8mm^2$), using a Megaohmmeter C.A 6541, C.A 6543, CHAUVIN ARNOUX (at room temperature, with relative humidity of 67%). The positive and the negative probe electrodes of a Megaohmmeter were places 25mm apart for all of composite rod specimens. The voltage was set to 5 volts. All specimens prepared by a phase II methods were tested for electrical resistance (R), and the resistivity (ρ), and conductivity (σ) were then calculated.

11.5.4 Dynamic mechanical analysis (DMA) test

In this study a Dynamic mechanical analysis (DMA) test was carried out using a *DMA DX04T*. The DMADX04T was connected to a computer which was controlled by windows software NT. The DMADX04T analysis system controlled the analyser and digitised the analog output from the detector before sending it to the computer. A single rod specimen was placed in the centre of the sample platform in a horizontal direction. A parallel plate measuring system with a diameter of 10mm was employed. The system analyser was driven by a linear force motor, which in turn was controlled by a computer. The probe was attached to the lower end of the core rod lowered down to hold the specimen in place for testing. The prescribed force generated by the force motor was applied to the sample through the core rod. Stresses induced in the sample were transmitted through the upper test fixture to a detector where deflections were converted to electrical signals and relayed to a DMADX04T machenical analysis instrument controller. The machenical analysis instrument controller then resolved the signals into elastic components of the complex modulus and the phase angle as their function. The samples were equilibrated at 26 ± 0.3 $^{\circ}C$ during testing. The results were the mean and standard deviation of 20 composite rod specimens. Static scans to obtain a value for the elastic modulus of the rods were performed between 0 and 10000mN at a maximum loading rate of 500 mN/min. Dynamic scans was set at frequency of 1 Hz, oscillation of

0.1mm amplitude and at 20 minute testing time per specimen. From the dynamic scans, a wide variety of measurements can be obtained. Here, the storage modulus E', loss modulus E" and deformation as functions of dynamic force were recorded.

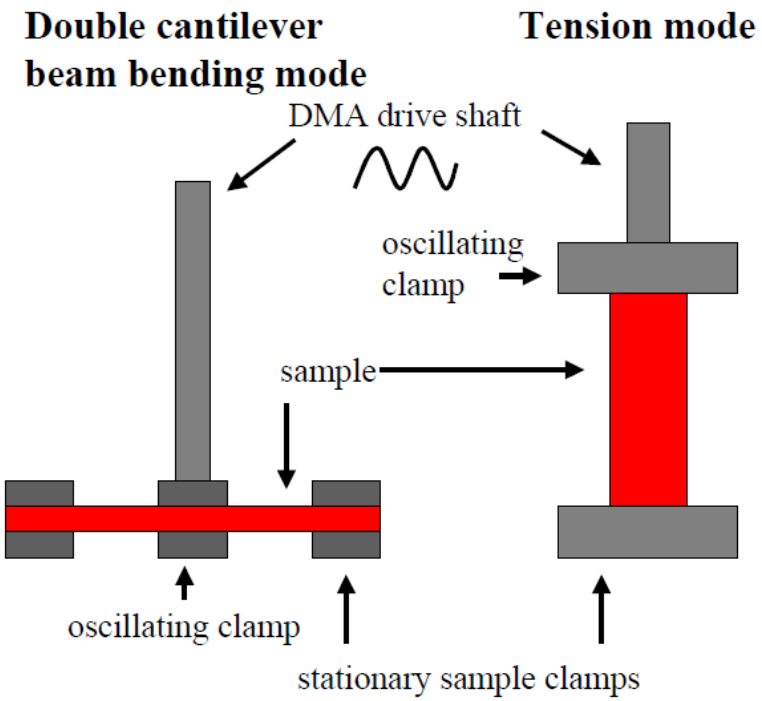

Figure 32: DMA Configuration

11.5.5 Copper Electroplating test for phase II samples

A copper solution was prepared by placing 20g of Copper sulphate crystals ($CuSO_4.5H_2O$) into a beaker, 5ml of ethanol, 1 ml of 96% H_2SO_4, were added as well. All the copper sulphate particles were dissolved by shaking and stirring of the electrolyte solution. The specimen with BF:CF [33:66] and 900g/l was used as a test sample for this part of the experiment. This carbon rod specimen was used as cathode (-) connected to the negative terminal and a copper plate was used as a anode (+) connected to the positive terminal. A power supply device (Diametral) was set to deliver 8 volts, and about 95% of the carbon rod was plated with copper in just 15 minutes.

11.5.6 Thermal damage of phase II sample

Equal weights with BF: CF ratio of (0:100, 33:66, 50:50, 66:33, and 100:0) with 900g/l of carbonised matrix were heated in the oven at 550^{o}C for about 15 minutes. The weight was recorded before and after the heating process. The weight loss was then calculated and recorded in mass %.

---

12. PHASE II RESULTS

12.1 Electrical Conductivity results

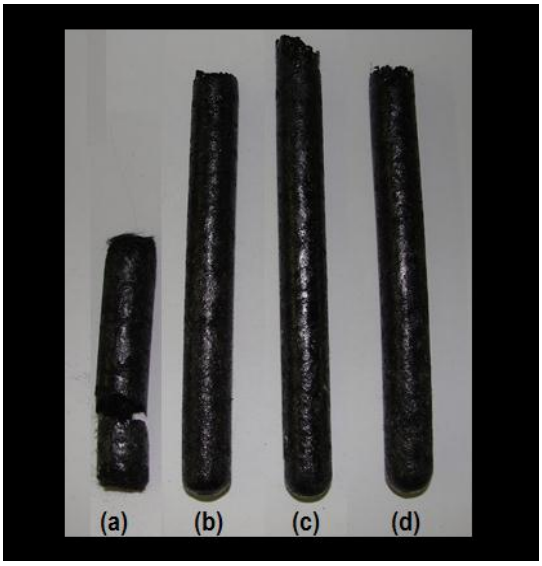

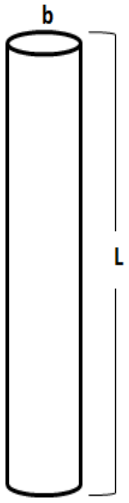

Figure 32, Electrical conductive composite rods with different concentrations of carbonised sucrose matrix, i.e. (a) 300g/l (b) 600g/l, (c) 900g/l and (d) 1200g/l

The electrical conduction was ohmic in nature and the electrical conductivity was given by the following relationship of equations.

Resistivity

$$\rho = R\ \frac{b}{L} \tag{15}$$

Conductivity

$$\sigma = \frac{L}{R.b} \tag{16}$$

where, ρ = Resistivity (Ohm-mm),R = Magnitude of impedance (resistance) obtained from Megohmmeter C.A 6541, C.A 6543 (Ohms), b = Cross sectional area of electrode (mm^2)

L = Distance between the electrodes (mm) σ = Electrical conductivity (S/mm).

Mix Ratio of BF:CF	Sucrose Matrix conc. 300g/		Sucrose Matrix conc. 600g/l		Sucrose Matrix conc. 900g/l		Sucrose Matrix conc. 1200g/l	
	Resistivity [Ω.mm]	Conductivity [S/mm]	Resistivity [Ω mm]	Conductivity [S/mm]	Resistivity [Ω.mm]	Conductivity [S/mm]	Resistivity [Ω.mm]	Conductivity [S/mm]
0:100	1.74	0.57	1.96	0.51	1.85	0.54	2.61	0.38
33:66	2.02	0.49	2.52	0.40	2.12	0.41	2.44	0.41
50:50	3.72	0.27	4.16	0.24	3.75	0.27	3.32	0.30
66:33	7.15	0.13	13.70	0.073	8.90	0.11	17.38	0.18
100:0	$9.6x10^8$	0.00	$8.4x10^8$	0.00	$9.4x10^8$	0.00	9.910^8	0.00

The separating distance between the electrodes (L) was 25 mm and the cross sectional area of the electrodes was 8mm^2. The value of real impedance (R) for each point on the plot is an average of three readings of each type of specimen.

Table 13: Room temperature conductivities and resistivity's of for basalt reinforced carbon fibre with different concentrations of sucrose matrix

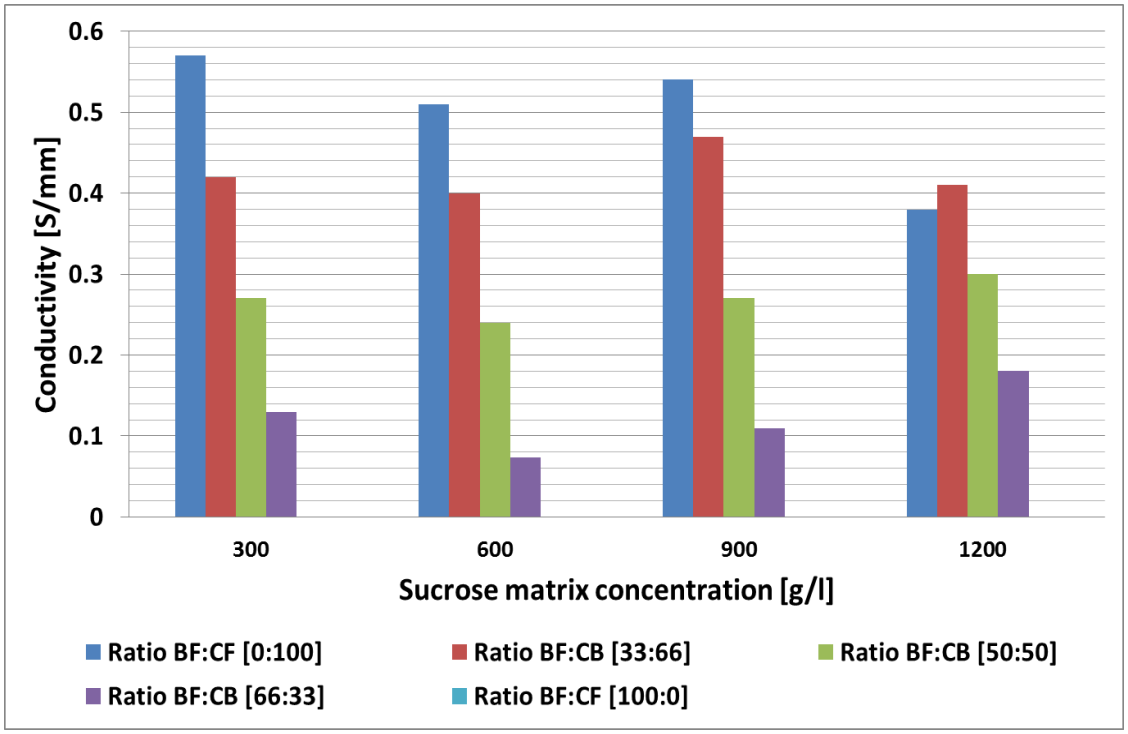

Figure 33: A graph of electrical conductivity vs. different concentration of carbonised sucrose matrix.

Carbon fibres are known for their good electrical conductivity properties. However they are very expansive and they are also known for being brittle when used for composite materials. On a contrary, basalt fibres are relatively cheaper, and they have good mechanical, thermal and chemical properties. Thus it makes logical sense to use a combination of the two fibres one wants to produce composite material with all of the above mentioned properties from each type of fibre and cheaper at the same time.

Based on the results from the graph above, it was realised that, the best mixing combination of carbon fibre to basalt fibre was a ratio of BF: CF [33:66], which was impregnated with 900g/l matrix. The conductivity of that specimen was the second best, as compared with the other specimen containing carbon alone. There other specimen had quite high conductivity as well, however it was realised that samples with lower concentration of matrix were slightly higher in conductivity as compared to the ones with a high contrition. This could be explained by the assumption that, high concentration of sucrose terns to insulate the fibres more, therefore prohibiting a free flow of electrons, during resistivity test. These results come about my determining the conductivity of each sample. This behaviour could be further explained by percolation threshold phenomena.

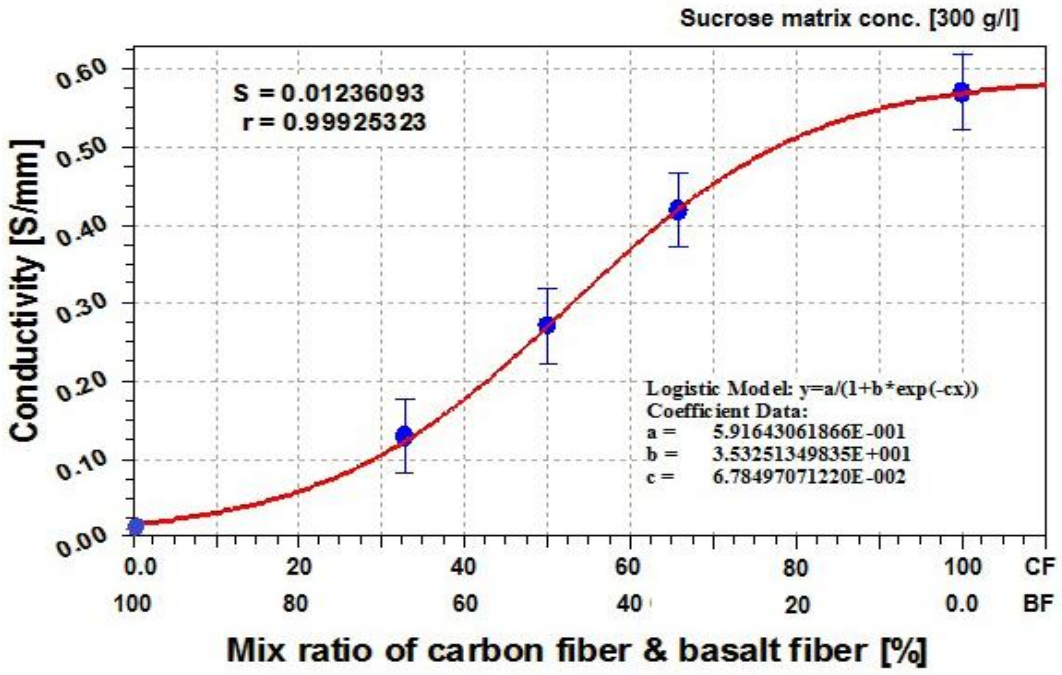

Figure 34: Graph of electrical conductivity vs. different mixing fraction (ratio's) of CF:BF impregnated with 300g/l C-matrix.

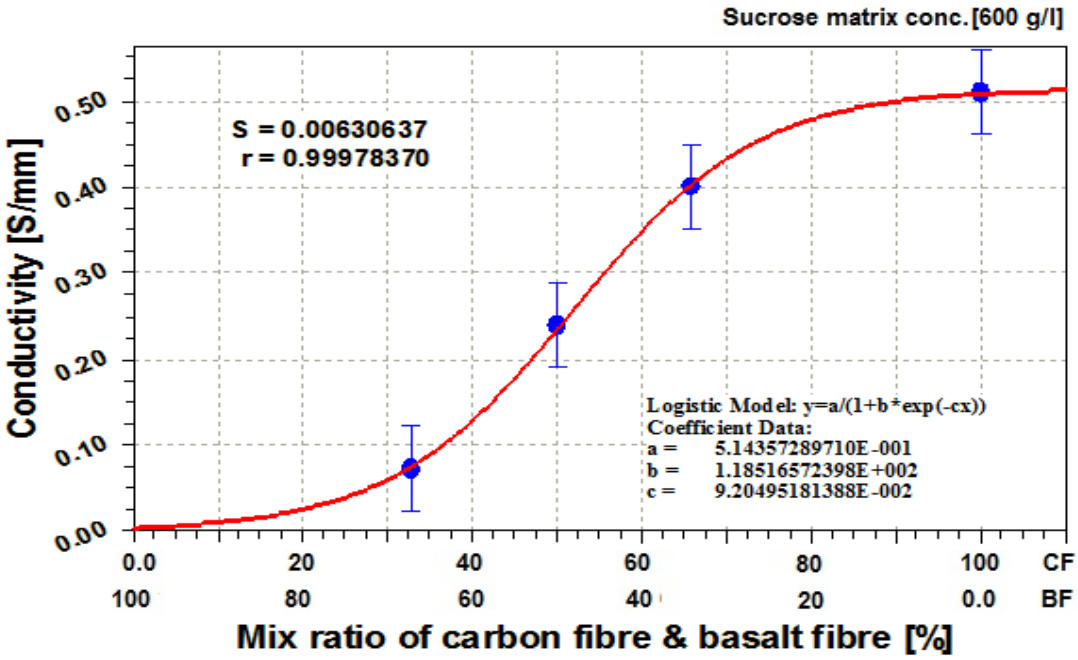

Figure 35: Graph of electrical conductivity vs. mixing fraction (ratio's) of CF:BF impregnated with 600g/l C-matrix

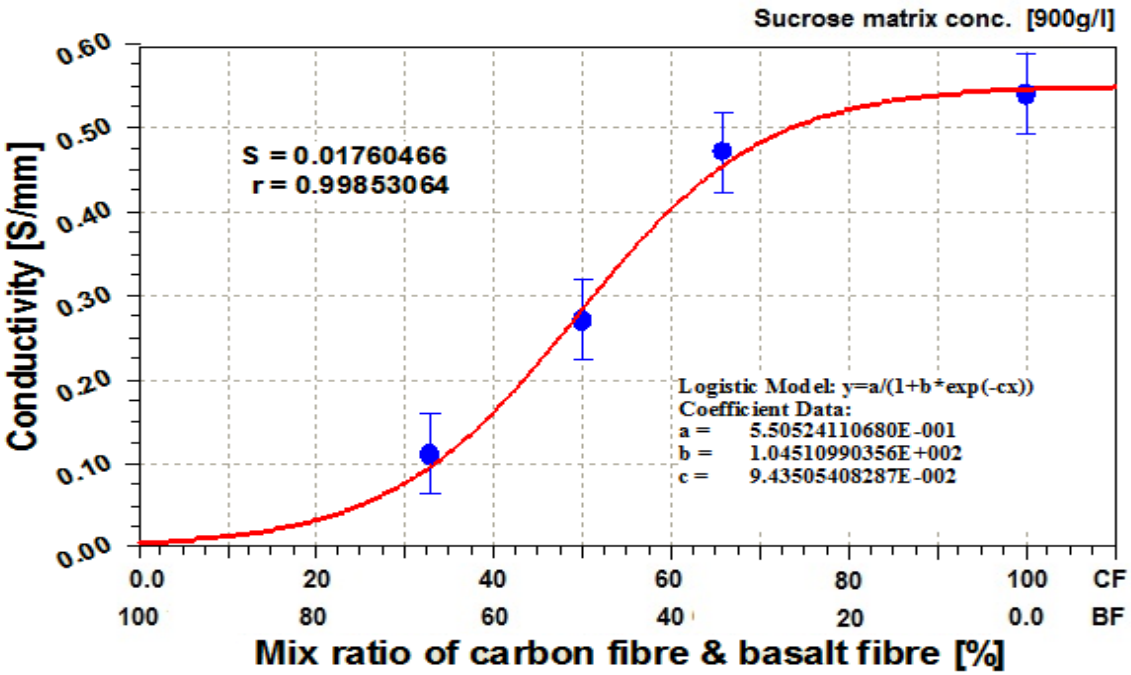

Figure 36: Graph of electrical conductivity vs. mixing fraction (ratio's) of CF:BF impregnated with 900g/l C-matrix.

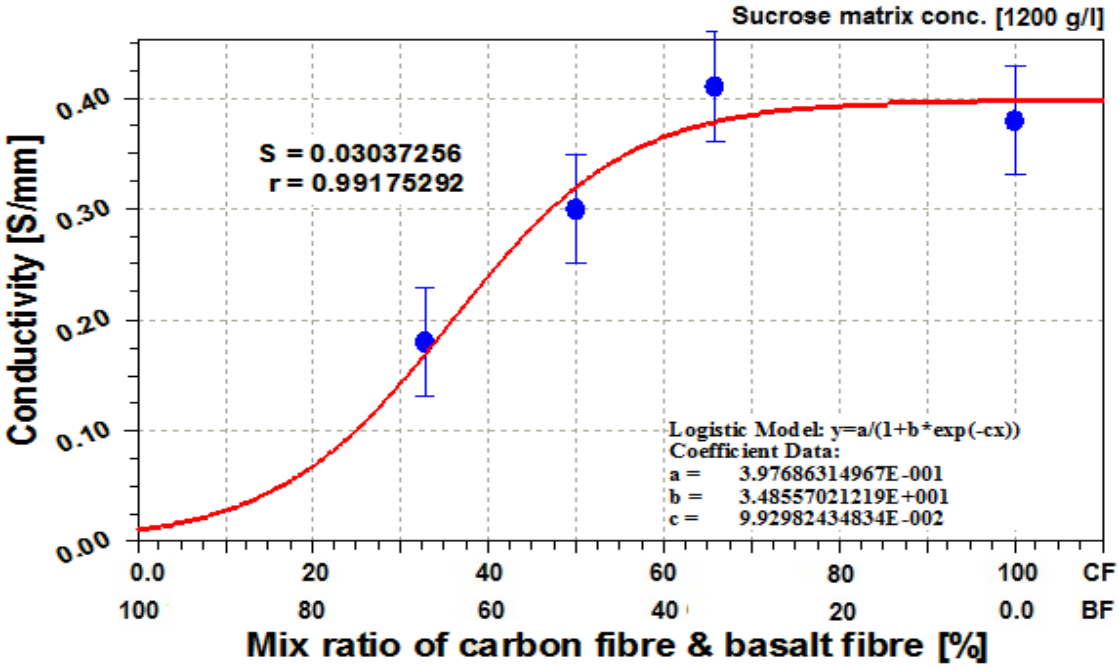

Figure 37: Graph of electrical conductivity vs. mixing fraction (ratio's) of CF:BF impregnated with 1200g/l C-matrix

The graphs above were generated from following empirical mathematical model:

$$\boldsymbol{\sigma = \frac{a}{1+b.e^{-c.m_{cf}}}} \tag{16}$$

a, b and c are empirical values , m_{cf} -mass % of carbon fibre and m_{bf} -mass% of basalt fibre. Assumptions were that, a standard deviation from an average mean value of conductivity was 0.04 [S/mm]. This assumption was based on the fact that the resistivity was influenced by the each individual measurement conditions, surface texture and geometry of the specimen.

12.1.1 PERCOLATION THRESHOLD

One way to discuss the electrical conductivity of carbon rod composites produced is with reference to percolation threshold phenomena. This refers to the volume ratio above which the fibres touch one another to form a continuous electrical path [34]. A D.C. current was applied on dry specimens and calculated the electrical conductivity of the reinforced with carbon fibres, basalt fibre. It can be seen that, the conductivity changes

by several orders of magnitude when the fibres volume approaches a critical value (percolation threshold). This phenomenon could be observed on figures 34-36, where by the fibre volume mix ratio is above 60% CF and below 40 % BF. Also, it was observed that the carbonised matrix does not have much influence on electrical conductivity, however at high concentrations it act as an insulator, therefore preventing a free flow of electrons. Therefore this explains the importance of fibre to fibre connectivity. The higher there carbon fibre connectivity order, the lesser the reliance to flow of electrons, therefore the composite material which obey this principle tends to be more conductive then others. The matrix also plays a huge role in this regard, by binding there fibre together, however there is a critical concentration that can be used in order to obtains better conductivity results. Composite impregnated with 900g/l matrix, proved to be the best BF: CF combination with less resistance, this was because CF-fibres were in contact with each other.

12.2 Dynamic mechanical analysis (DMA) results

The principle and device for measurement of DMA was carried out using a *DMA DX04T, according to the ASTM D4065, ISO6721 standard*

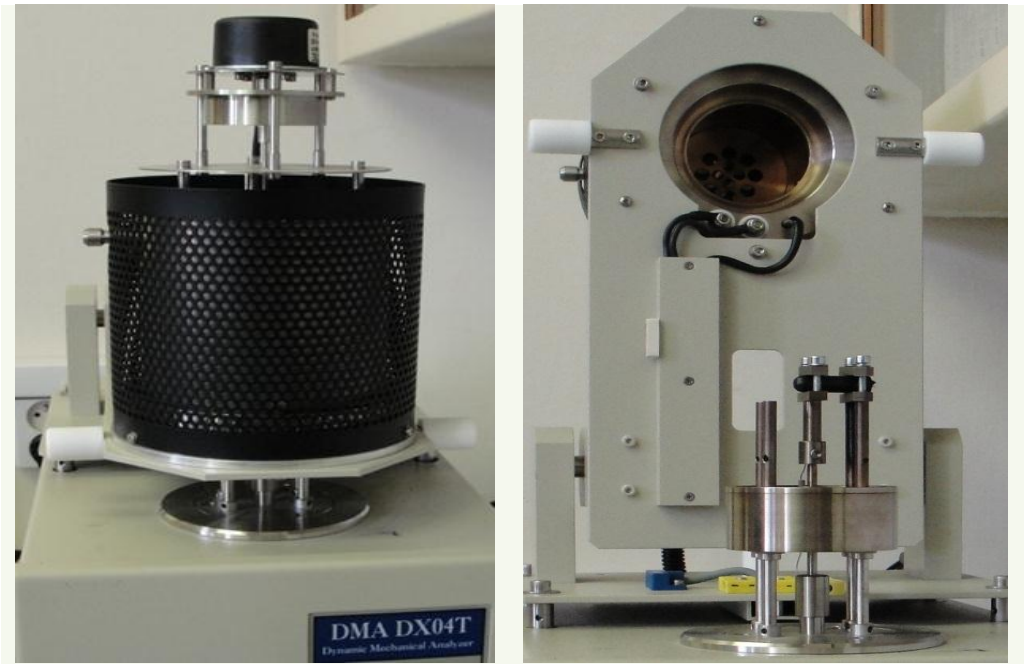

Figure 38: DMA DX04, machenical analysis device used to measure bending deformation, storage (E') and loss modulus (E'')

Specimen # 7,: mass % mix ratio of BF: CF [33:66], and impregnated with 900g/l carbon matrix. Refer to Appendix:

Table 14: DMA results of composite rod, impregnated with 900g/l C-matrix and a ratio of BF: CF [33:66], tested for 20 minutes

Sample # 7, BF: CF [33:66] Matrix conc. 900g/l		**At starting time**		**At finishing time**	
F-force (Max) [mN]		5209.8		5229.95	
F-force (Min) [mN]		-5277.93		-5303.64	
X Deformation (Max) [mm]		0.181		0.181	
X Deformation (Min) [mm]		-0.28		-0.281	
		Up	**down**	**Up**	**down**
δ		8.37E-02	8.95E-02	6.81E-02	8.04E-02
tanδ		8.39E-02	8.97E-02	6.83E-02	8.05E-02
E	[MPa]	1.80E+01	1.79E+01	1.86E+01	1.79E+01
E'(cos)	[MPa]	1.79E+01	1.78E+01	1.79E+01	1.78E+01
E''(sin)	[MPa]	1.51E+00	1.60E+00	1.23E+00	1.43E+00

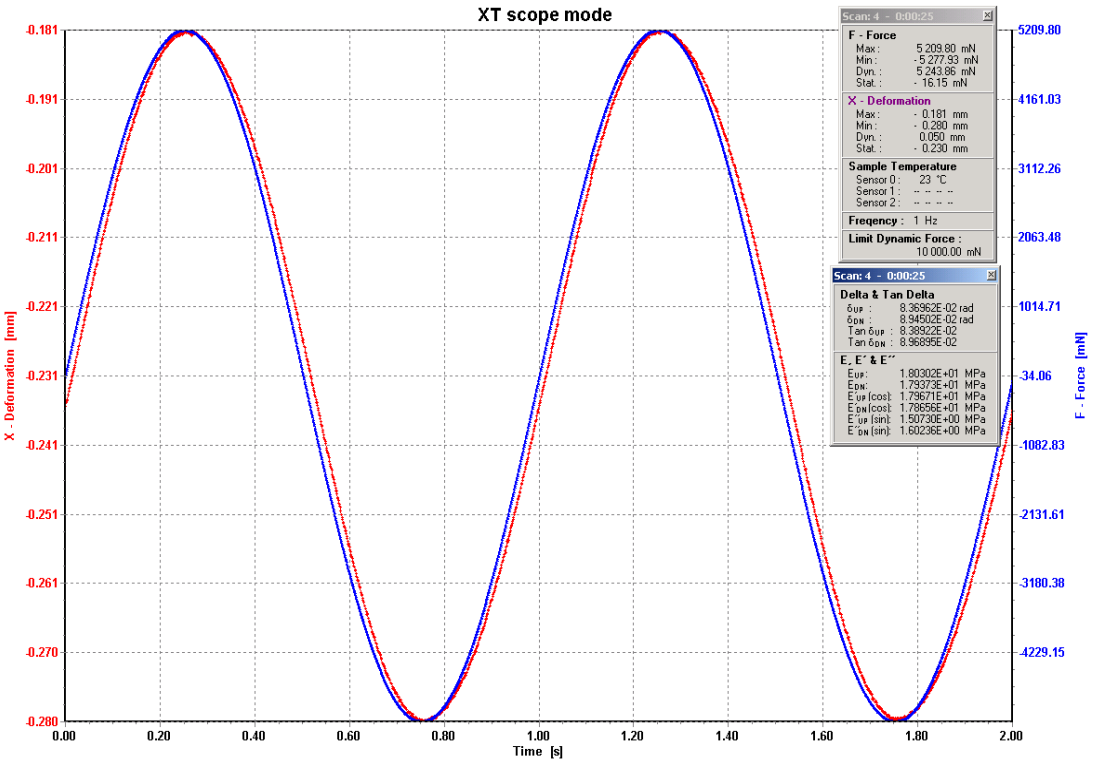

Figure 39: Deformation at the start of DMA test

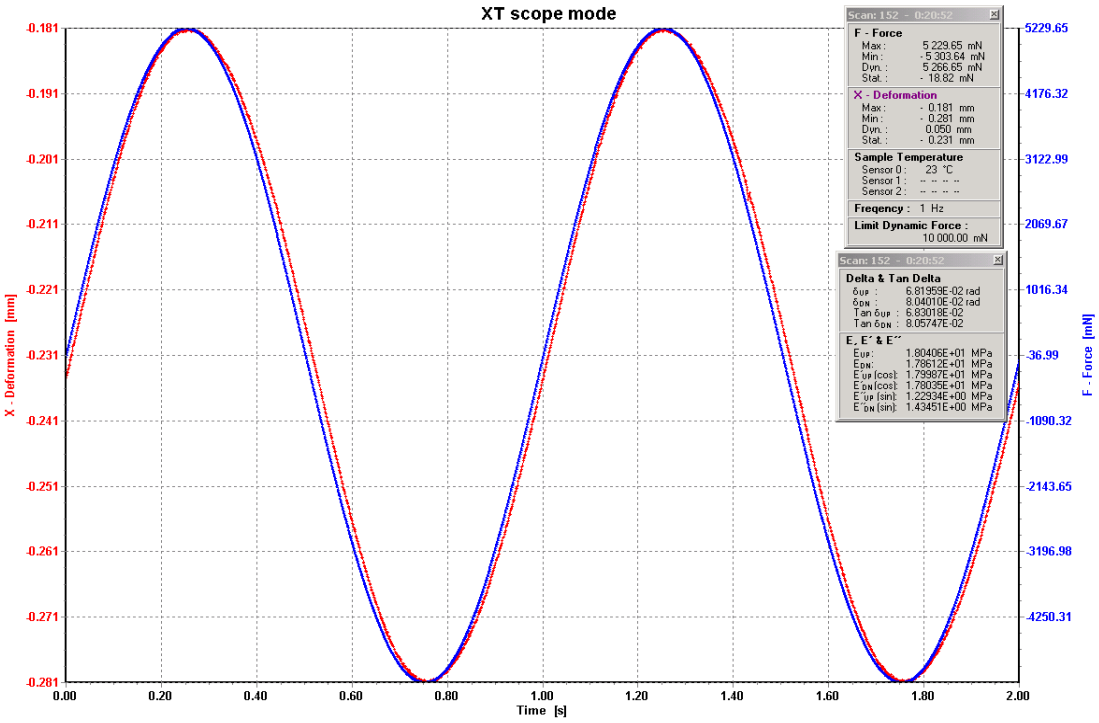

Figure 40: Deformation at the end of DMA test

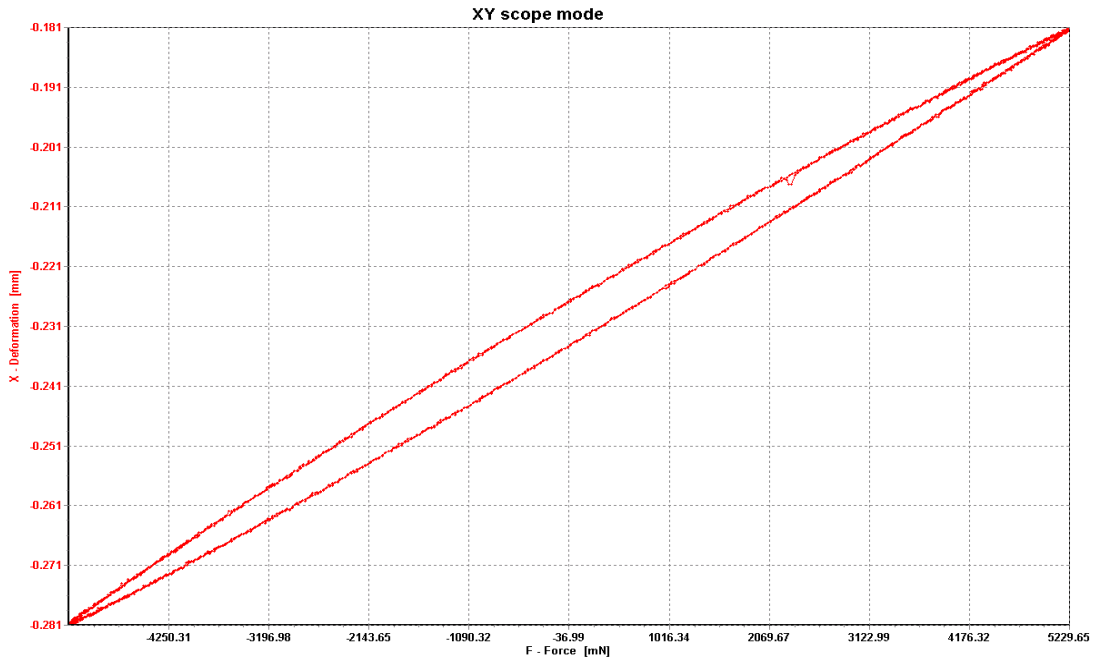

Figure 41: X- Defamation vs. Dynamically applied force on a rod specimen

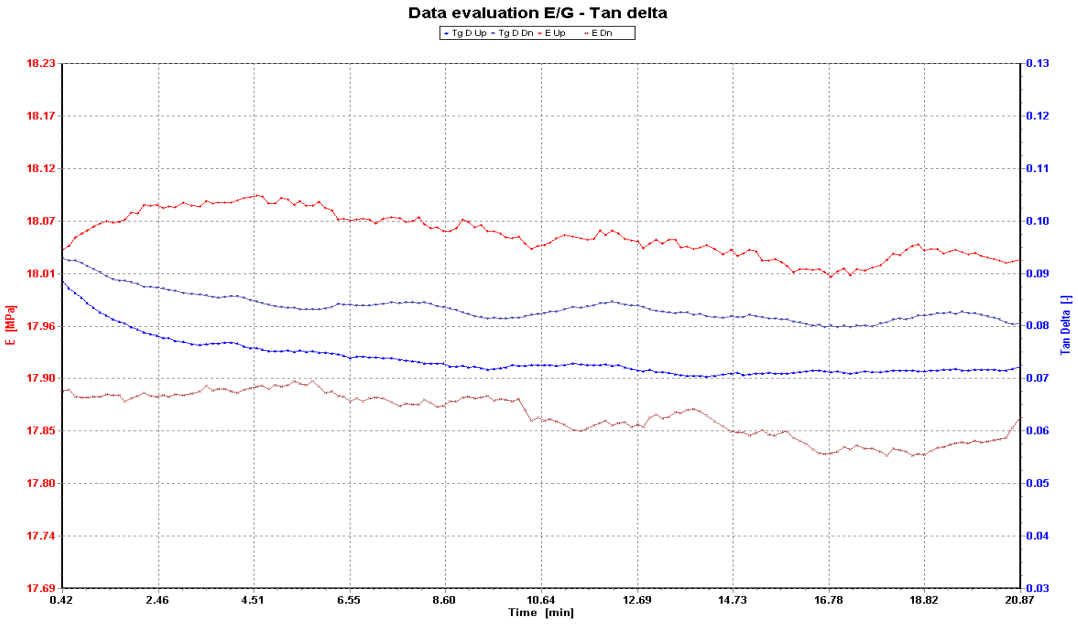

Figure 42: Complex modulus E and the loss tangent (tanδ), at *Up* and a *down* defamation direction.

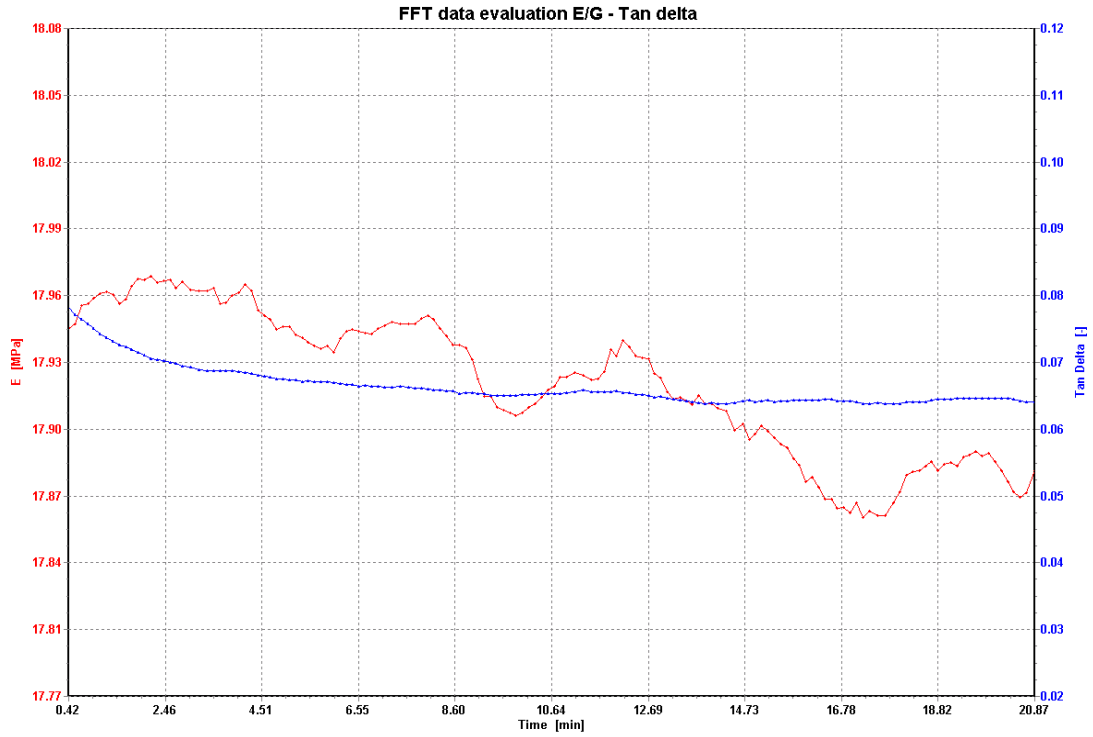

Figure 43: Complex modulus E and the loss tangent (tanδ) for the longitudinal direction of a tested sample.

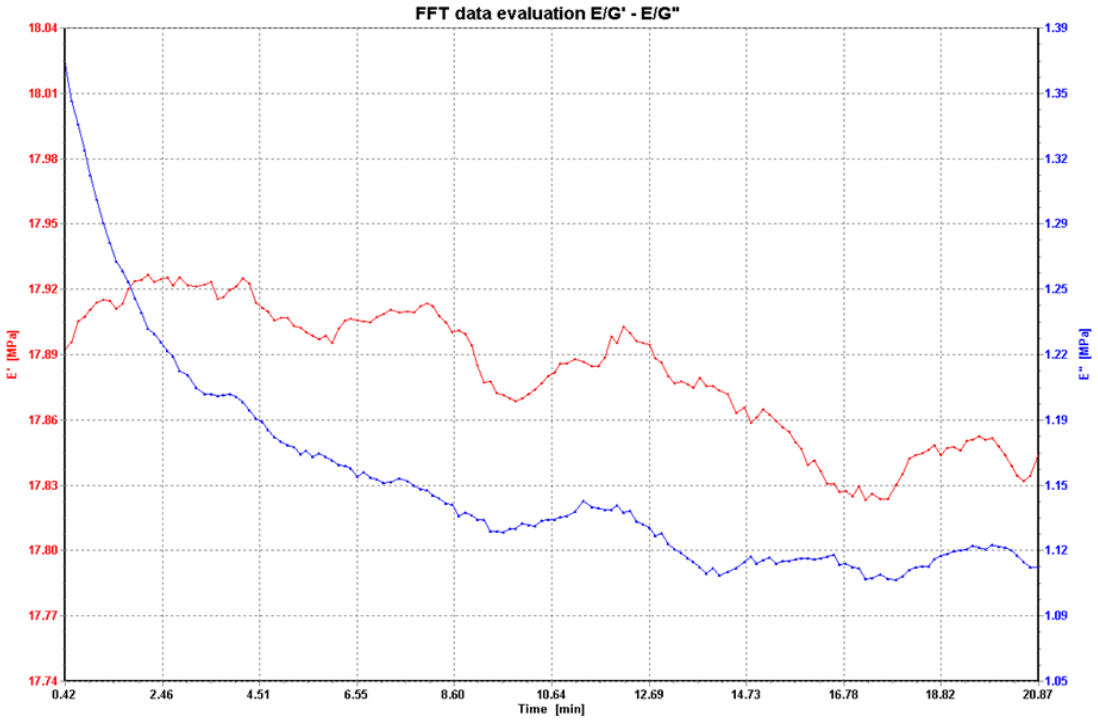

Figure 44: Storage modulus E′, & loss modulus E" of a sample in a longitudinal direction.

Dynamic mechanical testers apply a small sinusoidal stress or strain to a sample and measure the resulting strain or stress response (figure 39 and 40). The observed complex modulus, E^{**}, is defined as the instantaneous ratio of stress/strain ($\sigma_0/\mathcal{E}_0$).

$$E^{**} = \left(\frac{\sigma_o}{\varepsilon_o}\right) cos\delta + i\left(\frac{\sigma_o}{\varepsilon_o}\right) sin\delta \qquad (17)$$

This was due to the time dependent properties of viscoelasticity of the rod composite materials; as a result the response was out-of-phase with the applied stimulus. In order to understand the deformation mechanics occurring in the composite rod material this is resolved into an in-phase or elastic response, being recoverable as stored energy, defined as:

$$E' = \left(\frac{\sigma_o}{\varepsilon_o}\right) cos\delta \qquad (18)$$

And out-of-phase or viscous response, this being proportional to the irrecoverable or dissipated energy

$$E'' = \left(\frac{\sigma_o}{\varepsilon_o}\right) sin\delta \tag{19}$$

The angle, δ, is the measured phase lag between the applied stimulus and the response. tan δ is given by the ratio of loss (*E'*) to storage (*E"*) modulus and is proportional to the ratio of energy dissipated/energy stored

$$tan\delta = \left(\frac{E''}{E'}\right) \tag{20}$$

This is known as the loss tangent or damping factor, the experimental results were recorded on table 14 above. The results revealed that the dynamic machenical properties of sample #7 were relatively stable, with only 18.39% loss in strength in an up direction and 10.25 % on down direction after 20 minutes of DMA testing.

12.3 SEM results

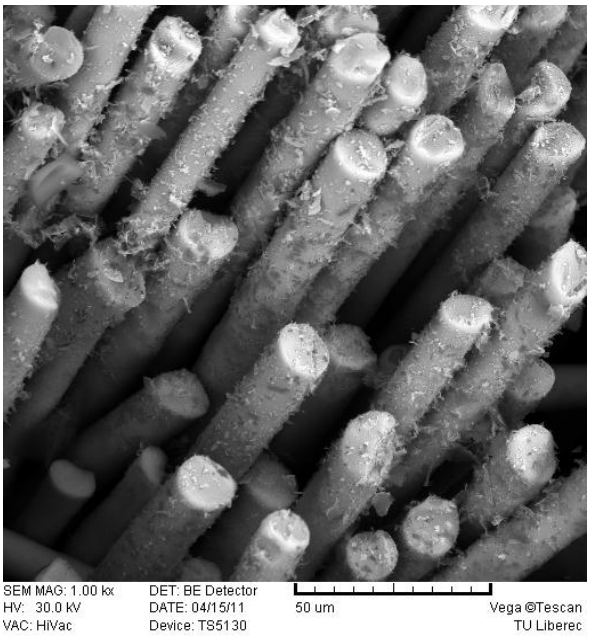

a

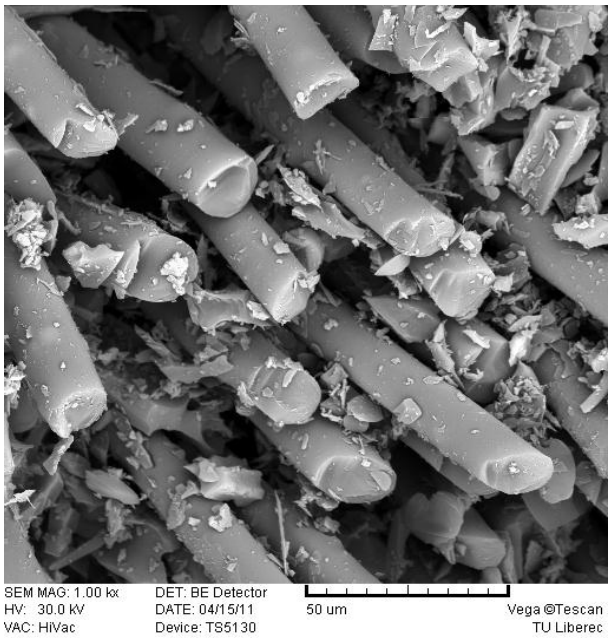

b

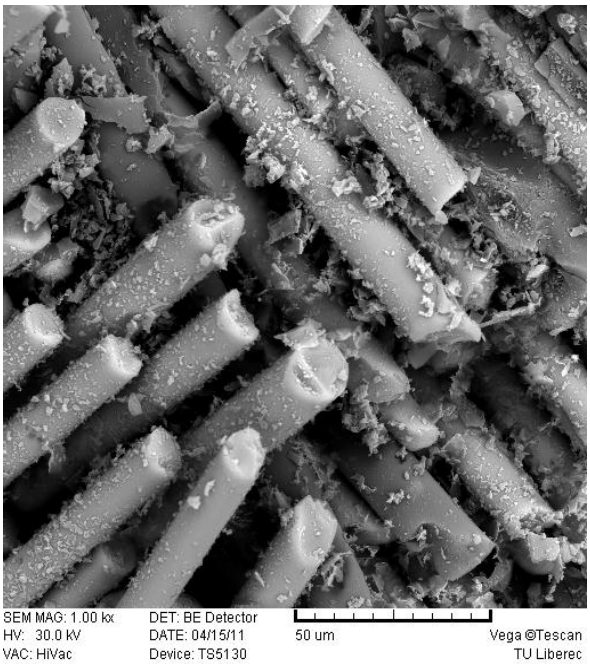

c

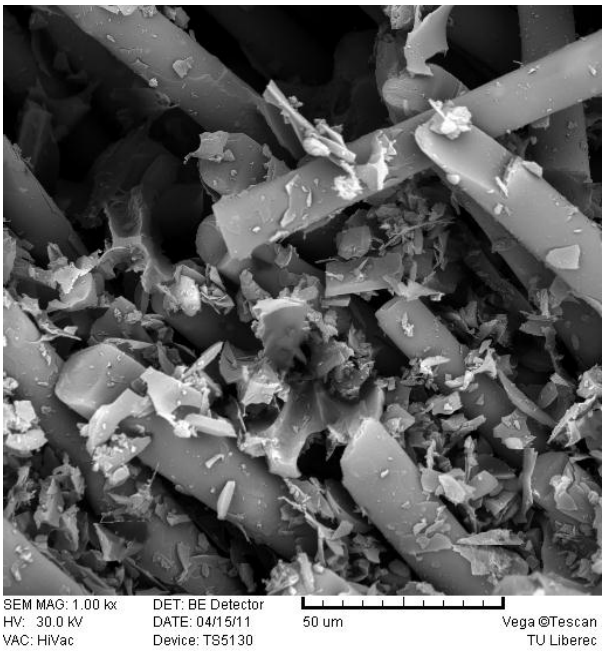

d

Figure 45: SEM image of BF:CF [33:66], with different concetration of carbonised sucrose matrix, i.e (a) 300g/l (b) 600g/l, (c) 900g/l and (d) 1200g/l. The magnification of 1000x was used.

12.4 Porosity results

Porosity (ϕ) of each composite rod was calculated from the following equation:

$$\phi = (1 - \frac{\rho_c}{\rho_s}) \quad (21)$$

The total volume V_T and total mass of each composite rod were measured (fig. 46) and calculated from equation 22 and volume of each component was calculated using the ratio of mass and density of each component. The ρ_c and ρ_s were calculated from the following equation: (see Appendix: table).

Total volume of a composite rod

$$V_T = (pi .r^2) .l \quad (22)$$

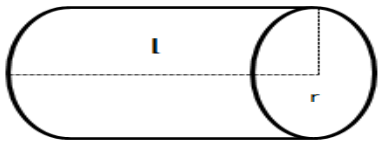

Figure 46: Composite rod

Density of composite rod

$$\rho_c = \frac{M_T}{V_T} \quad (23)$$

Volume of solid components

$$V_s = V_{BF} + V_{CF} + V_m \quad (24)$$

Overall density of solid components

$$\rho_s = \frac{M_T}{V_s} \quad (25)$$

Where ϕ – porosity of composite [%] , r- radius of a rod calculated from a 10mm diameter. V_T – total volume of a composite , V_s – total volume of solid components, V_{BF} –volume of basalt fibre, V_{CF} - volume of carbon fibre, V_m - volume of sucrose matrix. The overall density ρ_s of solid components was calculated from a ratio of M_T (Total

mass) and V_s for each specimen. A ratio of each specimen mass (g) and known densities of basalt (2.75g.cm^3), carbon fibre (1.77g/cm^3) and carbon matrix (1.95g/cm^3) were used for a calculation of V_s.

Table 15: show the relationship between the mix ratio, the concentration and the porosity of specimen 1 to 20, and their relative densities

Conc. [g/l]	Density [g/cm^3]	Porosity [%]	Density [g/cm^3]	Porosity [%]	Density [g/cm^3]	Porosity [%]	Density [g/cm^3]	Porosity [%]	Density [g/cm^3]	Porosity [%]
	BF /CF [0:100]		BF /CF [33:66]		BF /CF [50:50]		BF /CF [66:33]		BF /CF [100:0]	
300	0.31	82.50	0.34	82.61	0.39	81.53	0.51	77.53	0.72	72.63
600	0.32	81.81	0.40	79.90	0.52	78.23	0.53	76.60	0.73	72.10
900	0.36	79.79	0.41	79.38	0.46	74.41	0.54	75.90	0.69	71.54
1200	0.37	79.61	0.42	78.66	0.54	73.94	0.55	76.41	0.79	69.28

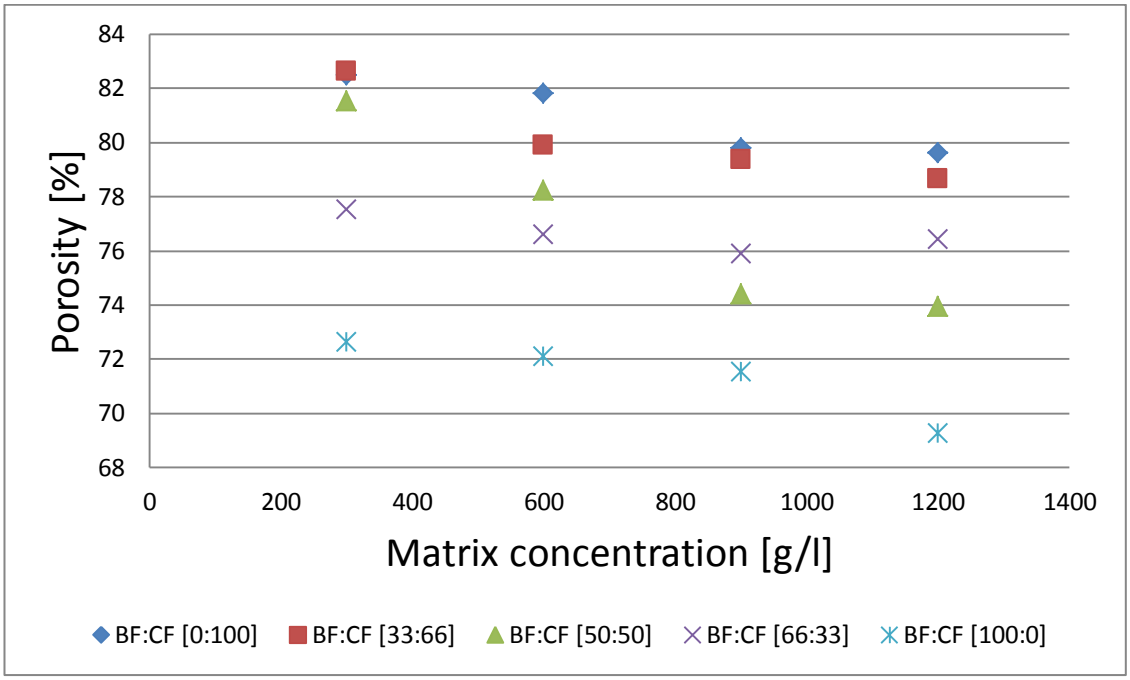

Figure 47: Porosity [%] vs. Matrix concentration [g/l] with different amounts of CF:BF components.

The composite material had very high porosity, which ranged from 82 to 69 %. The porosity was highly influenced by type fibre used, volume fraction of each component and the binding matrix concentration. SEM image (figure 45) also confirms the relationship between the matrix concentration, and the porosity of the composite rod.

12.5 Copper electroplating test results

A carbon rod was to be plated with copper. The carbon rod is connected to the negative terminal of a power supply, while the copper rod is connected to the positive terminal.

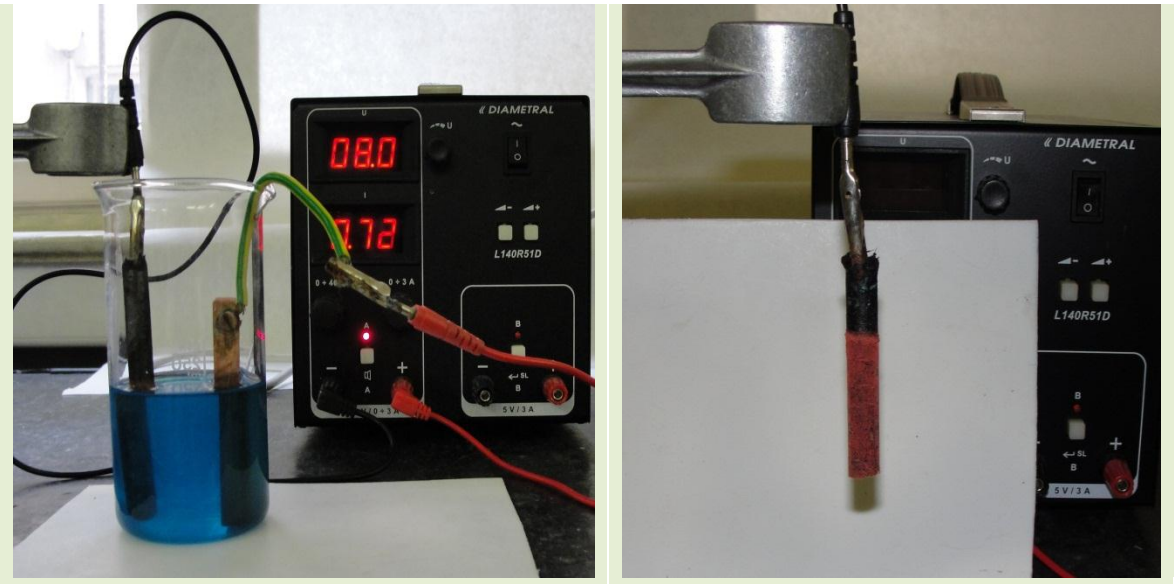

Fig. 48: Copper electroplating on carbon rod (specimen #7) . Voltage set at 8, 0v. At 15 minutes plating time

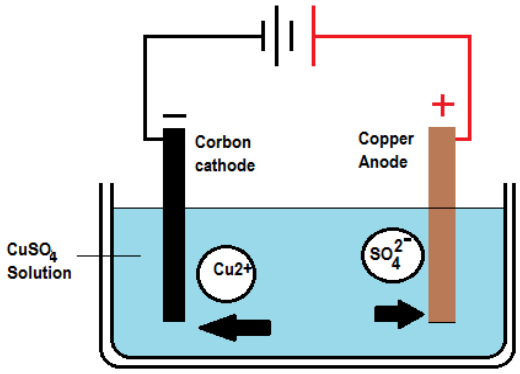

Fig. 49, Copper electroplating

In solution, copper sulphate exists as Cu^{2+} and SO^{-} ions. When a potential difference is applied across the electrodes, the Cu^{2+} ions move towards the cathode (the carbon rod here) and gains two electrons from it to become a neutral atom of copper. The liberated copper gets deposited on the carbon rod.

$$Cu^{2+} + 2e^{-} \longrightarrow Cu \quad \text{(at the cathode)} \qquad (26)$$

The SO_4^{2-} ions move to the anode and react with copper as given below.

$Cu \rightarrow Cu^{2+} + 2e-$ (27)

$Cu^{2+} + SO_4^{2-} \rightarrow CuSO_4$ (at the anode) (28)

So, two things happen. Firstly Copper goes into solution to form copper sulphate, and then it leaves behind 2 electrons on the copper electrode (fig. 49). These electrons flow to the power supply and from there to the cathode. And the copper sulphate formed ensures that the concentration of the electrolyte is maintained. These phenomena could be seen on our test sample on figure 48.

12.6 Thermal damage results

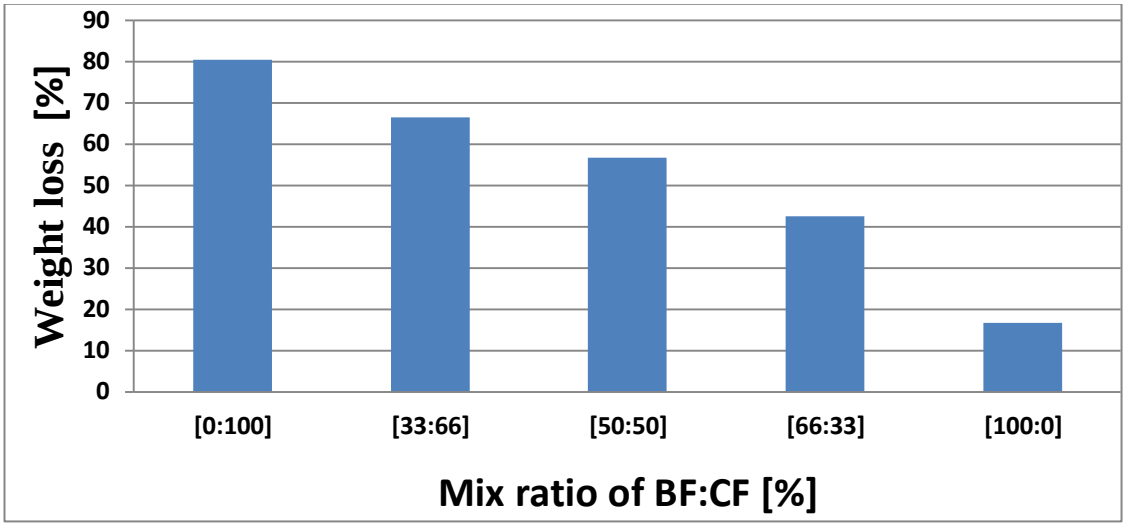

Fig. 50: Mass loss when a composite tube with a 900g/l of sucrose matrix was heated for 60 minutes at 550°C

It was proven that the thermo stability of our prepared specimen is limited. When carbon rods specimens were heated to very high temperature (550°C), carbon from a matrix reacted with O_2 to form CO_2. This resulted in a loss in binding properties of our carbon matrix. As a result the rods were damaged to a certain degree.

13. CONCLUSION

Finishing is a last and curtail step in the manufacturing process of any production line. This step determines the value, quality and applicability of a product. Hence it is known as a value adding step. In this study a series of attempts were made in order to find other possible techniques, to be used in basalt fibres finishing. This study serves as a building block, adding on a foundation laid down by other previous researcher in the field of material science, and textile engineering. Due to its good properties, basalt fibres have gradually gained a lot of attention over the years. However its use has been limited to a few applications, as compared to its counterparts like glass and carbon fibres.

To answer the problems at hand, this study first investigated the nature of basalt fibre by a qualitative analysis using Laser induced breakdown spectroscopy (LIBP). The results revealed that the tested specimen of basalt fibre had some Si, Ca, Fe and Al atomic elements. Their spectral wavelengths correlate with standard data obtained from NIST database [36], which listed the wavelengths and configurations of the corresponding elements. The downfall of this method is that some trace element can be hidden or captured by another element of similar size and charge or one having a higher ionic potential (cf. Goldschmidt's Rules of Substitution). Therefore for better qualitative analyses, there is a need to find multiple peaks of unmistakeably associated with each element. This work shows that for many trace elements, useful lines corresponding to emission from minor elements do exist and may be used for qualitative identifications and even quantitative analysis as well.

Basalt fibres may be damaged to a certain degree in the HCl and NaOH solutions with a concentration of 2g/l. In our real surrounding environments the concentration of acids and alkalis are generally in a diluted form, there for in this study a simulation of real environment acidity conditions was conducted. The results revealed that the stability of basalt in alkalis is slightly better as compared to acidic conditions. Prolonged acids and alkali action leads to flakes peeling off, from the fibre surface, and tensile strength of the fibres decreases with increasing treatment time. The rate of diffusion ions from BF which results to fibre corrosion could be even bigger if the material is exposed to acidic

environments with high turbulence flow. From this observation, it was deduced that there is a need to protect the fibres from acidic and alkali corrosion. This could be archived by applying or coating the fibres with thin sol-gel layer, of TiO_2 or ZiO_2 as a finishing technique.

Attempts to use IR laser for the modification of basalt fibre surface, proved to be less useful. At low energy levels not much effect could be observed, except a slights swelling of fibres. At high laser intensity, fibre formed bubble and holes which led to weakening of fibre tensile strength. However this technology could be useful when used as a cutting tool for basalt fibres. Further attempt to try and deposited carbon via IR laser dehydration of thin layer of sucrose led some negative effects. Thin layers of carbon were formed on the surface of basalt fibre, but high irradiation destroyed the substrate material.

An attempt to produce a carbon matrix with good binding properties, yet simpler and cheaper to prepare was rather success. Material treated with this carbon matrix possessed some electrical properties. The addition of TiO_2 in such a matrix produced a material with even better stability. Such materials could be applicable for photo-catalytic applications.

Composite rods reinforced with basalt fibre and carbons fibres were prepared by mixing mass fractions BF, CF and carbon matrix. These rods had high porosity, electrical conductivity and low relative density. Dynamic mechanical assessments of these carbon rods revealed that high concentrates of carbon matrix, binds the composite material better which results in high mechanical stability. Based on these properties, the carbon rods could well be suitable as carbon electrodes, which can be used in carbon-zinc batteries, and also other low duty electrical applications. Empirical mathematical models were generated, and they can be manipulated to optimise the electrical and mechanical properties.

14. REFERENCES

[1] Carmisciano S, et.al,. Basalt woven fibre reinforced vinyl ester composites: Flexural and electrical properties. Elsevier; Materials and design; 2010, 32:3-6.

[2] Weib B, Cao H, and Song S. Surface modification and characterization of basalt with hybrid sizing. Elsevier; Composites; 2010:1-4.

[3] Saravanan D, Spinning the Rocks - Basalt Fibres.,2006:1-2.

[4] Taylor G.J, Hawaii Institute of Geophysics and Planetology ,Mars Crust: Made of Basalt, PSR Discoveries; 2009: 7.

[5] Nelson S.A. Basaltic and Gabbric Rocks.,2004: 2-4.

[6] Militký J, Kovačič V and Křemenáková D; Basalt filaments- Properties and applications. TUL, GACR 106/531,(2005),1-26.

[7] Tomkova B, Textile Composites: Categorization of composites according to fibrous reinforcement, TUL, 2010: 6

[8] Ross A, Basalt Fibers: Alternative To Glass,CompositesWorld., 2010:1-2.

[9] Michael Z.,The main principles and device for continous basalt fibres production,BASALT-TECH, 1998: 2-5.

[10] Michael Z. , Basalt continuous fibre state of the art, market application problems and directions.BASALT-TECH, 05, 2008:1-7.

[11] Hearle J.: High Performance Fibres; The Textile Institute, Woodhead Publishing Limited, Cambridge, England, 2001, ISBN 1855735393.

[12] ASA.TEC CLASSICO Type of fiber: textile continuous fiber,www.asatec.at: pdf: 1

[13] Pasquini, J., Cortez, J., Silva, L. M. C., Gonzaga, F. B.: "Laser induced breakdown spectroscopy",Journal of the Brazilian Chemical Society, Vol. 18, No. 3, (2007): 463 - 512.

[14] Dyar M.D, and Clegg S.M, LIBS analysis of minor elemets in geological samples, Tucker, Department of Astronomy, Amherst College, Amherst, MA 01002, 40th Lunar and Planetary Science Conference, (2009):1-6.

[15] http://www.appliedspectra.com/technology/LIBS.html, 16/03/2011

[16] Andrew J., Effenberger Jr. and Jill R. Scott ,Effect of Atmospheric Conditions on LIBS Spectra. Idaho National Laboratory USA; Sensor ISSN 1424-8220: 10, (2010),:1-10.

[17] Wiener j., Prusovam M., Titenium nad carbon in textile structure by LIBS Method.,TUL, Czech Republic, 7th International Confrence, TEXCI; 2010:1-4.

[18] Shokrieh M.M., & Memar M., Stress Corrosion Cracking of Basalt/Epoxy Composites under Bending Loading., Elsevier: Corrosion Science, 53, (2009): 2-5.

[19] Wei B., Cao H. & Song S., Degradation of basalt fibre and glass fibre/epoxy resin composites in seawater. Springer Science., 53, 2010: 428-431

[20] Weib B, Cao H, and Songb S, Environmental resistance and mechanical performance of basalt and glass fibers, Harbin Institute of Technology, Elsevier: Materials science and engineering,2; 2010:1-6.

[21] Esteves E.F., H. Alonso, Effect of CO2 laser radiation on surface properties of synthetic fibres, University of Minho, Guimarães, Portugal,: 1-5.

[22] Warren S.W.: Physical Basis of Chemstry, 2nd edition, A Harcourt Science and Technology Company, Princeton University, New Jersey, 2000/2001,:178

[23] Avadhanulu M.N.: An Introduction to Lasers Theory and Applications, 1st Ed., S. Chand & Company Ltd., Ram Nagar, New Delhi-110055, 2001, ISBN: 81-219-2071

[24] Rubahn H. G.: Laser Applications in Surface Science and Technology, John Wiley & Sons Ltd, Chichester, 1999, ISBN 0-471-98450-7, pp 203-205.

[25] Kennedy L.J., Vijaya J., Sekaran G., Electrical conductivity study of porous carbons derived from rice husk, Central Leather Research Institute, Adyar, Chennai, Tamil Nadu, India:2-7

[26] Lysenko D, A. Shvets A.V., P. S. Yaremov, Effects of the conditions of the matrix carbonization of sucrose on the structure and adsorption of mesoporus carbon material,Vol.44.No.6.2008: 2-5.

[27] Abdel-Fattah T, Pyrolytic Synthesis of Carbon Nanotubes from Sucrose on Mesoporous Silicate Nanotubes, and Carbon Nanostructures, 14: 585–594, 2006: 2-10.

[28] Sakintuna B, Akta Z and Yürüm Y, Synthesis of porous carbon materials by carbonization in natural zeolite nanochannels, , Sabanci University Tandoğan, Ankara, Turkey,:1-2.

[29] Frackowiak E. et.al., Supercapacitor electrodes from carbon prepared in MCM-48 Template, 2002,: 4,5

[30] Tae-Wan Kim and Leonid A. Solovyovb, Synthesis and characterization of large-pore ordered mesoporous carbons using gyroidal silica template DOI: 10.1039/b516945c, Journal of Materials Chemistry, 2006,:1-8

[31] Chen B., el.al., Conductivity of carbon fibre reinforced cement-based composites., 26; 2004:1-5.

[32] Camila Ramos da Silva, Martin Wallau and Ernesto A. Urquieta-González Mesoporous Carbons Prepared by Nano-Casting with Meso- or Non-Porous Silica Nanoparticles. CP 676,Vol.17, No. 6, 2006.,1170-1180.

[33] Kopachevskii V.D., and Krivosheeva M.V., Refractories and Industrial Ceramics, 48(4), (2007),:255–258

[34] Cegarra Jose, Dyeing Of Textile Materials: the Scientific Base And The Techniques Of Application, 1992,:123-125.

[35] Ralchenko, Yu., Kramida, A.E., Reader, J., and NIST ASD Team (2010). NIST Atomic Spectra Database (ver. 4.0.1), [Online]. Available: http://physics.nist.gov/asd [2011, May 6]. National Institute of Standards and Technology, Gaithersburg, MD.

15. APPENDIX

15.1 Chemical corrosion resistance

Table 16: Calculated rest weights and relative degradation rates for acid

Time [hr]	1/ t [hr-1]	Rz %	ΔRz %	1/ΔRz [per %]	K [% hr-1]	ΔR∞ [mass %]	ΔRz [mass %]
0	-	100	0	-	0.011	0.788084	0
1	-			-	0.011	0.788084	0.082428
2	-	99.89	0.11	-	0.011	0.788084	0.116252
3	-			-	0.011	0.788084	0.14199
4	-	99.85	0.15	-	0.011	0.788084	0.163508
12	-			-	0.011	0.788084	0.277131
24	0.041667	99.64	0.36	2.777778	0.011	0.788084	0.379613
33	-	-	-	-	0.011	0.788084	0.434815
48	0.020833	99.5	0.5	2	0.011	0.788084	0.504753
55	-	-	-	-	0.011	0.788084	0.530964
72	0.013889	99.44	0.56	1.785714	0.011	0.788084	0.582896

Table 17: Table 16. calculated rest weights and relative degradation rates in 2g/l of NaOH

Time [hr]	1/ t [hr-1]	Rz %	ΔRz %	1/ΔRz [per %]	K [% hr-1]	ΔR∞ [mass%]	ΔRz [mass %]
0	-	100	0	-	0.027	0.359221	0
1	-	-	-	-	0.027	0.359221	0.05863
2	-	99.95	0.05	-	0.027	0.359221	0.082361
3	-	-	-	-	0.027	0.359221	0.1002
4	0.25	99.88	0.12	8.333333	0.027	0.359221	0.114935
12	-	-	-		0.027	0.359221	0.188976
24	0.041667	99.72	0.28	3.571429	0.027	0.359221	0.248073
33	-	-	-		0.027	0.359221	0.275866
48	0.020833	99.7	0.3	3.333333	0.027	0.359221	0.306156
55	-	-	-		0.027	0.359221	0.31593
72	0.013889	99.68	0.32	3.125	0.027	0.359221	0.332521

15.2 Mechanical test by Tera 2300

Table 18: Mechanical properties of laser irradiated woven basalt fabric, using Tera test 2300 in a weft direction

Pixel time (100 µs)	Amax mm	Fmax N	W J	E MPa	t sec	Amax %	E MPa
Number of tests	3	3	3	3	3	3	3
Average value	7.88074	1575.55334	12.486973	3135.24	8.11	3.72	3135.24
Standard deviation	0.5791	71.21367	1.913475	40.08	0.73	0.29	40.08
Variance coefficient	7.77896	4.51991	15.323773	1.28	9.04	7.78	1.28
Minimum value	7.37428	1493.45593	10.277534	3091.05	7.28	3.45	3091.05
Maximum value	8.05541	1620.65198	13.604712	3169.25	8.66	4.03	3169.25

Table 19: Mechanical properties of laser irradiated woven basalt fabric, using Tera test 2300 in a weft direction

Pixel time (500 µs)	Amax mm	Fmax N	W J	E MPa	t sec	Amax %	E MPa
Number of tests	3	3	3	3	3	3	3
Average value	6.6859	769.30298	5.087422	1954.35	7.59	3.34	1954.35
Standard deviation	0.21869	39.7676	0.1157	78.04	0.45	0.11	78.04
Variance coefficient	3.27086	5.1693	2.274236	3.99	5.92	3.27	3.99
Minimum value	6.46567	729.91339	4.986835	1880.8	7.1	3.23	1880.8
Maximum value	6.90301	809.43811	5.213861	2036.2	7.98	3.45	2036.2

Table 20: Mechanical properties of laser irradiated woven basalt fabric, using Tera test 2300 in a weft direction

Pixel time (500 µs)	Amax mm	Fmax N	W J	E MPa	t sec	Amax %	E MPa
Number of tests	3	3	3	3	3	3	3
Average value	5.1054	159.9489	0.94532	157.9	6.39	2.55	157.99
Standard deviation	0.2426	51.57466	0.166378	50.68	1.7	0.12	50.68
Variance coefficient	4.7522	32.24446	17.60017	32.08	26.55	4.75	32.08
Minimum value	4.86941	121.33081	0.762653	122.29	5.22	2.43	122.29
Maximum value	5.35417	218.519	1.088193	216	8.34	2.68	216

Table 21: Mechanical properties of laser irradiated woven basalt fabric, using Tera test 2300 in a weft direction

Untreated	Amax	Fmax	W	E	t	Amax	E
	mm	N	J	MPa	sec	%	MPa
Number of tests	3	3	3	3	3	3	3
Average value	7.87688	2111.39941	7.309371	4018.38	5.12	3.94	4018.38
Standard deviation	0.36675	112.17332	0.813067	130.63	0.26	0.18	130.63
Variance coefficient	4.65606	5.31275	11.123629	3.25	4.99	4.66	3.25
Minimum value	7.61526	2012.56604	6.370525	3881.55	4.84	3.81	3881.55
Maximum value	8.29609	2233.32007	7.781037	4141.76	5.34	4.15	4141.76

15.3 Porosirty measurements

Table 22: C-composite Porosity (ϕ) measurements and calculations results

Sample #	Sample [g]	BF [g]	CF [g]	CM [g]	Vol BF [cm3]	Vol CF [cm3]	Vol CM [g]	Vol S/s [g]	density [g/cm3]	Total vol	density of sample	porosity [%]
1	2.09	0	2	0.09	0	1.129943503	0.046153846	1.1760973	1.777063779	6.72281	0.310881908	82.50586661
2	2.257	0	2	0.257	0	1.129943503	0.131794872	1.2617384	1.788801899	6.9387881	0.325272938	81.81615648
3	2.492	0	2	0.492	0	1.129943503	0.252307692	1.3822512	1.802856101	6.8406163	0.364294664	79.7934697
4	2.656	0	2	0.656	0	1.129943503	0.336410256	1.4663538	1.811295524	7.194035	0.369194756	79.61708889
5	2.183	0.66	1.34	0.183	0.24	0.757062147	0.093846154	1.0909083	2.001084783	6.2751463	0.347880338	82.61541234
6	2.37	0.66	1.34	0.37	0.24	0.757062147	0.18974359	1.1868057	1.99695698	5.90602	0.401285468	79.90515209
7	2.446	0.66	1.34	0.446	0.24	0.757062147	0.228717949	1.2257801	1.995463957	5.9452888	0.411418201	79.38232864
8	2.469	0.66	1.34	0.469	0.24	0.757062147	0.240512821	1.237575	1.995030657	5.7999944	0.425690068	78.66247987
9	2.138	1	1	0.138	0.363636364	0.564971751	0.070769231	0.9993773	2.139332064	5.4112338	0.395103982	81.53143272
10	2.252	1	1	0.252	0.363636364	0.564971751	0.129230769	1.0578389	2.128868615	4.303855	0.523251829	75.42113096
11	2.403	1	1	0.403	0.363636364	0.564971751	0.206666667	1.1352748	2.116668175	5.2188169	0.460449189	78.24651048
12	2.504	1	1	0.504	0.363636364	0.564971751	0.258461538	1.1870697	2.109396018	4.555175	0.549704457	73.94019651
13	2.229	1.34	0.66	0.229	0.487272727	0.372881356	0.117435897	0.97759	2.280097018	4.3509775	0.512298673	77.53171602
14	2.309	1.34	0.66	0.309	0.487272727	0.372881356	0.158461538	1.0186156	2.26680207	4.3549044	0.53020682	76.6099199
15	2.404	1.34	0.66	0.404	0.487272727	0.372881356	0.207179487	1.0673336	2.252341786	4.429515	0.542723075	75.90405337
16	2.439	1.34	0.66	0.439	0.487272727	0.372881356	0.225128205	1.0852823	2.247341568	4.6022975	0.529952703	76.41868462
17	2.191	2	0	0.191	0.727272727	0	0.097948718	0.8252214	2.655044913	3.01584	0.726497427	72.63709463
18	2.214	2	0	0.214	0.727272727	0	0.10974359	0.8370163	2.645109725	3.0001325	0.737967406	72.10068832
19	2.312	2	0	0.312	0.727272727	0	0.16	0.8872727	2.605737705	3.3456975	0.691036772	73.4801868
20	2.334	2	0	0.334	0.727272727	0	0.171282051	0.8985548	2.59750441	2.9255219	0.797806374	69.28565853

15.4 DMA analysis results

Table 23: DMA test results for all 20 samples (BF: CF rods)

Sample # 1 [0:100] 300 g/l	**At starting time**	**At finishing time**		**Sample # 11 [50:50] 900g/l**	**At starting time**	**At finishing time**
F-force (Max) [mN]	not tested	not tested		F-force (Max) [mN]	4830.84	4840.77
F-force (Min) [mN]	not tested	not tested		F-force (Min) [mN]	4882.27	4.887
X Deformation (Max) [mm]	not tested	not tested		X Deformation (Max) [mm]	0.032	0.044
X Deformation (Min) [mm]	not tested	not tested		X Deformation (Min) [mm]	0.068	0.057
Sample # 2 [0:100] 600 g/l	**At starting time**	**At finishing time**		**Sample # 12 [50:50] 1200g/l**	**At starting time**	**At finishing time**
F-force (Max) [mN]	2289.55	2336.02		F-force (Max) [mN]	7276.04	7305.36
F-force (Min) [mN]	-2301.73	2.351.36		F-force (Min) [mN]	7396.4	7435.29
X Deformation (Max) [mm]	0.039	0.041		X Deformation (Max) [mm]	0.174	0.174
X Deformation (Min) [mm]	0.06	0.059		X Deformation (Min) [mm]	0.274	0.274
Sample # 3 [0:100] 900g/l	**At starting time**	**At finishing time**		**Sample # 13 [66:33] 300g/l**	**At starting time**	**At finishing time**
F-force (Max) [mN]	2995.14	3036.65		F-force (Max) [mN]	2457.83	2630.17
F-force (Min) [mN]	3038	3084.02		F-force (Min) [mN]	2487.15	2667.16
X Deformation (Max) [mm]	0.12	0.12		X Deformation (Max) [mm]	0.069	0.075
X Deformation (Min) [mm]	0.22	0.219		X Deformation (Min) [mm]	0.029	0.025
Sample # 4 [0:100] 1200g/l	**At starting time**	**At finishing time**		**Sample # 14 [66:33] 600g/l**	**At starting time**	**At finishing time**
F-force (Max) [mN]	4229.47	4470.39		F-force (Max) [mN]	5711.47	6039.91
F-force (Min) [mN]	4270.07	4524.52		F-force (Min) [mN]	5796.74	6150.89
X Deformation (Max) [mm]	0.209	0.209		X Deformation (Max) [mm]	0.041	0.036
X Deformation (Min) [mm]	0.308	0.309		X Deformation (Min) [mm]	0.059	0.064
Sample # 5 [33:66] 300g/l	**At starting time**	**At finishing time**		**Sample # 15 [66:33] 900g/l**	**At starting time**	**At finishing time**
F-force (Max) [mN]	1343.5	1346.66		F-force (Max) [mN]	6814.94	7038.74
F-force (Min) [mN]	1366.51	1355.23		F-force (Min) [mN]	6927.76	7178.17
X Deformation (Max) [mm]	0.129	0.125		X Deformation (Max) [mm]	0.175	0.175
X Deformation (Min) [mm]	0.227	0.225		X Deformation (Min) [mm]	0.274	0.275
Sample # 6 [33:66] 600g/l	**At starting time**	**At finishing time**		**Sample # 16 [66:33] 1200g/l**	**At starting time**	**At finishing time**
F-force (Max) [mN]	4692.34	4867.84		F-force (Max) [mN]	5665.46	5929.83
F-force (Min) [mN]	4752.8	4938.67		F-force (Min) [mN]	5746.66	6023.67
X Deformation (Max) [mm]	0.048	0.048		X Deformation (Max) [mm]	0.038	0.037
X Deformation (Min) [mm]	0.052	0.052		X Deformation (Min) [mm]	0.061	0.062
Sample # 7 [33:66] 900g/l	**At starting time**	**At finishing time**		**Sample # 17 [100:0] 300g/l**	**At starting time**	**At finishing time**
F-force (Max) [mN]	5209.8	5229.95		F-force (Max) [mN]	6442.78	6574.51
F-force (Min) [mN]	5277.93	5303.64		F-force (Min) [mN]	6542.78	9700.83
X Deformation (Max) [mm]	0.181	0.181		X Deformation (Max) [mm]	0.2	0.199
X Deformation (Min) [mm]	0.28	0.281		X Deformation (Min) [mm]	0.299	0.3
Sample # 8 [33:66] 1200g/l	**At starting time**	**At finishing time**		**Sample # 18 [100:0] 600g/l**	**At starting time**	**At finishing time**
F-force (Max) [mN]	3816.22	3902.39		F-force (Max) [mN]	9728.91	9708.15
F-force (Min) [mN]	3858.18	3947.05		F-force (Min) [mN]	9965.31	9987.86
X Deformation (Max) [mm]	0.154	0.157		X Deformation (Max) [mm]	0.033	0.028
X Deformation (Min) [mm]	0.254	0.257		X Deformation (Min) [mm]	0.067	0.017
Sample # 9 [50:50] 300g/l	**At starting time**	**At finishing time**		**Sample # 19 [100:0] 900g/l**	**At starting time**	**At finishign time [20 minutes]**
F-force (Max) [mN]	2545.35	2770.92		F-force (Max) [mN]	7752.45	7808.84
F-force (Min) [mN]	2607.16	2813.33		F-force (Min) [mN]	7890.05	7961.33
X Deformation (Max) [mm]	0.163	0.17		X Deformation (Max) [mm]	0.199	0.203
X Deformation (Min) [mm]	0.07	0.07		X Deformation (Min) [mm]	0.298	0.305
Sample # 10 [50:50] 600g/l	**At starting time**	**At finishing time**		**Sample # 20 [100:0] 1200g/l**	**At starting time**	**At finishing time**
F-force (Max) [mN]	5766.97	5997.95		F-force (Max) [mN]	5665.46	5929.83
F-force (Min) [mN]	5890.88	6105.77		F-force (Min) [mN]	5746.66	6023.67
X Deformation (Max) [mm]	0.052	0.053		X Deformation (Max) [mm]	0.038	0.037
X Deformation (Min) [mm]	0.048	0.048		X Deformation (Min) [mm]	0.061	0.062

NB: The machenical strength of sample # 1so weak to an extent that it broke during initial DMA test, therefore it was “not tested”, and its results could not be included in the table above.

Figure 51: Graphs of DMA analysis for sample # 2, with 600g/l matrix and BF: CF [0:100].

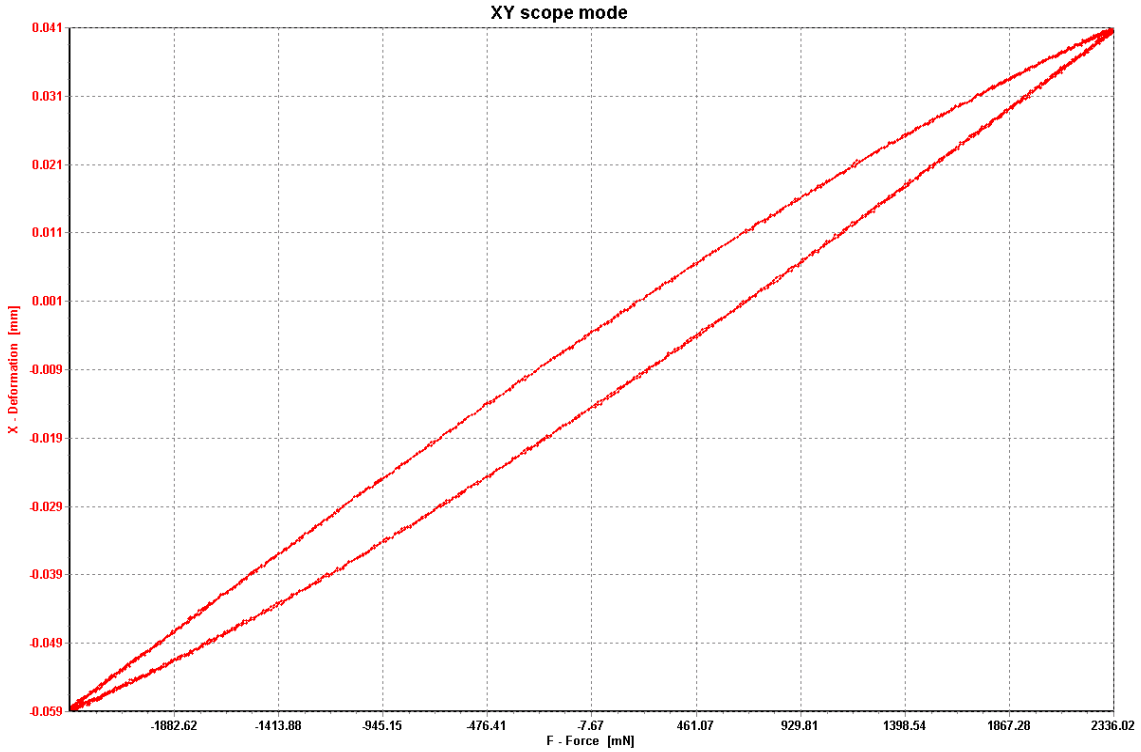

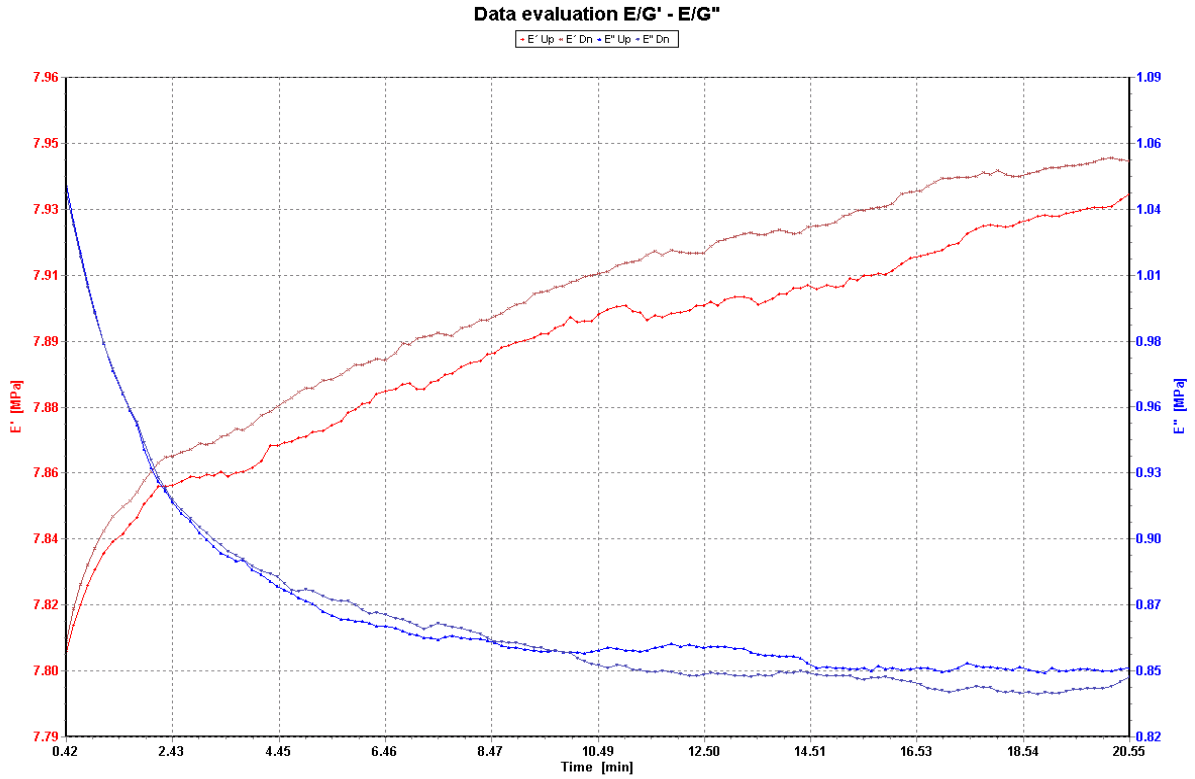

Figure 52: Graphs of DMA analysis for sample # 3, with 900g/l matrix and BF:CF [0:100].

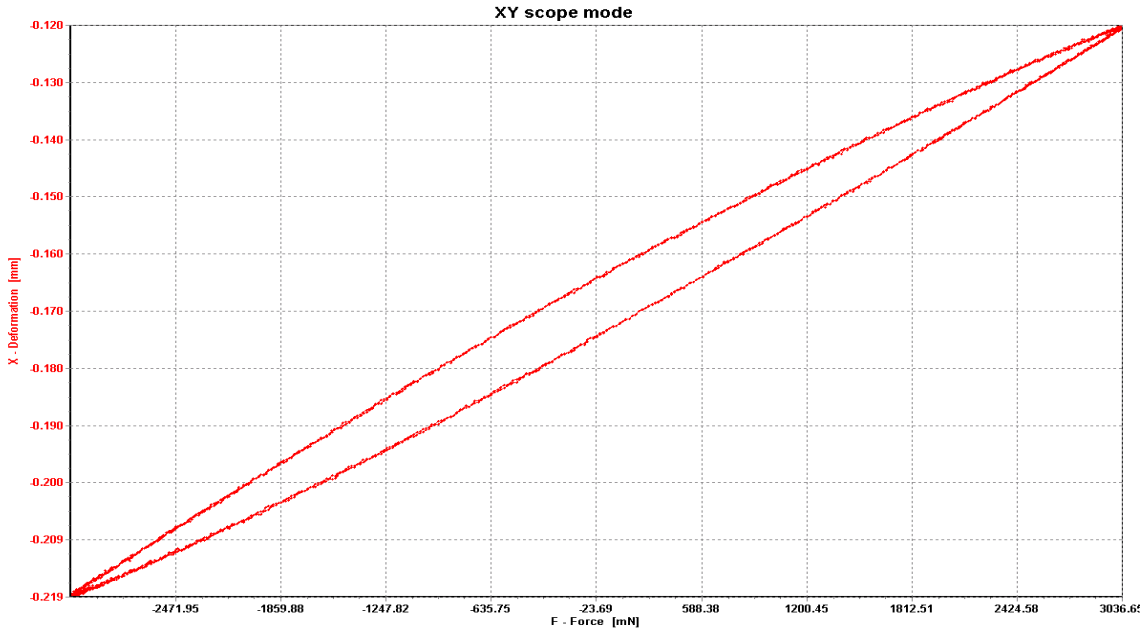

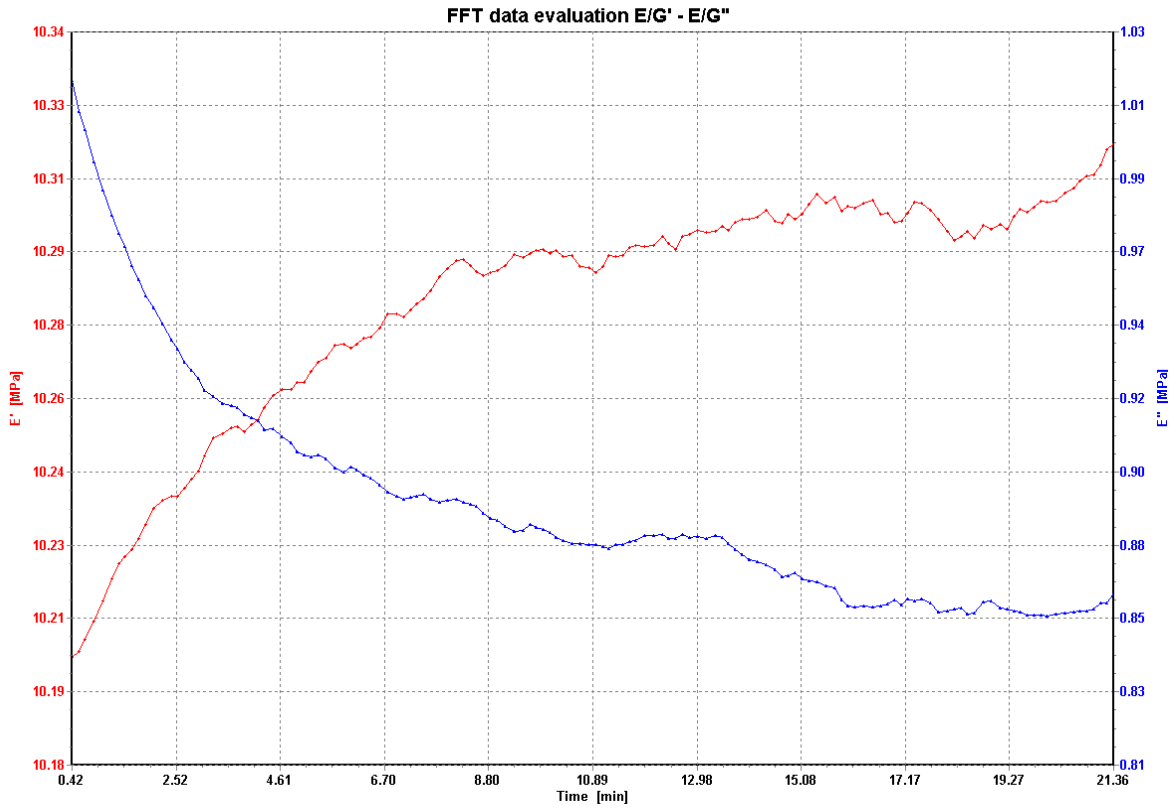

Figure 53: Graphs of DMA analysis for sample # 11, with 900g/l matrix and BF:CF [50:50]

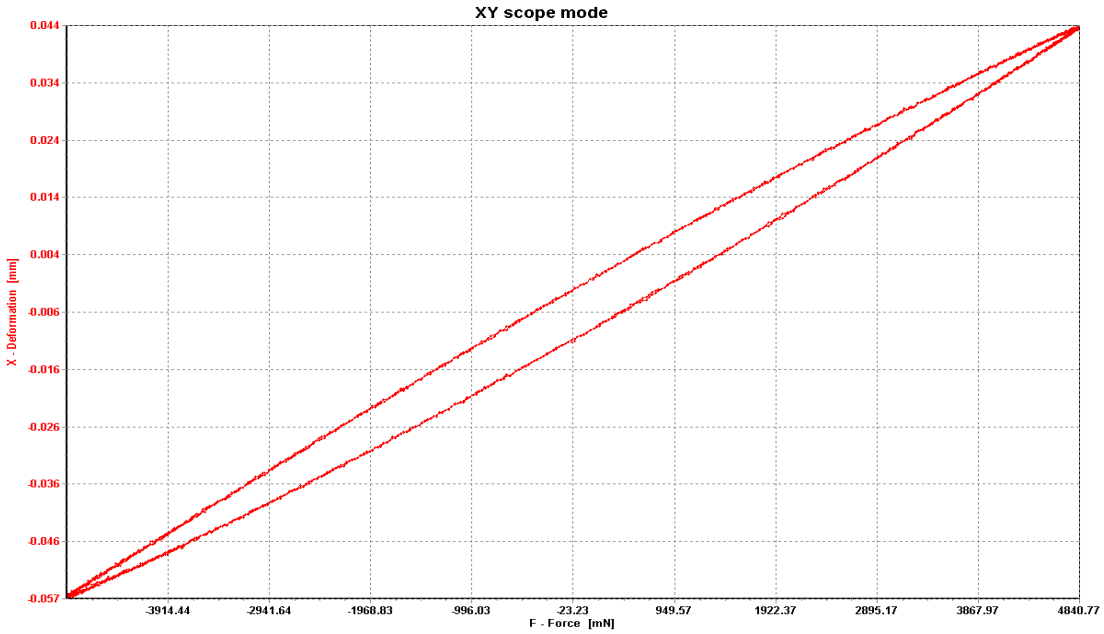

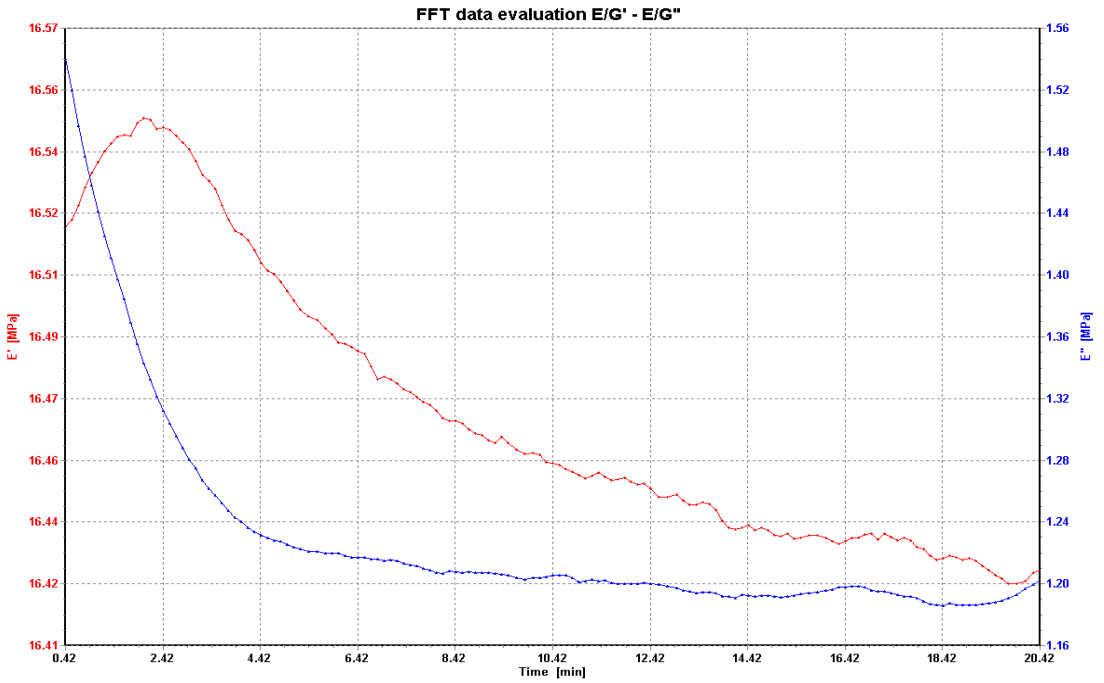

Figure 54: Graphs of DMA analysis for sample # 15, with 900g/l matrix and BF: CF [66:33]

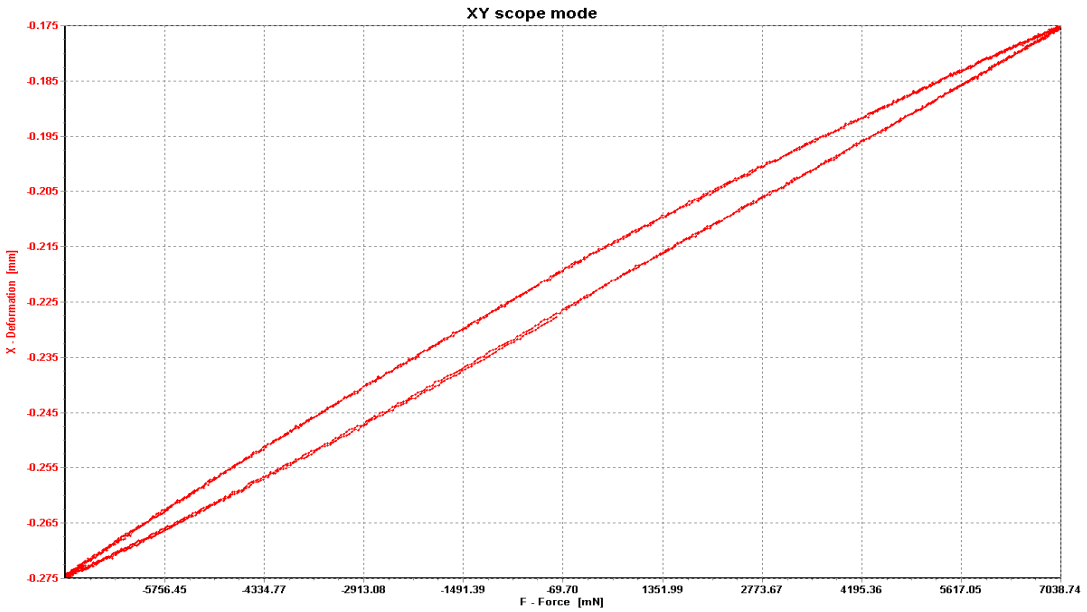

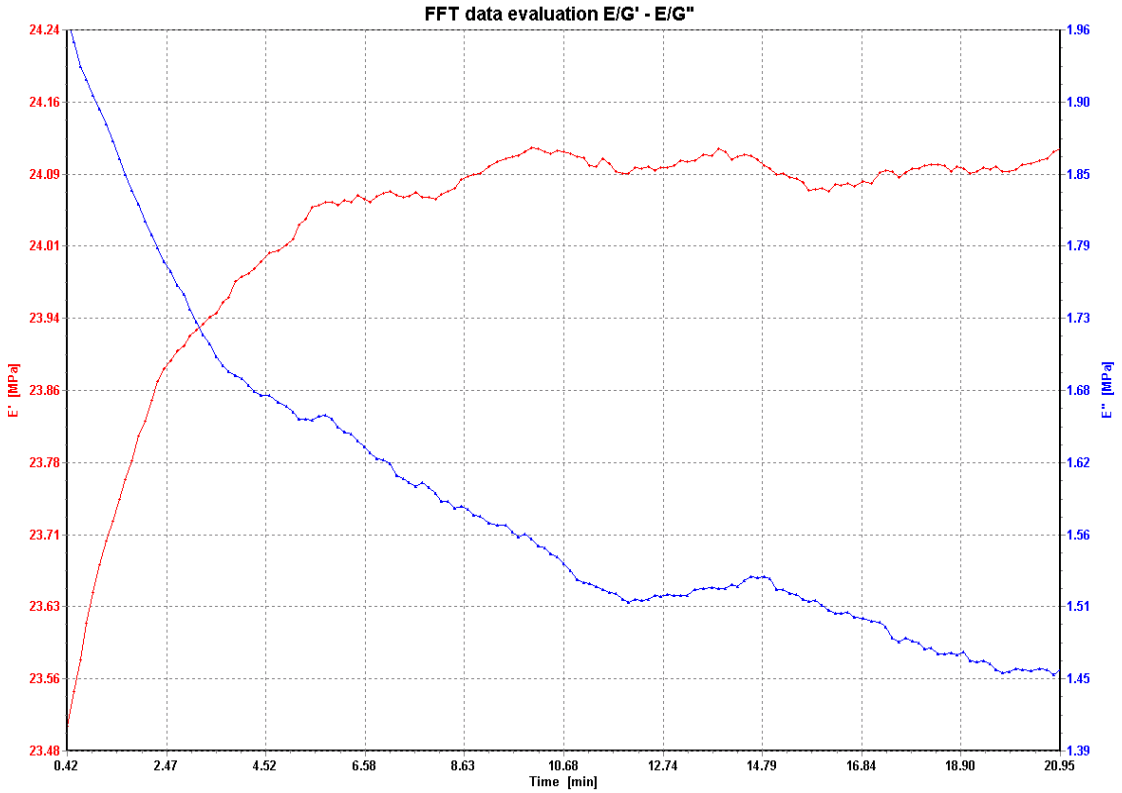

Figure 55: Graphs of DMA analysis for sample # 16, with 1200g/l matrix and BF:CF [66:33]

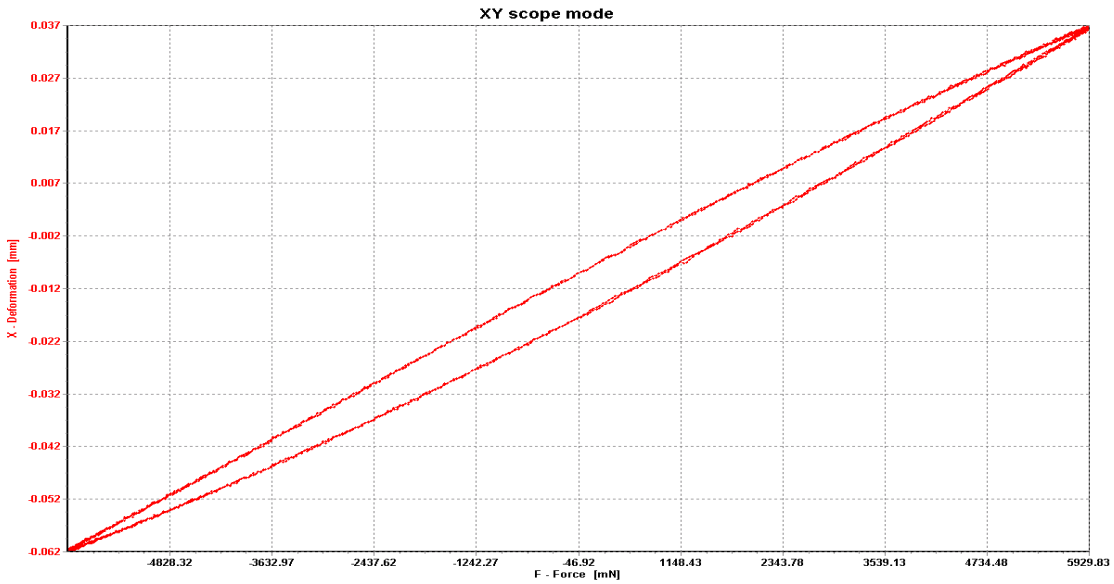

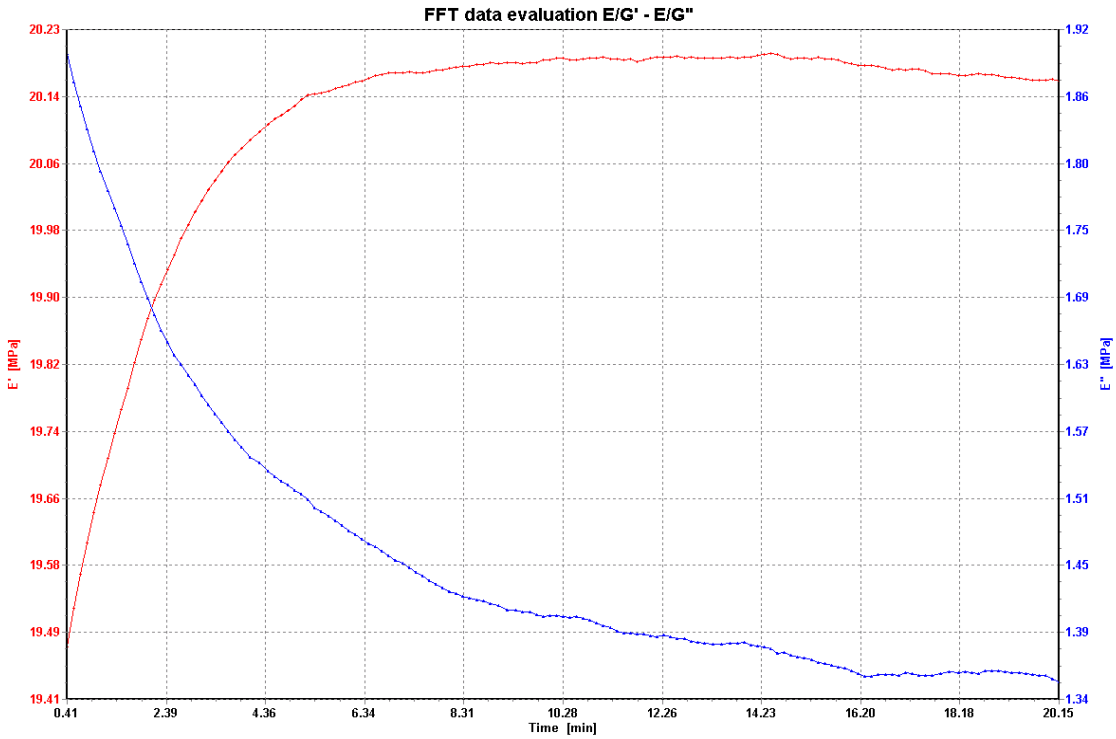

Figure 56: Graphs of DMA analysis for sample # 19, with 900g/l matrix and BF: CF [100:0]

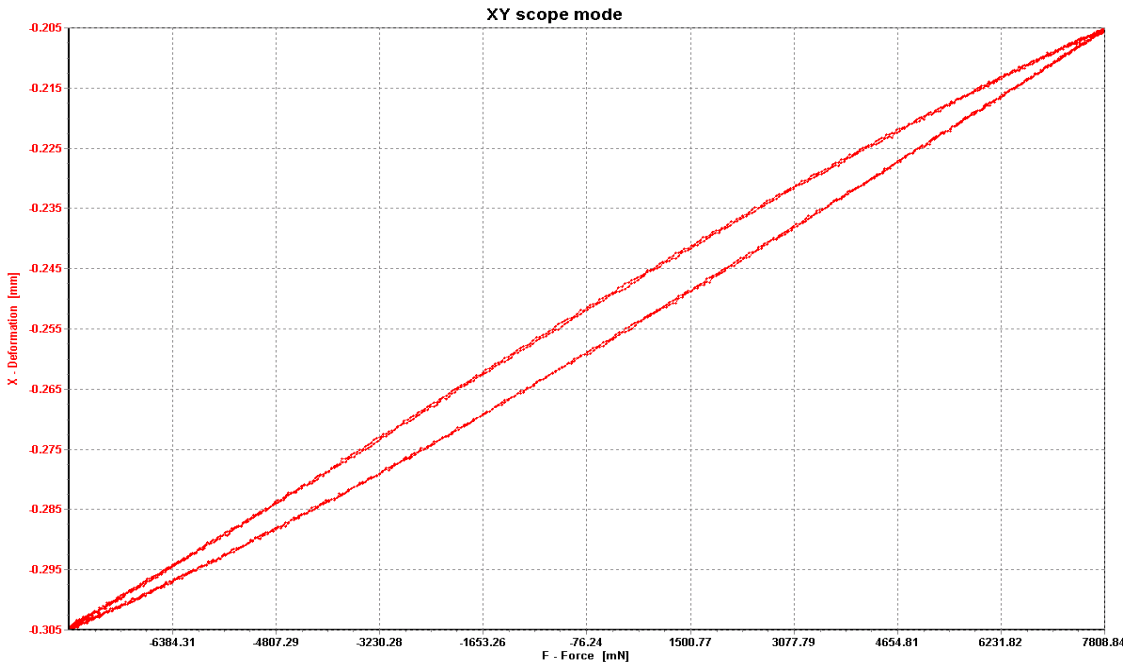

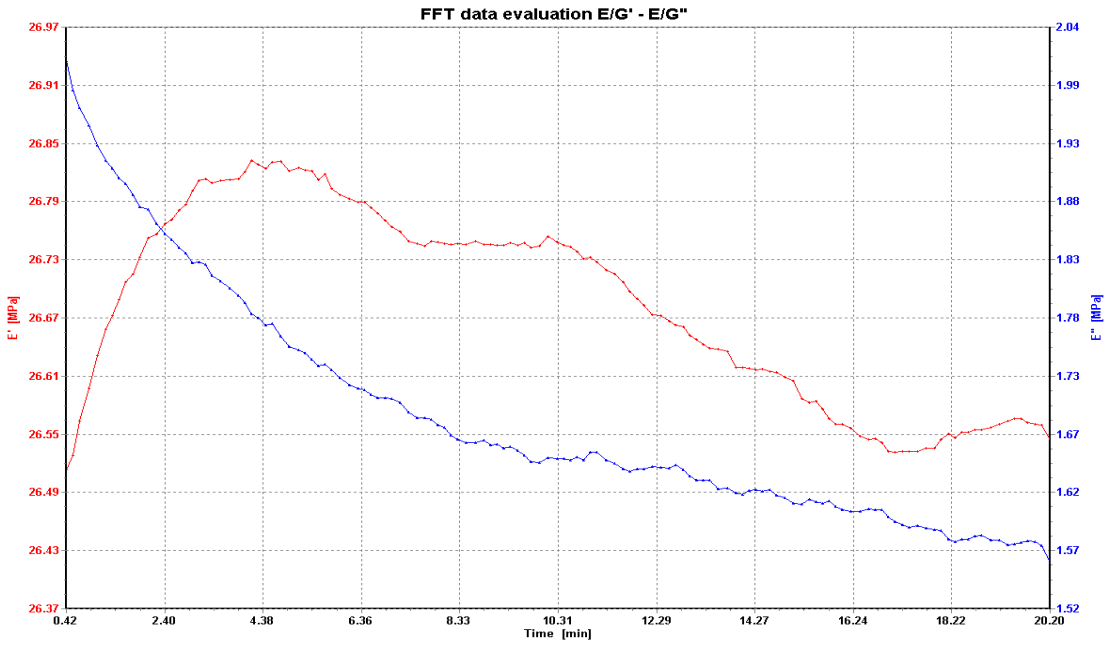

Figure 57: Graphs of DMA analysis for sample # 20, with 1200g/l matrix and BF: CF [100:0]